Experimental zircon alteration and baddeleyite formation in silica saturated systems: implications for dating hydrothermal events

Alexander Lewerentz

Dissertations in Geology at Lund University,
Master's thesis, no 293
(45 hp/ECTS credits)

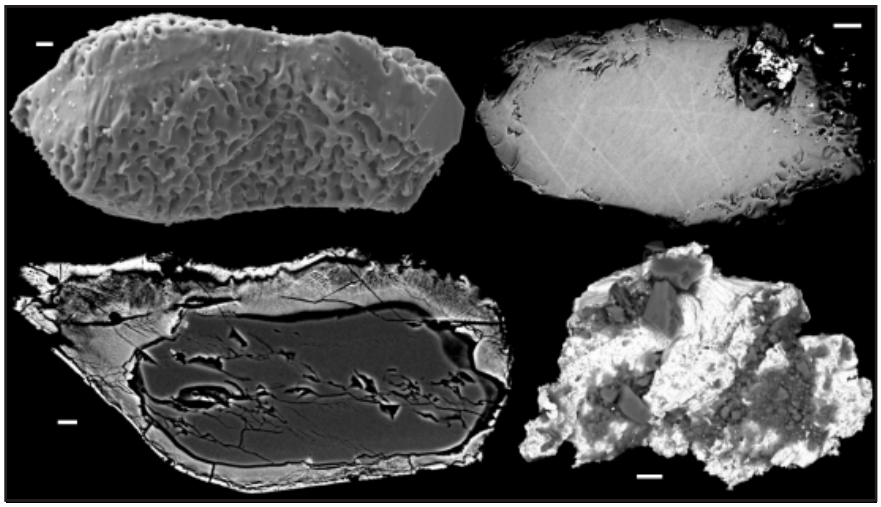

Department of Earth- and Ecosystem Sciences
Division of Geology
Lund University
2011

Experimental zircon alteration and baddeleyite formation in silica saturated systems: implications for dating hydrothermal events

Master's thesis

Alexander Lewerentz

Department of Earth and Ecosystem Sciences
Division of Geology
Lund University

2011

Contents

Cover Picture: SEM-BSE and SE, cross-section and surface, images of zircon grains that are partially dissolved and altered to baddeleyite. From top left to bottom right: ZrBd-09, ZrBd-09, ZrBd-14 and ZrBd-12. All scale bars are 20 μm long.

Experimental zircon alteration and baddeleyite formation in silica saturated systems: implications for dating hydrothermal events

ALEXANDER LEWERENTZ

Lewerentz, A., 2011: Experimental zircon alteration and baddeleyite formation in silica saturated systems: implications for dating hydrothermal events. *Dissertations in Geology at Lund University*, Master's Thesis, No. XXX, 56 pp. 45 hp (45 ECTS credits).

Abstract: Zircon ($ZrSiO_4$) and baddeleyite (ZrO_2) are two common zirconium bearing minerals which are important for U-Pb geochronology. Zircon is stable at silica saturated conditions, while baddeleyite should react with the free silica to form zircon under the same conditions. Yet, baddeleyite have been observed as intergrowths within zircon grains in silica saturated rocks, e.g. from southern West Greenland (Lewerentz, A., 2010: On the occurrence of baddeleyite in zircon in silica-saturated rocks. *Dissertations in Geology at Lund University*, Bachelor's Thesis N.o. 261, 54 pp.). This study is focused on replicating this phenomenon and the textures seen in natural zircon with baddeleyite intergrowths, using experimental petrological methods (piston cylinder and hydrothermal autoclave experiments). Experiments were conducted at 1,000 MPa and 900°C or ~400 MPa and 600°C in a closed system containing natural zircon, H_2O and $Ca(OH)_2$ or $CaCl_2$. Both silica saturated and under-saturated systems were used. SEM imaging (cross-section BSE and CL, surface SE and BSE), SEM-EDS analyses and EMP analyses were used to evaluate the experiments. Zircon is known to be perfectly stable at the experimental conditions. Yet, partial alteration of zircon to baddeleyite is observed in most experiments conducted in a silica under-saturated system, but also in a number of experiments conducted in a saturated system. Baddeleyite is appearing as blobs concentrated in thin semi-continuous bands or seemingly at random scattered within grains, or as thicker bands of a baddeleyite-Ca silicate intergrowth. I conclude that baddeleyite formation in zircon in a silica saturated system is possible due to fluid induced lowering of the silica activity in the system, making it under-saturated. A conceptual model on how the silica activity may be lowered is also proposed. Furthermore, it is concluded that the natural textures seen in zircon from e.g. southern West Greenland have formed through the process of coupled dissolution-reprecipitation (i.e. metasomatism), and are induced by a Ca bearing fluid. It is assumed that the reacted parts of zircon grains undergo trace element loss and that the U-Pb geochronometer is reset. Newly formed baddeleyite should incorporate U but not Pb. Subsequently, it would be possible to date hydrothermal (metasomatic) events, using U-Pb geochronological techniques on either the baddeleyite itself or on reacted parts of zircon grains.

Keywords: zircon, baddeleyite, silica saturated system, hydrothermal alteration, coupled dissolution-reprecipitation, experimental petrology, scanning electron microscopy, electron microprobe analysis, energy dispersive x-ray spectroscopy, southern West Greenland.

Alexander Lewerentz, Department of Earth and Ecosystem Sciences, Division of Geology, Lund University, Sölvegatan 12, SE-223 62 Lund, Sweden. E-mail: alexander.lewerentz@gmail.com

Experimentell omvandling av zirkon och baddeleyitbildning i kiselmättade system: betydelse för datering av hydrotermala händelser

ALEXANDER LEWERENTZ

Lewerentz, A., 2011: Experimental zircon alteration and baddeleyite formation in silica saturated systems: implications for dating hydrothermal events. *Examensarbeten i geologi vid Lunds universitet*, Masterarbete, Nr. XXX, 56 sid. 45 hp.

Sammanfattning: Zirkon ($ZrSiO_4$) och baddeleyit (ZrO_2) är två vanliga zirkoniuminnehållande mineral som båda är viktiga för U-Pb-geokronologi. Zirkon är stabilt under kiselmättade förhållanden medan baddeleyit under kiselmättade förhållanden torde reagera med det tillgängliga kislet och bilda zirkon. Trots detta har baddeleyit observerats som interna domäner i zirkon i kiselmättade bergarter från exempelvis sydvästra Grönland (Lewerentz, A., 2010: On the occurrence of baddeleyite in zircon in silica-saturated rocks. *Examensarbeten i geologi vid Lunds universitet,* Kandidatarbete, Nr. 261, 54 pp.). Den här studien är fokuserad på att återskapa detta fenomen och de texturer som observerats i naturlig zirkon med baddeleyitdomäner. Detta utförs genom att använda två metoder inom experimentell petrologi, cylinderpressexperiment och hydrotermalautoklavexperiment. Experimenten utfördes vid 1 000 MPa och 900°C eller ~400 MPa och 600°C i ett slutet system innehållandes naturlig zirkon, H_2O samt $Ca(OH)_2$ eller $CaCl_2$. Såväl kiselmättade som omättade experiment utfördes. För att utvärdera experimenten användes svepelektronmikroskopi (BSE och CL i tvärsnitt, SE och BSE på kornytor), energidispersiv röntgenemissionsspektroskopi samt elektronmikrosondanalys. Zirkon ska vara stabilt vid de förhållanden som använts i experimenten. Trots detta kan partiell omvandling av zirkon till baddeleyit ses i de flesta experiment som utförts under kiselomättade förhållanden, men också i att antal av de experiment som utförts under kiselmättade förhållanden. Baddeleyit uppträder som prickar, koncentrerade i tunna band, eller slumpmässigt spridda inom zirkonkornet, eller som tjockare band bestående av en sammanväxt mellan baddeleyit och ett kalciumsilikat. Av detta dras slutsatsen att baddeleyitbildning i zirkon under kiselmättade förhållanden är möjligt på grund av fluidorsakad sänkning av kiselaktiviteten i systemet, dvs. att system går från kiselmättat till kiselomättat. En konceptuell modell för hur detta sker är föreslagen. Vidare fastslås att de texturer som observerats i zirkon från t.ex. sydvästra Grönland har bildats genom processen kopplad upplösning-utfällning (metasomatism) och orsakats av kalciuminnehållande fluider. Det kan antas att de delar av zirkon som reagerar på detta vis också genomgår urlakning av spårämnen samt att U-Pb-geokronometern återställs. Den baddeleyit som bildas genom omvandling från zirkon bör inkorporera U men inte Pb. Summerat bör det vara möjligt att datera hydrotermala (metasomatiska) händelser genom att använda U-Pb-geokronologi, antingen på nybildad baddeleyit eller på reagerade delar av zirkon.

Nyckelord: zirkon, baddeleyit, kiselmättat system, hydrotermal omvandling, kopplad upplösning-utfällning, experimentell petrologi, svepelektronmikroskopi, elektronmikrosondanalys, energidispersiv röntgenemissionsspektroskopi, sydvästra Grönland.

Alexander Lewerentz, Institutionen för geo– och ekosystemvetenskaper, Enheten för geologi, Lunds universitet, Sölvegatan 12, 223 62 Lund, Sverige. E-post: alexander.lewerentz@gmail.com

1 Introduction

1.1 Background

Zircon ($ZrSiO_4$) and baddeleyite (ZrO_2) are the two most common zirconium bearing minerals. Both zircon and baddeleyite are important minerals for U-Pb geochronology as they incorporate U but not Pb in the crystal lattice, i.e. they can be used to date both igneous crystallisation and metamorphic events. Zircon forms under silica saturated conditions while baddeleyite forms under silica under saturated conditions. Hence, baddeleyite should not be stable in silica saturated systems since baddeleyite should react to form zircon in these cases. Yet, baddeleyite intergrowths are observed in zircon from silica saturated rocks from southern West Greenland (Lewerentz 2010). How is this possible?

The primary aim of this study is to establish how baddeleyite forms in seemingly silica saturated conditions, as well as what the underlying process or processes might be. To reach this aim, this study is focused on: 1) experimental replication of natural textures seen in rocks from southern West Greenland, 2) experimental alteration of zircon to baddeleyite under silica saturated conditions, 3) if possible, linking of the experimental conditions to the regional geology of southern West Greenland, and thereby answer the following questions. Is baddeleyite formation an effect of hydrothermal fluid induced metasomatic alteration of zircon? Is altered zircon chemically equilibrated with the fluid? Would it be possible to date metasomatic events? Possibilities to date metasomatic events are interesting from two angles; to my knowledge it has not been done on zircon before and would open up new possibilities for continent reconstruction and petrogenetic studies, hydrothermal fluids are documented to result in ore mineralisations containing elements such as Au, Ag and the REEs (e.g. Kolb et al. 2010; Páez et al. 2011; Smith et al. 2000). Movement of metamorphic and hydrothermal fluids are also interesting for other disciplines than the strictly geological, e.g. for the safety of storage of nuclear waste material.

1.2 Coupled dissoloution-reprecipitation

Coupled dissolution-reprecipitation is a process which results in re-equilibration within a rock at the influence of a metamorphic fluid, i.e. metasomatic alteration. Albitisation of plagioclase is perhaps the best known example of this process, where plagioclase is pseduomorphically replaced by albite (Putnis & Austrheim, 2010). Dissolution-reprecipitation processes have been subject to numerous experimental studies, concentrated on both zircon and other minerals such as plagioclase and monazite (e.g. Harlov et al. 2011; Geisler et al. 2001; 2003a; 2003b; Geisler 2002; Lenting et al. 2010; Putnis 2002; 2009). The impact on other minerals is not considered here, as this study is focused on metasomatic alteration of zircon.

The process of coupled dissolution-reprecipitation takes place on the atomic scale, where a fluid in contact with a zircon grain is partially dissolving the zircon. As more of the zircon is dissolved, the fluid can reach deeper into the zircon, i.e. the reaction front is moving into the grain. Behind the reaction front recrystallisation takes place, creating a reaction rim which is re-equilibrated with the fluid. Reactiveness is increasing with increased metamictisation of the zircon, as radiation damage is implying atomic disorder within the lattice and making the zircon more readily dissolved (Geisler et al. 2007). However, it is important to realise that thermal annealing will heal radiation damage and that this process has increasing effectiveness with increasing temperature (Geisler 2002).

A number of effects may be observed as a result of coupled dissolution-reprecipitation, one being that the reaction rim and grain surface will have higher porosity compared to the unreacted core. The recrystallised material will be amorphous and consist of polycrystalline zircon and contain non-formula elements, which are enriched in the fluid before the reaction, e.g. Al, Fe and Ca. Depletion of trace elements (U, Pb, Th and REE) will take place in the reaction rim, as these elements most probably is enriched in zircon in comparison with a metamorphic fluid (Geisler et al. 2007).

In nature, coupled dissolution-reprecipitation has been proposed to be the process behind the formation of zircon coronas around Fe-Ti oxides (Austrheim et al. 2008). Another example is alteration and breakdown of zircon from the Lanzo Massif in Italy, where trace elements are depleted in the altered areas (Rubatto et al. 2008). Alteration of zircon has also been observed in an alkaline pegmatite in Zomba-Malosa in Malawi. In this case the cores are unaltered and show high amounts of trace elements. In contrast, the outer grain parts are altered, show trace element depletion, increased porosity as well as several types of inclusions such as thorite ($ThSiO_4$) and yttrialite ($(Y,Th)_2Si_2O_7$) (Soman et al. 2010).

1.3 Geological background

The regional geology of southern West Greenland (Fig. 1) is dominated by a number of Mesoarchaean terranes, accreted between ca. 2.9 and 2.7 Ga in island arc settings or active continental margins (Friend et al., 1996; Windley & Garde 2009). The dominating rock types are the TTG orthogneisses (grey tonalites, trondhjemites and granodiorites), all plagioclase dominated rocks of granitoid composition. Between and within the gneiss complexes mafic intrusives and supracrustal belts occur as slivers. Additionally, a few anorthosite complexes, such as the Fiskenæsset complex, are found within the orthogneissic terranes (Keulen et al. 2009; Næraa & Scherstén 2008; Schiøtte et al. 1989; Steenfelt et al. 2005).

Several stages of metamorphism have affected the area. Granite intrusions around 2.8 Ga are related with granulite facies metamorphism. Later (2.72-2.68 Ga) the region was subject to amphibolite facies metamorphism. Metamorphic fluids associated with this latter

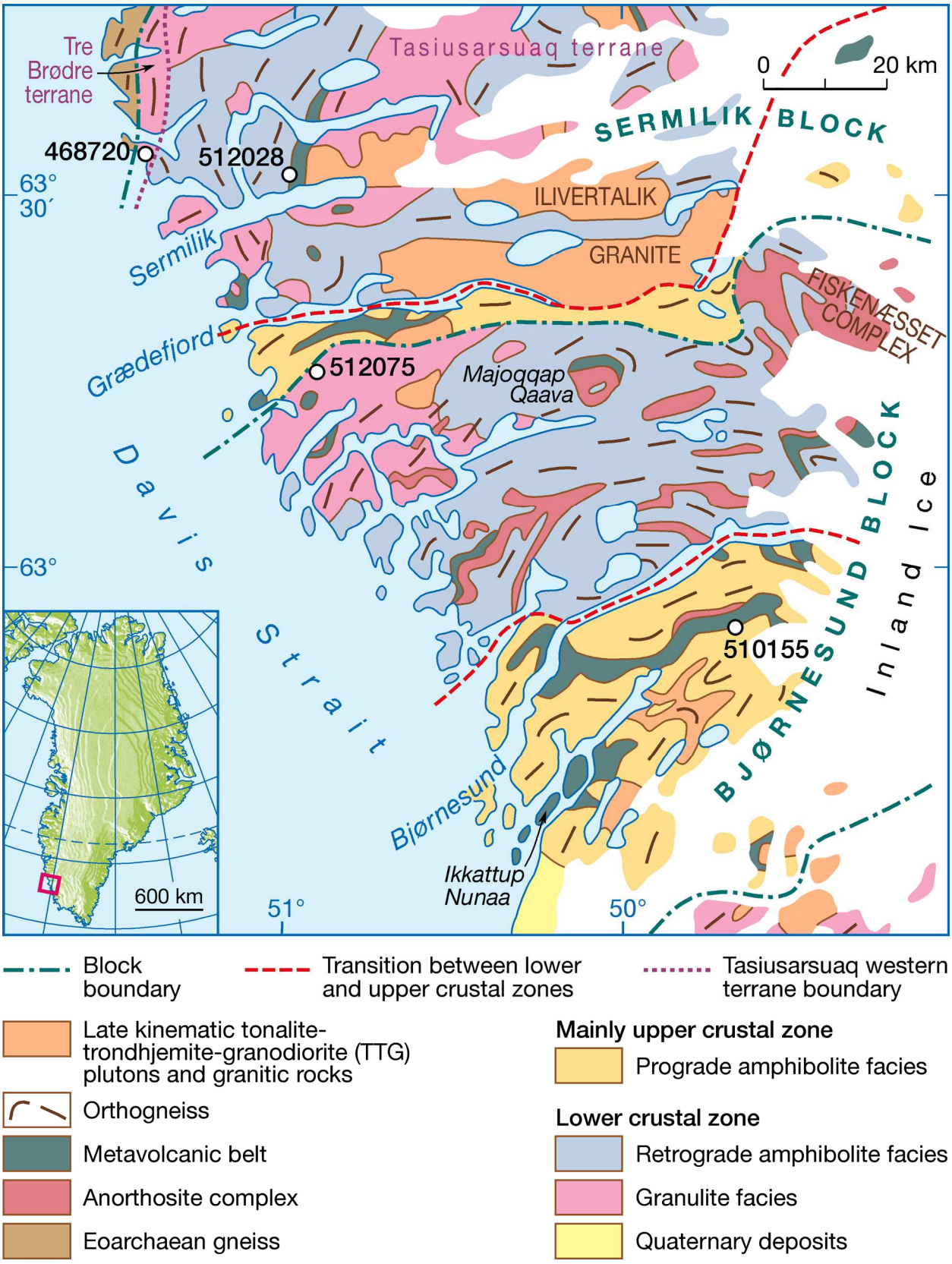

Fig. 1. Geological map of the Sermilik and Bjørnesund blocks in southern West Greenland. Marked sample locations are rocks containing zircon with baddeleyite intergrowths (modified after Keulen et al. 2009; Windley & Garde 2009).

event have resulted in fluid induced alteration along zones within the TTG complexes. P-T conditions have been estimated to 5-6 kbar and 700 °C. These alterations have resulted in recrystallisation of TTG, forming peraluminous rocks such as sillimanite bearing schists (Keulen et al. 2009; Schumacher et al. 2011).

The different terranes (parts of or completely) have been assigned to a number of blocks by Windley & Garde (2009), being a different way of explaining the geology of southern West Greenland and contrasting to the terrane model proposed by Friend et al. (1996). Each block can also be divided into a lower and an upper crustal zone, where the upper zone mainly consists of prograde amphibolite facies rocks while the lower zone yields granulite and retrograde amphibolite facies rocks (Windley & Garde 2009). This study is concentrated on the Bjørnesund and Sermilik blocks, where zircon grains containing baddeleyite intergrowths have been observed (Lewerentz 2010).

The Bjørnesund block extends from the glacier Fredrikshåb Isblink northwards to Grædefjord. The upper crustal zone of this block contains prograde amphibolite facies biotite-hornblende orthogneisses of tonalitic and granodioritic composition. The Bjørnesund area has reached garnet-kyanite or sillimanite grade metamorphism, but never as high as granulite facies (Thomas 1973; Windley & Garde, 2009). Within the gneisses, metavolcanic amphibolite layers up to 2 km thick are occurring. At places the amphibolite is bordered by up to 1 km thick anorthosite-leucogabbro layers that are folded with the amphibolite into refolded isoclines (Windley & Garde 2009). The deposition ages of one of the largest metavolcanic belts, the Ikkattup Nunaa belt, has been dated to 2908 ± 13 Ma (Nutman et al. 2004). A muscovite granite intruding the Ikkattup Nunaa belt has been dated to 2660 ± 20 Ma and this age marks the end of amphibolite facies metamorphism (Pidgeon & Kalsbeek 1978).

At the boundary between the upper and lower crustal zones of the Bjørnesund block a northward prograde amphibolite-granulite facies transition takes place and orthopyroxene is growing at the cost of amphiboles. The lower crustal zone is dominated by retrogressed amphibolite facies gneisses. Areas of relict granulite facies gneisses up to over 10 km across are found within the retrogressed gneisses, in greatest abundance near the base of the block. The Fiskenæsset anorthosite complex is part of the lower crustal zone of Bjørnesund block (Windley & Garde 2009 and references therein).

Sermilik block is the adjacent block to the north of Bjørnesund block. It extends from Grædefjord in the South to Ameralik fjord and Buksefjorden in the North. This block mainly consists of three terranes; Tasiusarsuaq, Tre Brødre and Færingehavn terranes from south to north (Nutman et al. 1989; Windley and Garde 2009). The Tasiuasarsuaq terrane consists mainly of gneisses, tonalitic to dioritic in composition. Granulites are common, ranging from isolated patches to semicontinuous belts (Coe 1980; Compton 1978; Nutman et al. 1989). Other litholigical units are vastly migmatised metabasic rocks, such as meta- and leucogabbros, of amphibolite facies metamorphism (Nutman et al. 1989). The Tre Brødre terrane is mainly made up by Ikkattoq gneisses which are rocks of granodioritic composition and grey in colour, showing a widely spread pegmatite banding (Nutman et al. 1989). These gneisses are intruding mafic rocks (mainly amphibolites derived from volcanic rocks and gabbros) and metasedimentary rocks such as metapilites and quartz-cordierite gneisses (Beech & Chadwick 1980). The main lithological units of Færingehavn terrane are pegmatite banded, tonalitic grey gneisses as well as iron rich granitic augen gneisses, both known as Amîtsoq gneisses (Nutman et al. 1989). These gneisses have been dated to between 3600 and 3820 Ma (Schiøtte et al. 1988).

Hydrothermal alteration and mineralisation (e.g. Au) have been observed in area between and around Sermilik and Grædefjord fjords. In the Sermilik fjord area plagioclase destructive hydrothermal alteration is present in mafic granulites and meta-sedimentary rocks. Alteration is concentrated to zones in the rocks, identified in field by alteration haloes, and structurally interpreted as post peak metamorphic. In the Grædefjord area, hydrothermal alteration is found in zones between pegmatite intrusions in mafic granulites, and in TTG gneisses where an alteration assemblage of biotite-quartz-pyrrohtite replaces the peak metamorphic orthopyroxene-plagioclase-K-feldspar-quartz assemblage. Gossan zones are present in breccias derived from the TTG gneisses, and both alteration zones and gossans are concentrated to fault intersections. Structures and fabrics within quartz suggest that alteration took place at greenschist facies (Kolb et al. 2010).

1.4 Natural zircons

Examples of baddeleyite within natural zircon from southern West Greenland are presented in Figure 2. Lewerentz (2010) described a large number of zircon grains from these rocks and described them in terms of mineralogical and petrological habitus. The internal baddeleyite domains are showing a large variety of textures, ranging from small (<1 µm) blobs and larger (~10 µm) irregular domains, to bands concordant with the zircon growth zonation and other regular textures that apparently are controlled by an external factor other than growth zonation. Areas of zircon that are adjacent to baddeleyite domains are commonly showing a darker BSE appearance than the rest of the zircon. SEM-EDS analyses of these areas reveal that they are enriched in non-formula elements, such as Al, Fe, Ca and Na (Lewerentz 2010).

Zircon containing baddeleyite intergrowths have been observed in four different rocks, and were described in detail by Lewerentz (2010), but a brief summary is given below. Field interpretations were made by Thomas Kokfelt, Nynke Keulen and Anders Scherstén respectively (drawn from unpublished

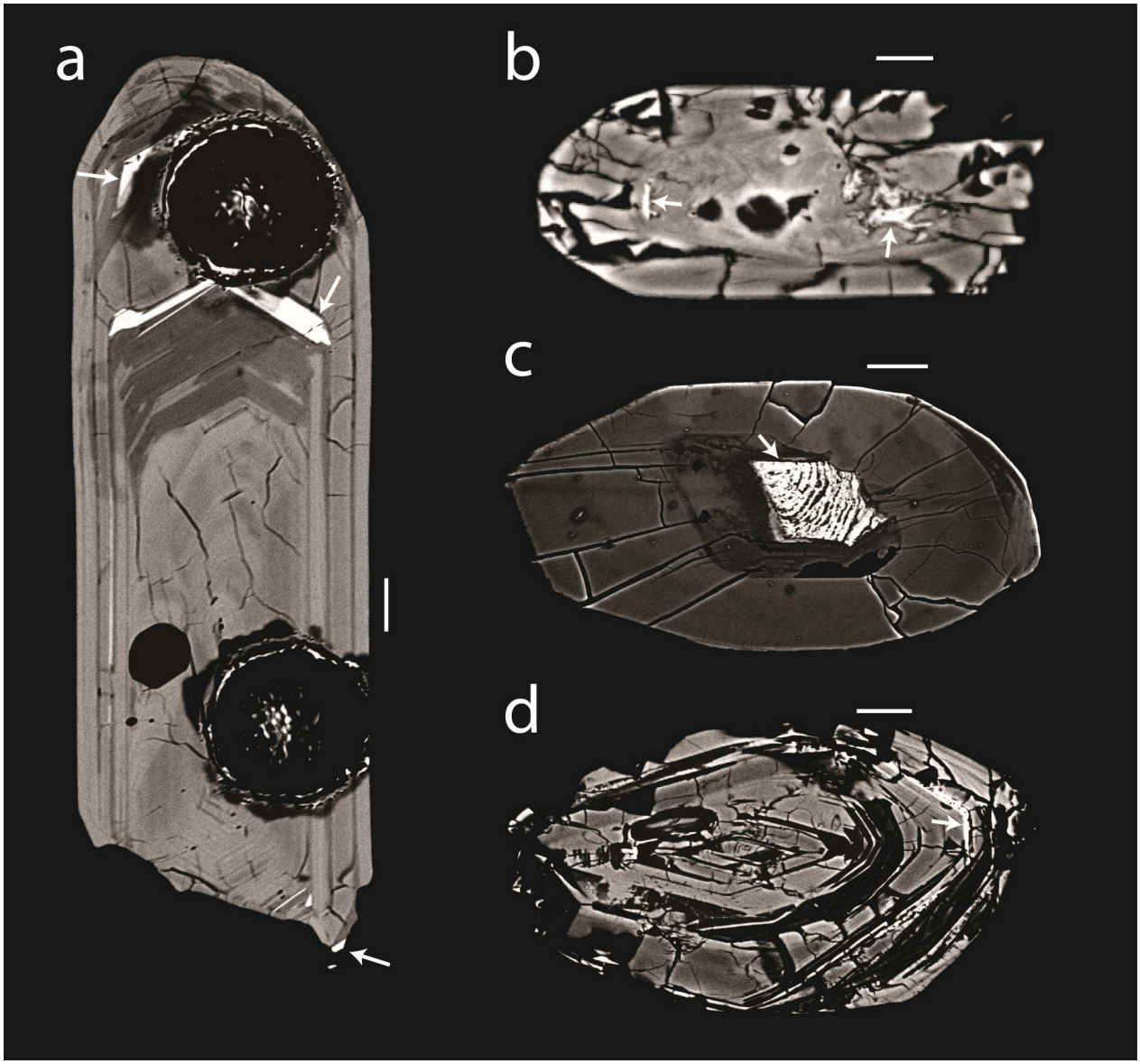

Fig. 2. SEM images (BSE) of natural zircon grains with baddeleyite intergrowths from four different rocks from southern West Greenland. Baddeleyite is white and is marked with white arrows. All scale bars are 10 µm. a) sample 510155, the ~20 µm wide black circular spots are LA-ICP-MS pits unrelated to this study, b) sample 512075, c) sample 512028, d) sample 468720 (compiled after Lewerentz 2010).

GEUS databases). Six digit combinations are GEUS (Geological Survey of Denmark and Greenland) sample reference numbers.

The Tre Brødre mica schist (468720) is a rock metamorphosed to amphibolite facies, mapped as garnet-sillimanite-biotite schist and possibly a meta-sediment. Average anorthite content of the plagioclase in this rock is 28.65 % An (σ=0.66), SEM-EDS data is presented in Appendix X. The mineral content have been estimated to 65 % quartz, 15 % sillimanite, 10 % biotite, 5 % K-feldspar, <5 % muscovite, <5 % plagioclase, apatite and zircon as accessory minerals. A foliation is defined by bands of biotite, sillimanite and muscovite. Sillimanite occurs as fibrolite associated with muscovite, abundantly as sillimanite-muscovite intergrowth (Lewerentz 2010).

The Nukagpiarssuaq (NGI) granite (510155) has an estimated mineral content of: 35 % quartz, 30 % plagioclase, 15 % K-feldspar, 15 % biotite, < 5% biotite, <5 % apatite. Zircon, hematite, opaque minerals and allanite occur as accessory minerals. The average An content of plagioclase is 19.75 % An (σ=0.93). Plagioclase and K-feldspar is occasionally showing an altered appearance (heterogeneous grains and partial replacement by Al silicates). Plagioclase-quartz intergrowths (myrmekite) are occurring. This rock holds a large number of zircon grains, with over 40 grains observed in a 4x2 cm thin section (Lewerentz 2010).

Sample 512028 consist of a more fine grained part of a pegmatite, with an estimated mineral content of: 35 % quartz, 35 % K-feldspar, 25 % plagioclase, <5 % biotite, <5 % muscovite, <5 % garnet, zircon as an accessory mineral. Average An content of the plagioclase is 35.29 % An (σ=0.98). Most plagioclase and K-

feldspar grains are showing an altered appearance (see above), and myrmekite occurs as inclusions in plagioclase and K-feldspar grains (Lewerentz 2010).

Sample 512075 consists of a more fine grained part of a pegmatite from the Grædefjord shear zone, just south of the boundary between the Sermilik and Bjørnesund blocks. Estimated mineral content: 50 % quartz, 25 % plagioclase, 15 % K-feldspar, 5 % biotite, 4 % muscovite, 1 % garnet, zircon as an accessory mineral. Average plagioclase An content is 43.49 % An (σ=1.30). Plagioclase is abundantly showing an altered appearance, and muscovite is only occurring within altered plagioclase grains. Metamorphic twinning is occasionally visible in plagioclase grains. K-feldspar and biotite are also showing an altered appearance (Lewerentz 2010).

All these rocks show a few mutual features; they are rich in quartz (35-65 %), plagioclase is either showing an altered appearance (commonly with inclusions such as muscovite) or is more or less absent, myrmekite (plagioclase-quartz intergrowth) is abundant, K-feldspar is commonly showing an altered appearance. SEM studies of thin sections have shown that in all cases of baddeleyite intergrowths, the zircon grains are in direct connection with cracks in the respective host rocks. However, a majority of the zircon grains found in these samples are not altered, and many of these are also in contact with cracks. Altered zircon grains are seemingly distributed randomly with respect to petrological factors, such as host rock mineralogy (Lewerentz 2010).

Baddeleyite intergrowths in zircon grains have also been observed in a Birimian quartzite from southern Ghana, West Africa. This sample was collected at the contact to a granitic intrusion, a possible fluid source. An additional sample of the same quartzite was collected 2 meters from the intrusion contact and is not showing any baddeleyite (Anders Scherstén, personal communication). Although this shows that baddeleyite might be an isolated process within a rock volume, it is clearly not a geologically isolated phenomenon restricted to southern West Greenland. It should be safe to assume that these processes and their effects would be observable on a global scale, as fluids are part of the petrogenesis of most metamorphic rocks.

2 Starting material

2.1 Varberg charnockite zircon

This sample consists of zircon from the charnockite inliers associated with the Torpa granite (Varberg Charnockite-Granite Association), sampled in the outskirts of the town of Varberg, SW Sweden. The Charnockite intrusion host rock has been subject to later metamorphism and deformation and is now described as a migmatised gneiss, as the whole area was subject to high grade Sveconorwegian metamorphism, i.e. 1.1-0.9 Ga (Åhäll et al. 1997). Emplacement age for the Charnockite has been indirectly dated (U-Pb geochronology) to 1380±6 Ma (Åhäll et al. 1997) and 1399 +12/-10 Ma (Christoffel et al. 1999).

SEM-BSE imaging (Fig. 3 and Appendix 2) of the zircon grains show oscillatory zoning with bands showing homogeneous BSE (back scattered electron) brightness, although some grains are seemingly lacking growth zonation (Fig 3). Under CL (cathodoluminescence), nearly all grains show distinct oscillatory zoning, but a few cases of more intricate CL patterns are also observed. The grains are abundantly cracked and showing inclusions, although crack and inclusion free grains are also present. Many grains are fragments of larger grains, but whole crystals are also present. Nearly all grains show euhedral appearance (excluding fracture surfaces). SE (secondary electron) and BSE imaging of grain surfaces confirms that most grains are euhedral, although a number of partially rounded grains are also present. Those grains that are fragments of larger crystals sometimes show conchoidal-like fracture surfaces. Partially exposed inclusions (e.g. K-feldspar) can also be observed on grain surfaces.

2.2 Önnestad syenite zircon

This sample contains zircon from a syenite sampled near the village of Önnestad, ca. 14 km west from the town of Kristianstad, NE Skåne, southernmost Sweden. This rock is situated within an intraplate tectonic zone, the Protogine Zone. U-Pb zircon dates of 1230-1200 Ma have been interpreted as the emplacement age of the syenite (Johansson 1990).

Under SEM-BSE (Fig. 3 and Appendix 2) oscillatory zoning is observed in a few cases but most grains show more or less homogeneous BSE-brightness. However CL reveals that almost all grains have some sort of oscillatory zoning, mainly simple growth zonation. Inclusions, pores and cracks are abundant. The grains are euhedral and consist of either whole crystals or fragments of crystals. SE imaging of grain surfaces confirms that most grains are euhedral, although a slight rounding of certain faces is rather common.

2.3 ASGH007A zircon

This sample consists of zircon from a tonalite, sampled near the Atlantic coast in SW Ghana. This tonalite is part of the SW-NE striking Ashanti granitoid belt (Grenholm 2011). Emplacement has been dated to 2172±12 Ma (Anders Scherstén, unpublished data).

BSE imaging (Fig. 3 and Appendix 2) shows mainly small (50-100 μm) and euhedral zircon grains. Most grains show distinct oscillatory zoning, an observation, which is also confirmed by CL imaging. In one case the grain interior (and oscillatory zoning) is seemingly overprinted by BSE homogenous and CL bright zircon. Most grains are cracked and host inclusions and or pores. SE surface imaging shows a range of varieties, ranging from perfect euhedral and completely pristine grains to grains with slightly rounded edges and uneven surfaces, although most grains are euhedral. A few grains are seemingly partially draped with another zircon phase, where the non-covered areas

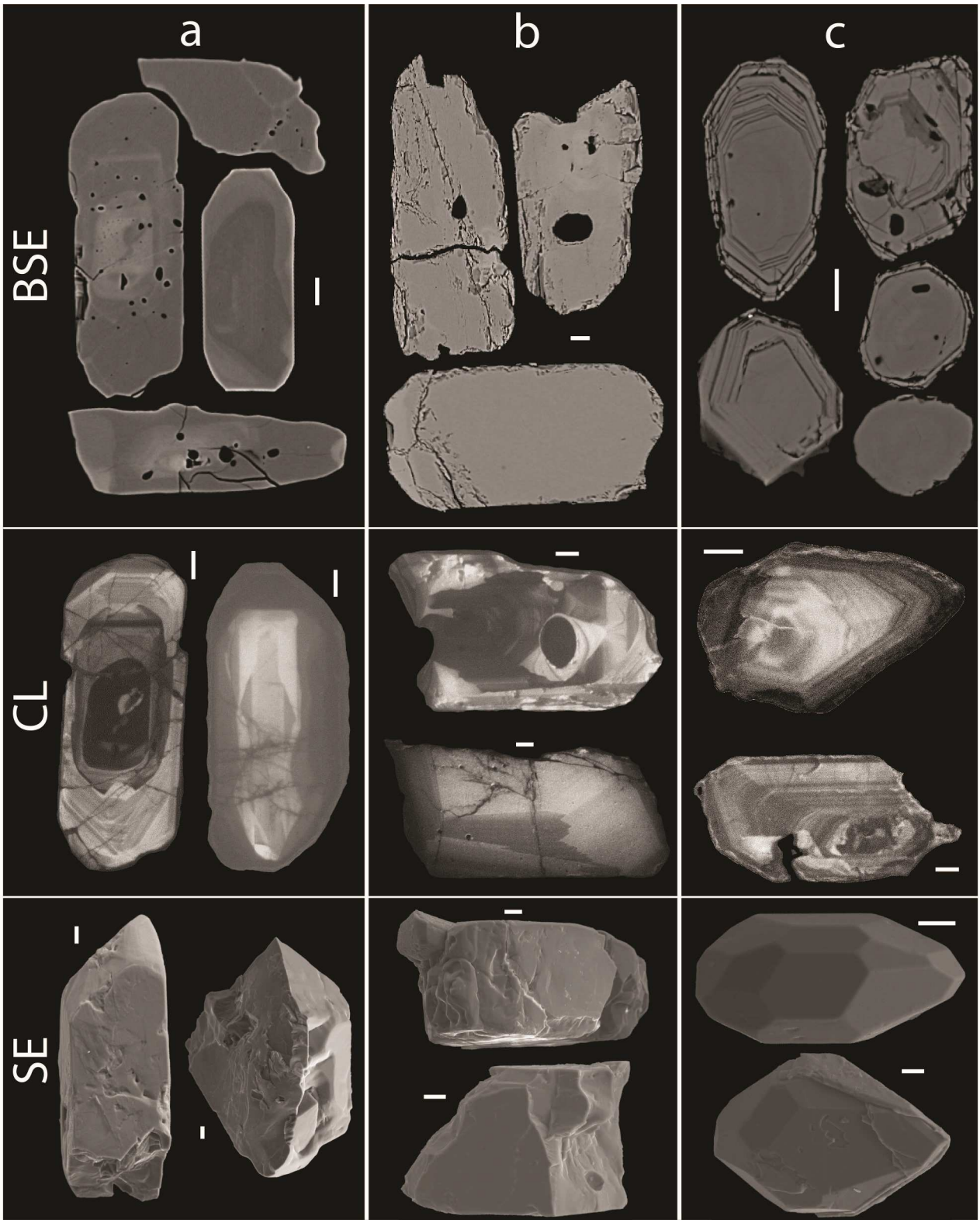

Fig. 3. SEM images of the different starting materials. BSE and CL are in cross-section, SE from surface imaging. All scale bars are 20 µm. a) Varberg charnockite zircons, b) Önnestad syenite zircons, c) ASGH007A tonalite zircons.

show perfect euhedral appearance while the draped areas are more irregular.

3 Methods

3.1 Experimental petrology

3.1.1 Piston cylinder experiments

All experiments using the piston cylinder apparatus were conducted according to Johannes et al. (1971) and Johannes (1973) at 900 °C and 1 000 MPa. Platinum capsules were cut in 1 cm long pieces from a 3 mm wide Pt tube, cured for several hours in an oven at 900 °C to remove any stress within the material and arc weld shut in one end using an argon plasma welder. ~7 mg of zircon, 5 mg of H_2O, 5 mg of SiO_2 and 1-2 mg $Ca(OH)_2$ or $CaCl_2$ were loaded into the capsules using a funnel. The capsules were pinched and arc weld sealed. To confirm that no contents had been lost from the capsules during the making process, they were weighed after each step. The capsules were put in an oven at 100 °C for at least 18 hours to confirm that the seals were tight.

After inserting the capsules, separated by biotite leaves, in the inner CaF_2 bottom piece (Fig. 4), any remaining cavities were eliminated by tapping in CaF2 powder. The CaF_2 bottom piece was fastened to the bottom piston by threading it on the thermocouple. A graphite oven was pushed on the CaF_2 piece and the CaF_2 top piece inserted. An outer CaF_2 piece, encapsulating the graphite oven, was applied. Over and under the CaF_2 cell pyrophyllite rings (for sealing) and Cu rings (for electrical conductivity) were fitted. The inside of the water cooled bomb was coated with MoS_2 powder for lubrication, after which the CaF_2 set-up was inserted into it. After inserting the bomb into the press, the apparatus was first taken up to pressure (corrected for friction within the CaF_2 cell) and secondly up to temperature. P and T were kept stable within less than 1 % variation for ca. 4 days. A NiCr thermocouple, with the tip covered with Al_2O_3 for protection against corrosion, was used to monitor and control the temperature.

The capsules were removed from the set-up, punctured, dried in a 100 °C oven and weighed to determine the water content. The remaining content was extracted and washed three times with triple distilled water to remove any remaining free $Ca(OH)_2$ or $CaCl_2$. The reaction products were either embedded in epoxy to make polished grain mounts for evaluation of grains in cross-section, or sprinkled on adhesive carbon tape, fastened on small circular pin-type mounts for evaluation of grain surfaces.

3.1.2 Hydrothermal autoclave experiments

All experiments using the hydrothermal autoclave apparatus were aimed to be conducted at 600 °C and 500 MPa. However, due to defect autoclaves or seals, the pressure was not stable at 500 MPa. Actual stable pressures ranged between 370 and 440 MPa. Platinum capsules were prepared, loaded and tested in the same manner as for the piston cylinder experiments. The capsules were put in a cold sealed autoclave which was inserted into a ceramic insulated oven. The water pressurised autoclave was kept at stable P and T for ca. 8 days and in one case for 50 days. A NiCr thermocouple was used to monitor and control the temperature. During quenching procedure, the pressure was lowered to 200 MPa, allowing the autoclave to cool isobarically to room temperature after which it was completely depressurised. Extraction and sample preparation was conducted in the same manner as for the piston cylinder experiments.

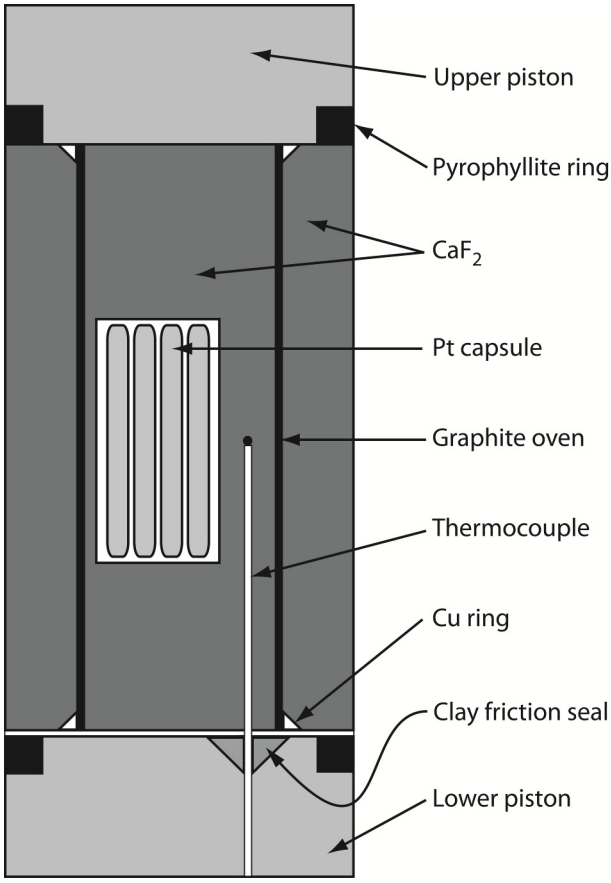

Fig. 4. Schematic drawing of the CaF_2 set-up, used in the piston cylinder experiments at 1,000 MPa and 900 °C. The cell itself was inserted into a bomb and pressurized vertically. Cu rings are applied to allow an electrical current flow through the set-up, being the source of heat (modified after Harlov et al. 2011).

3.2 Scanning electron microscopy

Scanning electron microscopy (SEM) images are obtained during scanning of an electron beam hitting the surface a the sample (Reed 1995). The used SEM techniques were: Secondary Electron (SE) detection, Back Scattered Electron (BSE) detection and Cathodoluminescence (CL) detection. High vacuum and 15 kV were used for SE and BSE, where the samples were coated by a thin layer (~25 nm) of carbon. In contrast to the other techniques, CL was conducted without carbon coating and at low vacuum (80 Pa). Most of the

SE and BSE imaging was carried out at the German Research Centre for Geosciences (GFZ) in Potsdam, Germany. CL imaging, as well as SE and BSE of samples ZrBd-19 and 20, were done at the Department for Earth and Ecosystem Sciences, Lund University in Lund, Sweden.

3.2.1 Secondary electron detection

Secondary electrons are dislodged from the sample surface due to bombardment by the incident electron beam. A detector collects these electrons, producing a SEM-SE image. The brightness of the SE signal is dependent of the number of secondary electrons reaching the detector. The number of secondary electrons increases with increased surface area being hit by the incident beam, thus a surface perpendicular to the beam will have the smallest possible area being hit by the beam at one instance and also give the smallest possible number of secondary electrons. With decreased angle between the beam and the surface, the surface area being hit by the beam and the number of secondary electrons will increase, therefore a edges and steep surfaces will appear brighter than flat surfaces (Reed 1995).

3.2.2 Back-scattered electron detection

The SEM-BSE signal is obtained by the measurement of electrons, derived from the incident beam, which have been subjected to large deflection within the sample and re-emerged from the surface. Contrast in BSE-images is dependent of the atomic number of the sample, or mean atomic number if the sample is a compound (Reed 1995), i.e. the contrast will show the difference in density between compounds within an image. A less dense compound will appear darker than a more dense.

3.2.3 Cathodoluminescence detection

A cathodoluminescence (CL) picture is obtained by imaging of the light emitted during electron bombardment of the sample. This light is almost only produced by trace elements, such as manganese and the rare earth elements (Long 1995), i.e. CL reflects compositional contrasts.

3.2.4 Energy-dispersive X-ray spectroscopy

Energy Dispersive X-ray Spectroscopy (EDS) is an analytical technique with many applications. It is often used together with the SEM technique. On a broad scale it works as follows. When the electron beam hits the sample, X-ray radiation is emitted. The radiation is measured with an EDS detector and the various energy values are then sorted into 20 eV wide channels. The results are displayed as a spectrum with a number of peaks (spectral lines). This spectrum depends on the composition of the analysed spot. In a spectrum, all elements have several peaks, depending on the emitting energy level. The various peaks are then compared with a known mineral standard to establish the composition of the analysed spot (Champness 1995). This comparison involves corrections for atomic number, absorption and fluorescence (ZAF-corrections). It is done using synthetic or natural mineral standard for all elements. The standards have been measured in the same way as the unknown sample.

To make quantitative analyses a calibration of the microscope is needed. In the used instrument (Oxford INCA system), this is done by analysing a cobalt standard. The calibration associates a specific count rate for any channel with the settings of the SEM. This calibration has been performed for both sample and mineral standards, which makes it possible to compare the analysed sample with the mineral standard.

3.3 Electron microprobe

An electron microprobe (EMP) is basically a SEM fitted with different x-ray spectrometers. The technique is similar to SEM-EDS (described above); in fact most EMPs are also fitted with an EDS detector. Hence, an EMP relies on the fact that any material emits x-ray radiation when being hit by an electron beam and that the resulting spectrum is composition dependent as all elements have a unique set of peaks at different energy levels (Reed 1995).

In contrast to most ordinary SEMs the EMP is also fitted with a wavelength-dispersive spectrometer (WDS). In a WDS the x-ray radiation is refined by a curved crystal that reflects the radiation towards the detector. Such a crystal may only reflect a certain interval of wavelengths, i.e. a certain portion of the spectrum, and by moving the crystal horizontally it is possible to choose one certain wavelength that is permitted to reach the detector. Different crystals have different wavelength windows, and to measure all relevant wavelengths several (typically four) crystals are needed, implying that one EMP also is fitted with several WDS detectors (Reed 1995).

The fact that a WDS only analyses one wavelength at a time implies sequential measurement of elements, but with several WDS detectors several portions of the spectrum can be measured at the same time which means that several elements can be measured simultaneously, decreasing the amount of time needed to analyse the selected elements in one point. Precision is often better than ±1 % and detection limits around 100 ppm by mass (Reed 1995).

The EMP analyses in this study were done on a JEOL JXA-8500F Fieldemission Electron Probe Microanalyzer at the GFZ in Potsdam, Germany. Analysed elements were: P, Nb, Si, Ti, Zr, Hf, Th, U, Al, Y, Ce, Pr, Nd, Sm, Gd, Dy, Ho, Yb, Lu, Ca, Mn, Fe, Pb and Na.

4 Results

4.1 Description of experimental runs

Examples of altered zircon grains are presented in Figures 5 and 6. A complete collection of SEM images

from all experiments is provided in Appendix 3. A summary of all experimental conditions, capsule contents and brief results is presented in Table 1.

4.1.1 ZrBd-01

This experiment was executed at 600 °C and 370 MPa, using the hydrothermal autoclave apparatus, and run for 186 h. With exception of some minor problems maintaining the pressure, the run was mechanically perfect. Contents of the capsule were; Varberg zircon, H_2O, SiO_2 and $Ca(OH)_2$. Due to difficulties with the first attempt of sealing the capsule, zircon + SiO_2 + $Ca(OH)_2$ were loaded as a mix with a total mass of 10.65 mg. After the run the capsule was determined to have held 4.17 mg of H_2O.

Under BSE little or no effect on the zircon grains is observed (Appendix 3). A few grains show BSE-lighter areas appearing as rims or bulges reaching inwards from the outer parts. Approximately half of the grains show pores and or inclusions, amounts varying from grain to grain and with no systematic distribution within the grains. The original growth zoning can be seen in a few grains, under CL in nearly all grains. SE imaging of grain surfaces show that some grains are rounded, a few cases of pits or cavities, as well as a needle shaped phase commonly growing on zircon grains.

4.1.2 ZrBd-02

This experiment was executed contemporaneously with ZrBd-01. The capsule was containing Varberg zircon, H_2O, SiO_2 and $Ca(OH)_2$. Zircon + SiO_2 + $Ca(OH)_2$ were loaded as a mix with a total mass of 8.58 mg. The capsule was determined to have held 1.87 mg of fluid. SEM imaging (BSE, SE, and CL), cross section and surface, show no difference to ZrBd-01 (Appendix 3).

4.1.3 ZrBd-03

This experiment was executed contemporaneously with ZrBd-01 and ZrBd-02. Contents of the capsule were: Varberg zircon, H_2O (1.66 mg), SiO_2 and $CaCl_2$ (0.90 mg). Zircon + SiO_2 were added as a mix with a total mass of 4.62 mg. SEM imaging (BSE, SE, CL), cross section and surface, show no difference to ZrBd-01 and 02 except for that the needle shaped phase is much less abundant (Appendix 3).

4.1.4 ZrBd-04

This experiment was executed at 900 °C and 1 000 MPa, using the piston cylinder apparatus, and ran for 96 h. The run was mechanically perfect, meaning that the pressure was increased slow and evenly without any sudden movements, indicating that the set-up was evenly and successively deformed, as well as that the temperature was held constant during the whole run with very little or no fluctuation. The capsule was loaded with Varberg zircon (7.55 mg), SiO_2 (4.50 mg), H_2O (1.47 mg) and $CaCl_2$ (0.65 mg).

Under BSE, most of the grains show homogenous brightness, but a few grains with darker or brighter domains are observed, growth zoning is scarcely seen, which is confirmed by CL. About half of the grains show pores and or inclusions and the smaller inclusions seem to have a preferred distribution along cracks or in continuous and undulating bands. SE images of the grain surfaces show abundant rounding and surface porosity (Appendix 3).

4.1.5 ZrBd-05

This experiment was executed contemporaneously with ZrBd-04 and the capsule was containing Varberg zircon (5.32 mg), H_2O (4.73 mg), SiO_2 (4.68 mg) and $CaCl_2$ (0.04 mg). Under BSE the grains are very similar to those of ZrBd-04, although pore and or inclusion bands are less abundant and less developed (Appendix 3). CL shows that oscillatory zoning is scarce, although a few grains with prominent zoning are observed. SE imaging of grain surfaces show that most grains are rounded, have surface porosity, and a few cases of a needle shaped phase as well as small quartz spheres (10 µm).

4.1.6 ZrBd-06

This experiment was executed at 600 °C and 370 MPa and left running for 166 h, using the hydrothermal autoclave apparatus. Contents of the capsule were; Varberg zircon (5.28 mg), SiO_2 (1.86 mg), H_2O (1.46 mg) and $CaCl_2$ (0.60 mg).

BSE imaging shows that, with the exception of a few rims, the grains show homogenous BSE-brightness (Appendix 3). However, CL imaging reveals that most grains show rather distinct oscillatory zoning. The grains are extensively cracked, and in some grains small pores and or inclusions have formed along the cracks. Almost all grains show areas where the surface resembles an uneven or pitted appearance, mainly but not entirely distributed along edges and cracks. Surface SE imaging show rounded grains and surface porosity.

4.1.7 ZrBd-07

This experiment was run contemporaneously with ZrBd-04 and 05. The contents of the capsule were: Varberg zircon (6.87 mg), H_2O (5.38 mg), SiO_2 (5.31 mg) and $Ca(OH)_2$ (0.87 mg). Under BSE and surface SE this sample shows a similar appearance as ZrBd-04 (Appendix 3). Although, CL reveals a more distinct and abundant oscillatory zoning than ZrBd-04.

4.1.8 ZrBd-08

This experiment was executed contemporaneously with ZrBd-04, 05 and 07. The contents of the capsule were: Varberg zircon, H_2O (2.93 mg), SiO_2 and Ca(OH)2. Zircon + SiO_2 + $Ca(OH)_2$ was added as a mix with a total mass of 9.72 mg. SEM imaging (BSE, CL, surface SE) shows high similarity to ZrBd-07

Table 1. Summary of experiment conditions, capsule contents and experiment results. Baddeleyite producing experiments are bold.

Experiment	Conditions			Capsule contents (mg)							Results	
	P (MPa)	T (°C)	Time	Zircon	$Ca(OH)_2$	$CaCl_2$	H_2O	SiO_2	Mix 1[1]	Mix 2[2]	Bd?	Ca:Si[4]
ZrBd-01	370	600	186 h				4.17		10.65		No	n.a.[5]
ZrBd-02	370	600	186 h				1.87		8.58		No	n.a.
ZrBd-03	370	600	186 h			0.90	1.66			4.62	No	n.a.
ZrBd-04	1000	900	96 h	7.55		0.65	1.47	4.50			No	0.08
ZrBd-05	1000	900	96 h	5.32		0.04	4.73	4.68			No	0.00
ZrBd-06	370	600	166 h	5.28		0.60	1.46	1.86			No	0.17
ZrBd-07	1000	900	96 h	6.87	0.87		5.38	5.13			No	0.14
ZrBd-08	1000	900	96 h				2.93		9.72		No	n.a.
ZrBd-09	**1000**	**900**	**120 h**	**7.42**	**3.20**		**5.92**	**1.24**			**Yes**	**2.09**
ZrBd-10	**1000**	**900**	**120 h**	**7.99**	**2.92**		**5.89**				**Yes**	∞
ZrBd-11	**1000**	**900**	**120 h**	**7.40**		**3.24**	**4.23**	**0.97**			**Yes[3]**	**1.81**
ZrBd-12	**1000**	**900**	**120 h**	**7.39**		**2.92**	**5.48**				**Yes[3]**	∞
ZrBd-13	440	600	240 h	8.13	3.42		4.59	1.71			No	1.62
ZrBd-14	**440**	**600**	**240 h**	**8.73**	**1.54**		**4.29**				**Yes**	∞
ZrBd-15	**440**	**600**	**240 h**	**7.21**		**1.31**	**3.87**	**1.18**			**Yes[3]**	**0.60**
ZrBd-16	440	600	240 h	5.73		2.71	6.36				No	∞
ZrBd-17	**1000**	**900**	**96 h**	**8.72**	**1.57**		**4.30**	**1.61**			**Yes**	**0.79**
ZrBd-18	**1000**	**900**	**96 h**	**4.00**	**1.31**		**1.40**	**1.45**			**Yes**	**0.73**
ZrBd-19	**420**	**600**	**50 days**	**7.10**	**1.70**		**3.98**	**1.41**			**Yes**	**0.98**
ZrBd-20	**420**	**600**	**50 days**	**6.64**	**1.78**		**3.93**				**Yes**	∞

[1]Mix 1 = Zircon + SiO_2 + $Ca(OH)_2$

[2]Mix 2 = Zircon + SiO_2

[3]Baddeleyite occurance exclusively on grain surfaces

[4]Ca:Si molar ratio (n_{Ca}/n_{Si})

[5]Ca:Si ratio is not calcuable as either or both of Ca and Si is added as a mix. The ratio should however be similar to those in experiments 04 to 07.

(Appendix 3). Additionally a BSE darker needle shaped phase is abundantly present on grain surfaces.

4.1.9 ZrBd-09

This experiment was run at 900 °C and 1 000 MPa, using the piston cylinder apparatus. It was run for 120 h. The capsule contained Varberg zircon (7.42 mg), H_2O (5.92 mg), $Ca(OH)_2$ (3.20 mg) and SiO_2 (1.24 mg). This run was regarded as mechanically perfect.

BSE imaging (Fig. 5a and Appendix 3) reveals a wide variety in terms of reactiveness, ranging from grains that are nearly unreacted to grains that are nearly completely dissolved. The least reacted grains show the uneven appearance, described under ZrBd-06. Most of these grains partially show bulging edges. Furthermore, a few grains show high porosity allocated to their outer parts. At the inner limits of these porous regions a fine continuous band of BSE-white (baddeleyite) blobs are present. In one of these grains a larger (Ø ~10 µm) baddeleyite domain is observed in its interior. In general, all grains show homogeneous BSE-brightness, with exception for the most heavily reacted grains. The near completely dissolved grains are observed as heaps of needles that are BSE-darker than the zircon grains, commonly accompanied by small amounts of baddeleyite blobs. Surface imaging (SE and BSE) shows rounded grains, dissolution textures of varying extensiveness, small blobs of baddeleyite, and needle shaped phases often clustered in heaps. CL shows that most grains have an interior with some kind of (oscillatory) zoning and that reaction rims (but not the baddeleyite) are CL bright.

4.1.10 ZrBd-10

This experiment was executed contemporaneously with ZrBd-09. Contents of the capsule were: Varberg zircon (7.99 mg), H_2O (5.89 mg) and $Ca(OH)_2$ (2.92 mg). This sample resembles many similarities with ZrBd-09 under SEM-BSE (Appendix 3), but in general this sample is more extensively reacted. Nearly all of the grains have been partially or near completely dissolved and partially altered to baddeleyite, only a few grains lack baddeleyite. Baddeleyite occurs as blobs, sometimes clustered together to form bands or other shapes of varying coherence. In a few cases several baddeleyite bands are found at different distance from the edge in the same grain. In a few of the grains con-

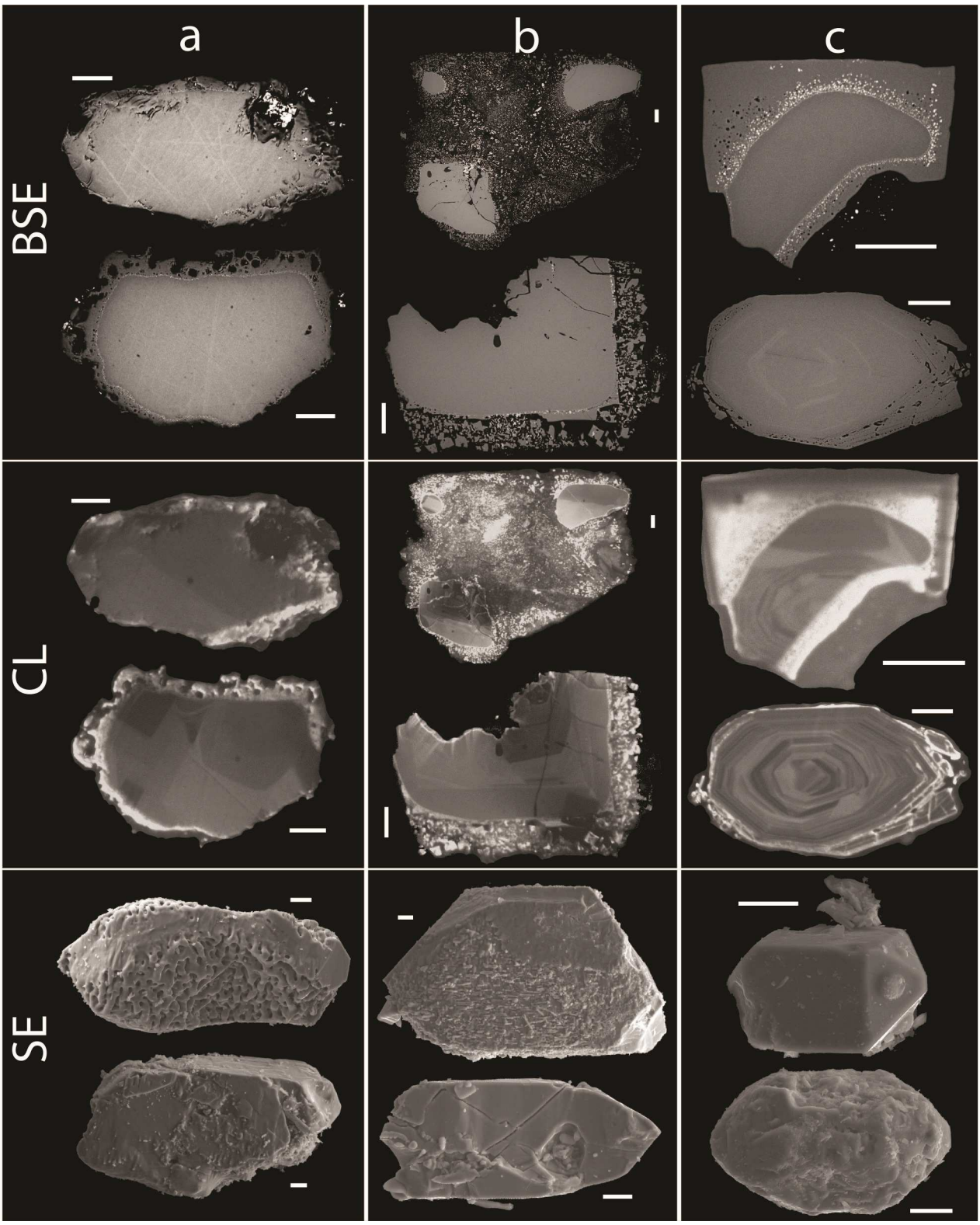

Fig. 5. SEM images of zircon grains from baddeleyite producing experimental runs. All scale bars are 20 µm. BSE and CL images are in cross-section, SE images from surface imaging. A) ZrBd-09, b) ZrBd-17 and c) ZrBd-18 are conducted at 900 °C and 1,000 MPa. The reaction rim consists of porous zircon, separated from the unaltered core by a thin band of baddeleyite blobs. Baddeleyite is also appearing as larger clusters. CL imaging shows that reacted zircon rims partially are CL bright. Surface imaging shows signs of dissolution (rounding, rough surfaces, dissolution pits and surface porosity), and the presence of a needle shaped phase other than zircon that is giving a furry impression.

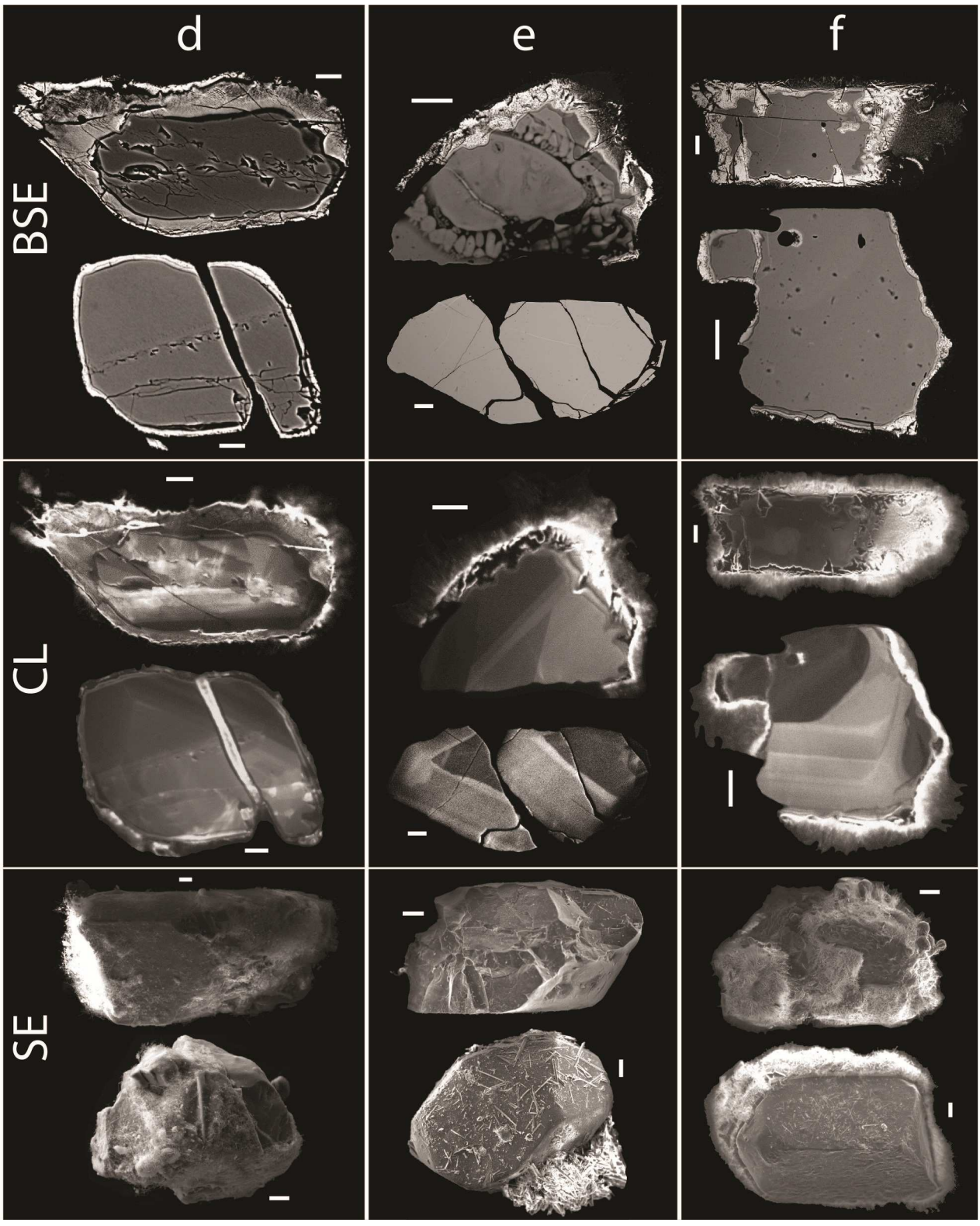

D) ZrBd-14, e) ZrBd-19 and f) ZrBd-20 are conducted at 600 °C and ~400 MPa. The reaction rim consists of one or several bands of varying baddeleyite content, baddeleyite is seemingly most abundant in the outer rim parts (brightest in BSE).

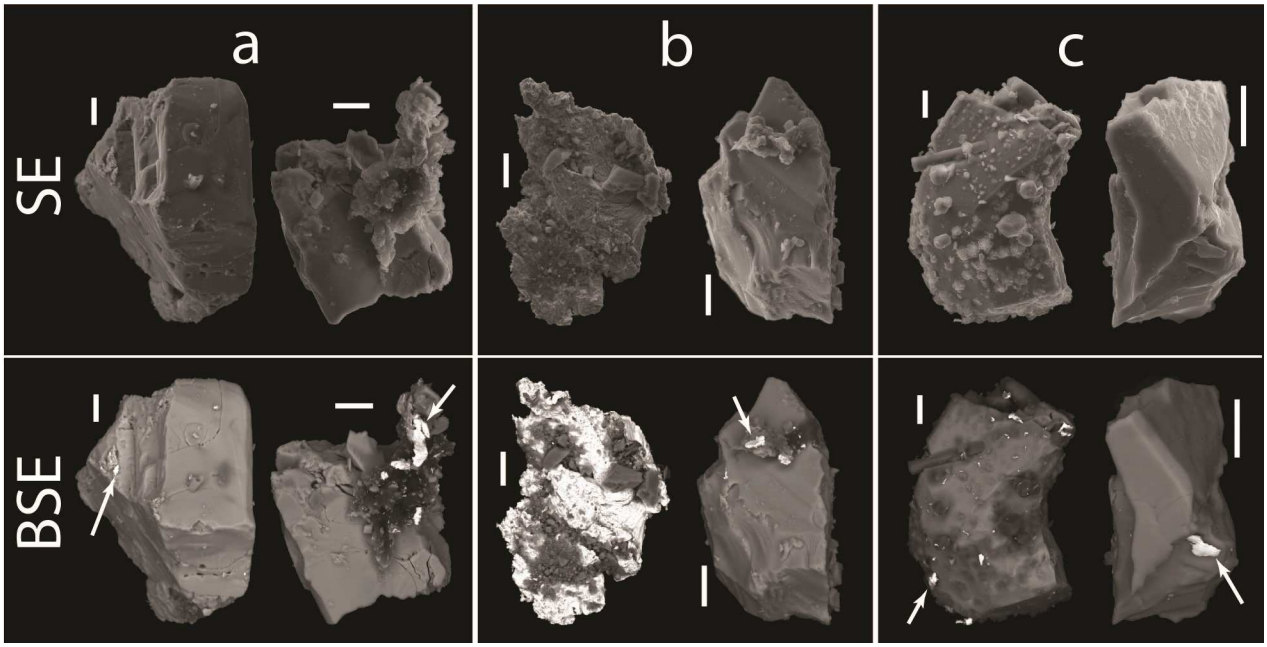

Fig. 6. Surface SEM images of zircon from experiments that only produced baddeleyite on grains surfaces. All scale bars are 20 µm. Baddeleyite appears as white in BSE and is marked with white arrows. A) ZrBd-11, b) ZrBd-12 (900 °C, 1,000 MPa) and c) ZrBd-15 (600 °C, 440 MPa).

taining inclusions, baddeleyite has formed at the boundary between the inclusion and the interior of the zircon grain. Surface and CL imaging show no difference compared to ZrBd-09.

4.1.11 ZrBd-11

This experiment was executed contemporaneously with ZrBd-09 and 10. Capsule contents were: Varberg zircon (7.40 mg), H_2O (4.23 mg), $CaCl_2$ (3.24 mg) and SiO_2 (0.97 mg). Under BSE, in cross-section, all grains appear in homogeneous BSE brightness and most of the grains show the uneven surface appearance described above. CL confirms that zoning is scarce and rather faint where it occurs. Some grains show CL-bright rims. Surface imaging (SE and BSE) show rounded grains, small amounts of porosity and baddeleyite blobs ranging from 1 to 10 µm in size (Fig. 6a and Appendix 3).

4.1.12 ZrBd-12

This experiment was executed contemporaneously with ZrBd-09, 10 and 11. The capsule contained: Varberg zircon (7.39 mg), H_2O (5.48 mg), $CaCl_2$ (2.92 mg) and SiO_2. BSE and CL images show little difference from ZrBd-11 with exception that some grains in this sample have been partially dissolved. Grains with CL bright rims are more abundant in this sample. Surface imaging (SE and BSE) is also showing similarities to ZrBd-11, but baddeleyite domains are generally larger, a few grain surfaces are almost completely altered to baddeleyite (Fig. 6b and Appendix 3).

4.1.13 ZrBd-13

This experiment was executed at 600 °C and 440 MPa using the hydrothermal autoclave apparatus. The experiment was left running for 240 h. Capsule contents were Varberg zircon (8.13 mg), H_2O (4.59 mg), $Ca(OH)_2$ (3.42 mg) and SiO_2 (1.71 mg). Cross-section BSE imaging reveals that some grains partially show the appearance of an uneven surface, that inclusions are abundant and that nearly all grains show almost completely homogenous BSE brightness (Appendix 3). On the contrary, CL shows that most of the grains have rather distinct oscillatory zoning. Surface imaging (SE) shows surface porosity in about half of the examined grains and that most grains are rounded. Additionally an abundant needle shaped phase is observed, either emplaced on the surface of zircon grains or as stack-like heaps.

4.1.14 ZrBd-14

This experiment was conducted contemporaneously with ZrBd-13. Capsule contents were: Varberg zircon (8.73 mg), H_2O (4.29 mg) and $Ca(OH)_2$ (1.54 mg). A few grains are seemingly unreacted, but most grains show some sort of reaction. The most common feature in cross-section is a banded texture where baddeleyite occupies the outermost band, separated from the unreacted zircon centre by a thin BSE black band (Fig. 5d and Appendix 3). The thickness of these bands are varying, where the grains showing the thickest reaction rims also show an additional light grey band between the baddeleyite and black bands. High magnification imaging of the thickest reaction rims show that the baddeleyite and light grey bands are spongy and contain black inclusions, resembling a stromatolite-

like texture. CL reveals that the areas located within reaction rims show oscillatory zoning and that the reaction rims (but not the baddeleyite) are CL bright. Surface imaging (SE and BSE) show that most grains are rounded and show other dissolution textures (porosity, preferential dissolution, etc.), baddeleyite blobs (1-20 μm). A needle shaped, than zircon BSE darker, phase is also observed.

4.1.15 ZrBd-15

This experiment was run contemporaneously with ZrBd-13 and 14. The capsule contained: Varberg zircon (7.21 mg), H_2O (3.87 mg), $CaCl_2$ (1.31 mg) and SiO_2 (1.18 mg). BSE and CL imaging shows no difference in cross-section, compared with ZrBd-13. Surface imaging (SE and BSE) is also showing little difference, with the exception for a few cases of small (< 5 μm) blob-like baddeleyite domains (Fig. 6c and Appendix 3).

4.1.16 ZrBd-16

This experiment was executed contemporaneously with ZrBd-13, 14 and 15. Capsule contents were Varberg zircon (5.73 mg), H_2O (6.36 mg) and $CaCl_2$ (2.71 mg). Cross-section BSE and CL show no difference compared to ZrBd-13 (Appendix 3). Surface imaging (SE) shows almost no difference, with the exception that the needle shaped phase is much less abundant.

4.1.17 ZrBd-17

This experiment was conducted at 900 °C and 1,000 MPa and run for 96 h using the piston cylinder apparatus, and was considered as mechanically perfect. The contents of the capsule were: Önnestad zircon (8.72 mg), H_2O (4.30 mg), SiO_2 (1.61 mg) and $Ca(OH)_2$ (1.57 mg). BSE imaging (Fig. 5b and Appendix 3) show that reaction intensity is varying from grains that are unreacted to grains that are partially or near completely dissolved. In a majority of the grains the zircon has partially been altered to baddeleyite, appearing as small blobs, mostly preferably distributed in bands following the reaction front but also scattered throughout the reaction rim or concentrated to cracks and pores in the otherwise unreacted grain centre. Reaction rims are highly porous. The unreacted grain centres show homogenous BSE brightness. CL imaging shows oscillatory zoning in most grains, but also a few grains that lack zoning, as well as that reaction rims (but not the baddeleyite) are CL bright. Surface imaging (SE and BSE) shows that most grains are rounded and porous. Other surface textures are e.g. a grain where almost the whole grain surface shows an intricate pattern of semi-concordant needles. A few examples of small (< 5 μm) blob-like baddeleyite domains are also observed.

4.1.18 ZrBd-18

This experiment was executed simultaneously with ZrBd-17. The capsule contained: ASGH007A zircon (4.00 mg), SiO_2 (1.45 mg), H_2O (1.40 mg) and $Ca(OH)_2$ (1.31 mg). Under BSE (Fig. 5c and Appendix 3) most grains show a reacted appearance, although a small number of seemingly unreacted grains are present. Most reacted grains are to a varying extent partially dissolved. In a majority of the grains baddeleyite is present as small blobs; oriented in continuous bands, scattered throughout the reaction rim, concentrated along cracks or pores in the otherwise unreacted grain interior, or as in a few cases scattered through the grain interior without any preferred orientation. Most of the grains show a highly porous reaction rim, but a few baddeleyite containing grains show no reaction rim at all. Under CL most grains show oscillatory zoning as well as CL bright reaction rims, also in grains where no baddeleyite is observed. The baddeleyite itself have approximately the same CL brightness as the unreacted zircon cores. Surface imaging (SE and BSE) shows that most grains are rounded and show other dissolution textures such as surface porosity. A few examples of small (~1 μm) blob-like baddeleyite domains are also observed.

4.1.19 ZrBd-19

This experiment was conducted at 600 °C and 420 MPa and run for 50 days using the hydrothermal autoclave apparatus. The contents of the capsule were: Varberg zircon (7.10 mg), H_2O (3.98 mg), SiO_2 (1.41 mg) and $Ca(OH)_2$ (1.70 mg). Most grains show little signs of reaction. Signs of reaction are: most grains are somewhat rounded and have thin (< 1 μm) BSE bright irregular lines where both ends are located to grain edges (Fig. 5e and Appendix 3). A few grains are heavily reacted and partially altered to baddeleyite. Baddeleyite is found as a highly porous BSE white outer rim, followed (inwards) by a thin BSE light grey band and a BSE dark grey band before reaching the BSE grey unreacted zircon. Baddeleyite rims are varying in thickness between 1 and 20 μm. Surface imaging (SE and BSE) shows that most grains are rounded and that dissolution pits are common on most surfaces. A fibrous BSE darker phase is present on the surface of almost all grains, appearing as heaps of needles covering the surface to varying degree. CL imaging shows that most grains are oscillatory zoned and that reaction rims are CL bright (except for baddeleyite rich parts that are CL dark).

4.1.20 ZrBd-20

This experiment was run contemporaneously with ZrBd-19. The contents of the capsule were: Varberg zircon (6.64 mg), H_2O (3.93 mg) and $Ca(OH)_2$ (1.78 mg). This sample is very similar to ZrBd-19 under SEM imaging (Fig. 5f and Appendix 3). In contrast all grains are partially altered to baddeleyite and the amount of baddeleyite per grain is much larger. Grains are also much more dissolved and rounded; only a few examples of euhedral zircon grains are present. In a

few grains baddeleyite appears in the grain interior, seemingly without connection to the grain edges.

4.2 Electron microprobe analyses

All EMP data is presented in Table 2, and plotted in Figure 7. Generally this data is confirming that the BSE white (in comparison with zircon) mineral is baddeleyite, showing that altered zircon rims are enriched in Ca, as well as a possible enrichment of Al in altered zircon rims. EMP element maps (Fig. 8) are showing that some larger pores in fact are filled with a Ca rich compound.

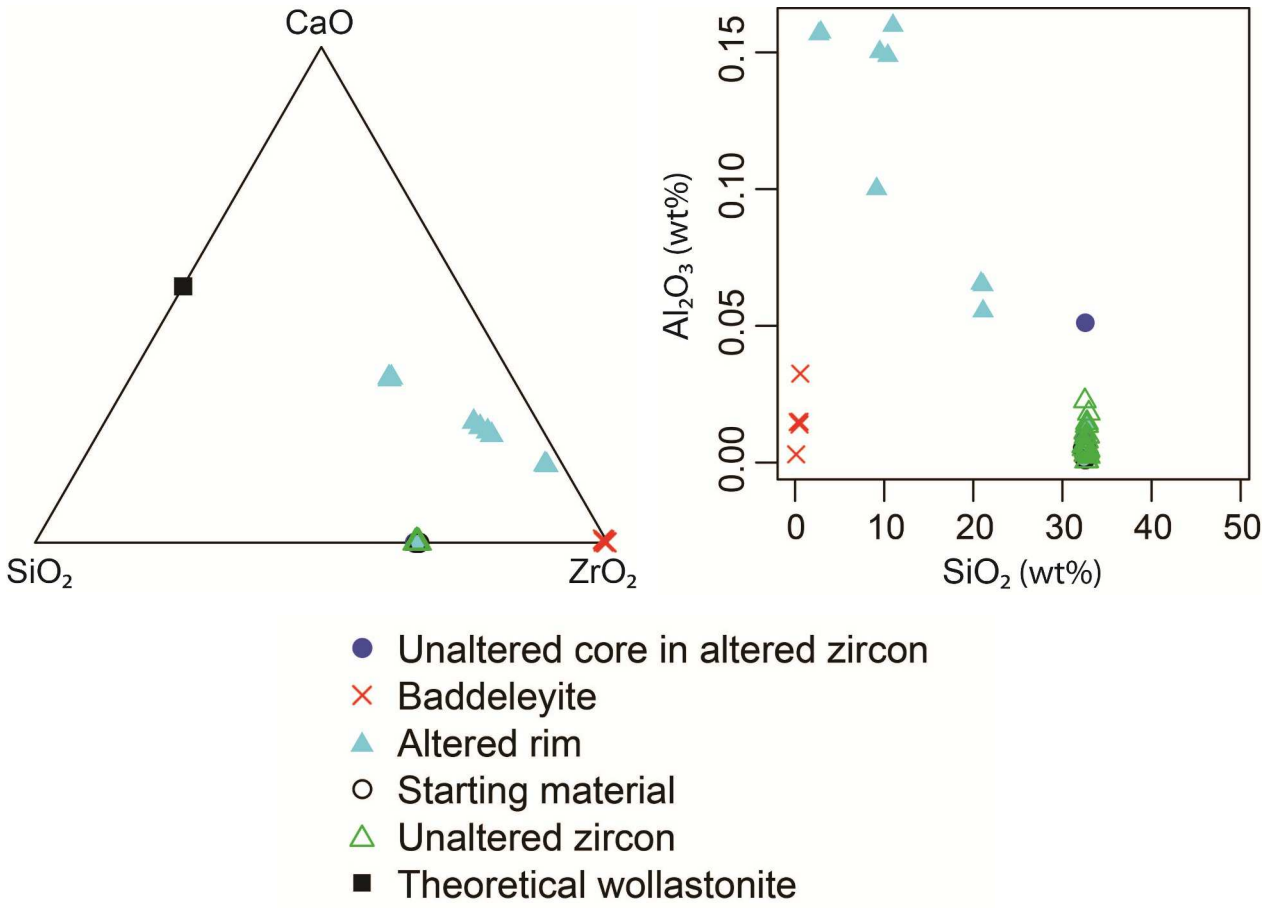

Fig. 7. ***Left:*** *Ternary Si-Ca-Zr plot of EMP data (Table 2) from experimental products from experiments using the Varberg zircon starting material. Note that a number of altered rims are plotting on a trajectory between the baddeleyite apex and a theoretical wollastonite point. Analyses from unaltered cores from altered zircons, as well as zircon analyses from experiments that did not produce any alteration, are plotting together with the starting material.*

Right: *Plot of Al_2O_3 vs. SiO_2 using the same data as in the previous plot, possibly indicating Al enrichment with decreasing Si-content (increasing alteration).*

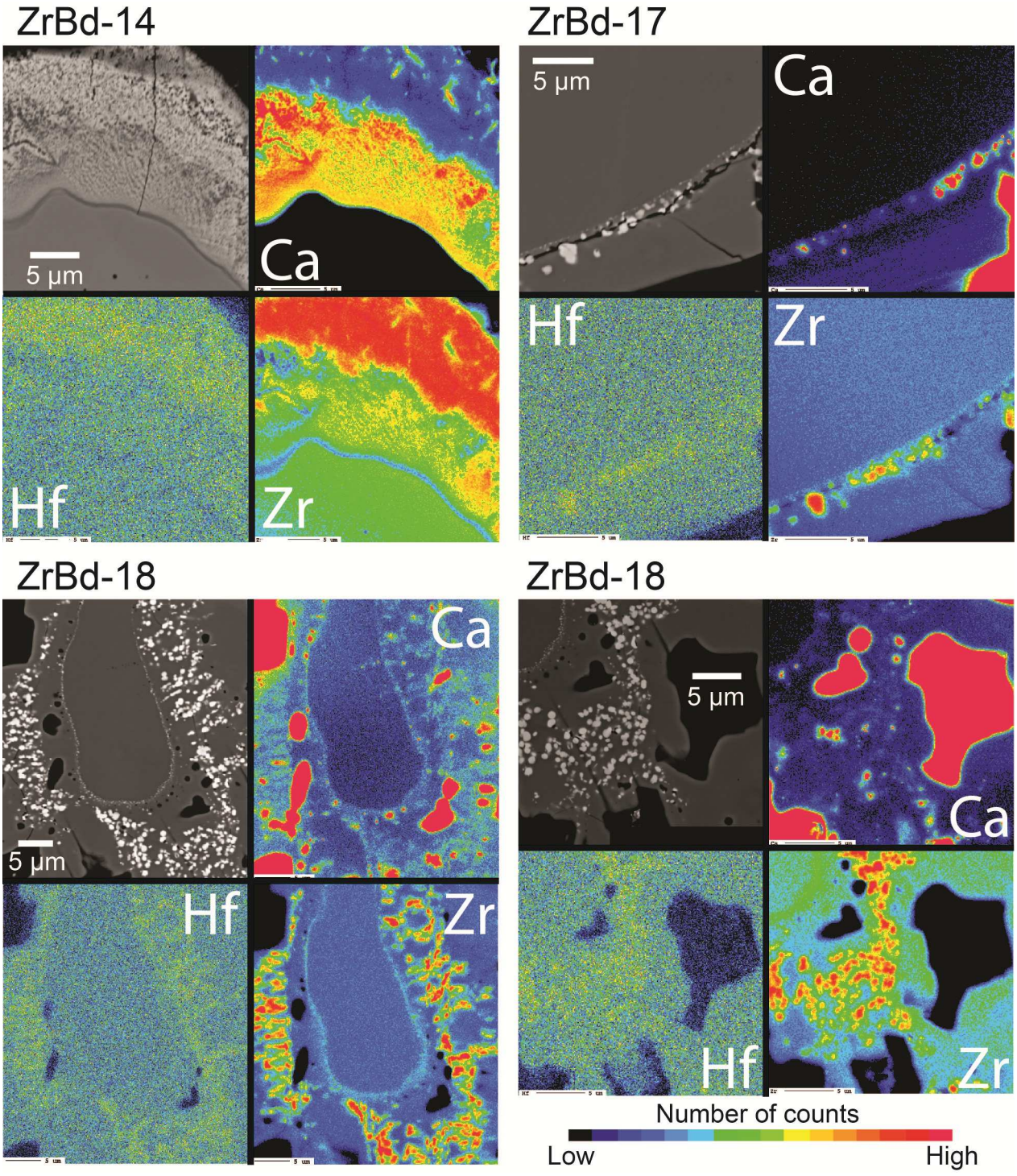

Fig. 8. EMP element maps of parts of zircon grains from ZrBd-14, 17 and 18. The bottom right set of maps are partially overlapping the bottom right corner of the bottom left set of maps. In the upper left set of maps it is notable that within the reaction rim Zr seemingly is low where Ca is high. In the bottom two sets of maps it is also noteworthy that what appears as pores (BSE black) show high Ca content, suggesting that these pores are filled with a phase other than zircon.

Table 2. Electron micro probe analyses of starting materials and experiment products. All element data is given in mass percent. Empty cell = below detection limit. Nb and Na are excluded (below d.l.). Analyses that are close to or at the d.l. are marked with italics and should be interpreted with caution.

Experiment	Comment	Fluid	P_2O_5	SiO_2	TiO_2	ZrO_2	HfO_2	ThO_2	UO_2	Al_2O_3	Y_2O_3	Ce_2O_3	Pr_2O_3	Nd_2O_3	Sm_2O_3	Gd_2O_3	Dy_2O_3	Ho_2O_3	Yb_2O_3	Lu_2O_3	CaO	MnO	FeO	PbO	Σ mass %	Σ cat ions
ZrBd-ÖP	Core		0.07	32.76	0.07	65.00	1.39	*0.01*	0.04			*0.02*	*0.01*	*0.05*	*0.05*		0.08				*0.01*	*0.01*	0.05		**99.62**	**8.004**
	Rim		0.04	32.03	*0.01*	63.86	1.61	*0.01*	0.05				*0.03*				*0.07*		*0.04*				*0.02*		**97.77**	**8.002**
ZrBd-ÖP	Core		0.15	32.42		64.33	1.32	0.12	0.13		0.16		0.07	*0.05*	0.14		*0.05*	0.15	*0.01*	0.07	0.04	*0.02*	0.07	*0.01*	**99.32**	**8.012**
	Zone		0.09	32.54	0.08	64.47	1.30	0.04	*0.01*		0.26			*0.05*	0.09	*0.06*	*0.07*		0.06	*0.02*	0.01	*0.01*			**99.17**	**8.007**
	Zone		0.06	32.49	*0.01*	65.18	0.82	0.02			0.06				*0.03*	*0.01*	*0.04*		0.10		*0.01*		*0.02*		**98.84**	**8.003**
	Rim		0.05	32.67	0.08	65.22	1.19	*0.01*	0.07					*0.05*	0.08	0.07	*0.05*	*0.03*	*0.03*	0.08	0.02				**99.69**	**8.004**
ZrBd-ÖP	Core		0.06	32.56		65.15	0.65	*0.01*	0.04			0.05	0.12		0.07	*0.04*						*0.02*	*0.02*		**98.80**	**8.004**
ZrBd-ÖP	Core		0.07	32.32	0.05	64.47	1.69	0.03	0.14						*0.04*		*0.05*	0.08	0.07	*0.01*	0.03	0.05		0.02	**99.13**	**8.006**
	Rim		0.04	32.50		65.48	0.73	*0.01*	0.02			*0.04*	0.10	*0.02*		0.09			*0.02*	*0.04*		*0.02*	*0.02*		**99.14**	**8.005**
ZrBd-GP	Core		0.05	32.10	*0.01*	65.20	1.10	0.02	0.04			0.08		*0.02*	0.08		0.18		*0.03*		0.01				**98.92**	**8.004**
	Zone		0.12	32.54	*0.01*	65.90	1.15	0.02	0.07			0.05					0.12	*0.06*	0.12	*0.04*		*0.02*	0.07	*0.01*	**100.28**	**8.005**
	Dark zone		0.08	30.84	0.21	58.63	1.11	0.02	0.12	0.71	0.14	0.99	0.22	0.59	*0.05*	*0.03*	*0.04*		0.08	0.09	0.72	0.10	0.73	0.03	**95.53**	**8.147**
	Rim		0.10	32.12		64.91	1.03		*0.01*		*0.01*	*0.02*	*0.05*			*0.02*	*0.05*	*0.05*	0.08		0.02		*0.03*		**98.49**	**8.003**
ZrBd-GP	Core		0.08	32.57		65.59	1.05	0.02							*0.05*	*0.03*						*0.02*	0.05		**99.46**	**8.002**
	Zone		0.05	32.51		65.45	0.83		0.03			*0.02*	0.16	*0.01*	0.10	0.09					*0.01*	*0.01*	*0.02*		**99.27**	**8.005**
	Zone		0.07	32.44	*0.01*	65.26	1.51	0.02	0.05				0.16	0.14	0.14			*0.04*					0.07		**99.92**	**8.007**
ZrBd-GP	Core		0.13	32.38		66.17	1.18	*0.01*		*0.01*					*0.01*						*0.01*				**99.89**	**7.998**
	Zone		0.05	32.72	0.03	66.12	1.58		0.03	*0.01*					0.09	*0.01*	0.21		0.08		*0.01*		*0.02*		**100.95**	**8.004**
	Zone		0.07	32.40	*0.01*	65.89	1.01			*0.01*					0.11		*0.07*			*0.01*	0.02	*0.02*	0.04		**99.65**	**8.005**
	Zone		0.09	32.32	*0.02*	65.80	1.07		*0.02*			0.08		0.09	*0.04*	0.08			*0.02*	0.11	*0.01*	*0.01*	0.05		**99.81**	**8.006**
ZrBd-GP	Core		0.08	32.49		66.09	1.19					*0.01*					*0.01*	*0.04*	0.06				0.03	*0.01*	**100.02**	**8.002**
	Zone		0.05	32.40	*0.01*	65.43	1.48		*0.02*			0.06	*0.02*	*0.04*	0.09		*0.06*	0.11		0.09		*0.03*	*0.02*	0.03	**99.92**	**8.007**
	Zone		0.11	32.55	*0.01*	65.95	1.49			*0.01*							*0.04*		0.08		0.01		*0.01*		**100.26**	**8.000**
ZrBd-P	Core		0.07	32.70		65.68	0.98					0.05		0.07		*0.01*			0.09	*0.01*	0.02	*0.02*	*0.02*		**99.72**	**8.004**
	Rim		0.06	32.56	0.04	65.20	1.71	*0.01*	0.08				*0.03*		0.15	0.17							*0.01*	*0.01*	**100.04**	**8.003**
ZrBd-P	Core		0.06	32.43	*0.02*	65.85	0.67		0.04				*0.01*	*0.04*					0.07	*0.03*	0.02	*0.02*	0.05	0.04	**99.35**	**8.006**
	Core		0.07	32.85	*0.02*	65.78	1.20		*0.01*					*0.05*					*0.03*	*0.03*	0.01		0.04		**100.10**	**8.003**
	Zone		0.04	32.54	*0.01*	65.26	1.40	*0.01*				*0.01*	*0.01*								*0.01*	0.04	0.03		**99.36**	**8.003**
	Rim		0.05	32.21	0.04	64.86	1.85	0.02	0.05	*0.01*		0.08			*0.05*			*0.04*	0.10			0.03	*0.02*	0.03	**99.44**	**8.005**
ZrBd-P	Core		0.05	32.40	*0.03*	66.06	1.04	*0.01*	0.14						*0.04*	*0.04*				*0.01*	0.02				**99.84**	**8.002**
	Rim		0.05	32.54	*0.03*	66.27	0.99						0.07						*0.04*	*0.02*			0.04		**100.05**	**8.003**
ZrBd-P	Core		0.08	32.65	0.07	65.99	1.15	0.02					0.07	0.10			*0.02*		0.06		*0.01*				**100.23**	**8.002**
ZrBd-P	Core		0.06	32.51	0.07	65.66	0.71					*0.02*		*0.02*		0.09			0.09	*0.03*		*0.02*			**99.29**	**8.001**
ZrBd-01	Inner core	$Ca(OH)_2$	0.10	32.39		65.21	1.13	0.04	0.09		0.06			*0.05*					0.07	*0.01*		0.05			**99.18**	**8.003**
	Outer core		0.06	32.41		65.58	1.18					0.05				*0.01*	*0.01*	*0.03*	*0.02*		*0.01*	*0.02*			**99.37**	**8.000**
	Unaltered rim		0.04	32.55	0.09	65.81	1.00	*0.01*	0.08			*0.01*			0.07	*0.07*		0.18		*0.02*	0.02		*0.02*	*0.01*	**99.96**	**8.005**
ZrBd-01	Core	$Ca(OH)_2$	0.06	32.61	*0.02*	65.59	0.96	*0.01*		*0.01*				*0.01*	0.09	*0.03*		*0.03*		0.06					**99.49**	**8.002**
	Unaltered rim		0.05	32.34	0.10	64.83	1.78		0.13	*0.01*		*0.02*	0.08		0.09		0.14					*0.01*			**99.59**	**8.004**

Table 2. (continued)

Experiment	Comment	Fluid	P_2O_5	SiO_2	TiO_2	ZrO_2	HfO_2	ThO_2	UO_2	Al_2O_3	Y_2O_3	Ce_2O_3	Pr_2O_3	Nd_2O_3	Sm_2O_3	Gd_2O_3	Dy_2O_3	Ho_2O_3	Yb_2O_3	Lu_2O_3	CaO	MnO	FeO	PbO	Σ mass %	Σ cat ions
ZrBd-02	Core	$Ca(OH)_2$	0.05	32.63	0.04	65.99	1.04							*0.06*	*0.06*		*0.02*				0.01	*0.01*			**99.92**	**8.002**
	Unaltered rim		0.04	32.55	0.06	65.32	1.32	*0.01*		*0.01*			*0.03*			*0.07*	*0.07*			0.06	0.03			**99.55**	**8.003**
ZrBd-02	Core	$Ca(OH)_2$	0.05	32.61	*0.01*	65.79	0.86	*0.01*				*0.03*		0.16	0.08	0.10		*0.07*		0.13			*0.01*		**99.91**	**8.005**
	Unaltered rim		0.03	32.79	0.05	64.94	2.07	*0.01*		*0.01*		*0.02*		0.09	0.08		*0.05*	0.10	*0.02*		0.01	0.04	*0.01*		**100.34**	**8.007**
ZrBd-03	Inne core	$CaCl_2$	0.07	32.55	0.05	65.38	1.14	0.02	0.07		0.23	*0.02*	*0.04*		*0.02*		0.10	*0.02*	0.18		0.02	*0.02*	*0.01*		**99.94**	**8.009**
	Outer core		0.07	32.35	*0.03*	66.09	0.91							*0.04*			*0.03*							0.03	**99.54**	**7.999**
	Unaltered rim		0.06	32.54	*0.02*	65.45	2.11	0.02	0.05	*0.01*		*0.01*	*0.04*		*0.06*	0.15					0.01	*0.03*	0.03		**100.60**	**8.006**
ZrBd-03	Inne core	$CaCl_2$	0.06	32.74		65.38	1.47	0.02	0.03		0.13		*0.06*	*0.02*		0.09			*0.02*	*0.01*					**100.04**	**8.002**
	Outer core		0.05	32.59		65.97	0.60	*0.01*		*0.01*		*0.01*	*0.04*						*0.04*		0.02				**99.33**	**8.001**
	Unaltered rim		0.04	32.68	*0.03*	65.60	1.32		*0.02*			*0.01*			0.07	*0.02*						*0.01*			**99.81**	**8.001**
ZrBd-04	Core	$CaCl_2$	0.05	32.64	*0.03*	65.23	1.55		*0.01*			*0.02*	*0.05*			*0.07*	*0.05*		*0.02*		0.01				**99.74**	**8.002**
	Unaltered rim		0.05	32.79	0.05	65.34	1.64		0.07				0.08		*0.03*		0.09	0.13	0.06	0.05		*0.01*		0.05	**100.43**	**8.004**
	Unaltered rim		0.03	32.79		65.57	1.52	0.02	0.12				*0.06*	0.13		0.24	0.08		*0.04*		0.02	0.04	*0.02*		**100.69**	**8.009**
ZrBd-04	Core	$CaCl_2$	0.06	32.64		66.00	1.02		*0.01*			*0.03*	0.11					0.09	*0.04*	*0.01*	*0.01*	0.05			**100.05**	**8.005**
	Unaltered rim		0.05	32.96	*0.03*	66.28	1.15			0.02				*0.05*		*0.07*	*0.07*	0.24	0.06		0.03		*0.03*		**101.05**	**8.008**
	Unaltered rim		0.08	32.62	*0.02*	65.80	1.45					0.07	*0.02*		0.11	*0.03*	*0.07*				0.01	*0.01*	0.07		**100.36**	**8.006**
ZrBd-05	Core	$CaCl_2$	0.04	32.84		65.91	1.42	0.02	*0.02*			0.07		0.08		0.15			0.05	*0.01*		0.03	*0.03*	*0.01*	**100.69**	**8.007**
	Core		0.10	32.88	0.06	65.37	2.01		0.10					0.15	0.10	0.14	*0.05*	*0.03*	0.08	*0.01*	0.02		*0.02*		**101.12**	**8.006**
	Core		0.03	32.85	*0.02*	65.61	1.90	*0.01*	*0.02*						*0.05*	*0.06*	0.11			*0.02*	0.01	*0.01*			**100.70**	**8.003**
	Unaltered rim		0.09	32.82	0.08	66.24	0.97					0.08		0.10			0.16	*0.07*			0.07				**100.69**	**8.006**
ZrBd-05	Core	$CaCl_2$	0.05	32.95		66.01	0.73			*0.01*		*0.01*		0.17	0.11	*0.02*	*0.06*	0.15			0.02	*0.01*			**100.30**	**8.007**
	Unaltered rim		0.05	32.73		65.20	1.88		0.06	*0.01*			*0.02*	0.07	*0.05*	*0.07*		*0.04*							**100.18**	**8.002**
	Unaltered rim		0.06	32.68	*0.03*	65.59	1.45		0.04	*0.01*		0.08				*0.04*	*0.05*	*0.03*	*0.01*	0.11					**100.20**	**8.003**
	Unaltered rim		0.03	32.61	*0.02*	65.26	1.99							*0.03*			*0.02*	*0.04*		0.08	*0.01*				**100.10**	**8.002**
ZrBd-06	Core	$CaCl_2$	0.09	32.52		64.93	1.49	0.03	0.06	0.02	0.18		0.08			*0.07*		*0.04*	0.05	0.06	0.02	*0.02*	*0.01*	0.03	**99.71**	**8.007**
	Unaltered rim		0.06	32.72	0.07	65.98	1.34	*0.01*		*0.01*			*0.02*	0.07	*0.05*	0.08	*0.06*	*0.04*			0.02				**100.55**	**8.005**
ZrBd-06	Core	$CaCl_2$	0.06	32.56		65.99	0.88	*0.01*	*0.01*				0.16		*0.02*				*0.03*	*0.01*			0.05		**99.77**	**8.003**
	Unaltered rim		0.09	32.61		65.93	1.10	*0.01*	*0.01*					*0.04*				*0.04*		*0.01*		0.06	*0.03*	*0.01*	**99.95**	**8.003**
ZrBd-07	Core	$Ca(OH)_2$	0.07	32.81		66.34	1.53										*0.05*	*0.07*							**100.88**	**8.000**
	Unaltered rim		0.07	32.67		65.65	1.22	*0.01*	0.03				*0.03*			*0.04*				0.09	0.01	0.03	*0.01*		**99.86**	**8.002**
ZrBd-07	Core	$Ca(OH)_2$	0.07	32.96	0.07	66.04	1.44		0.04			0.05	*0.04*				0.14		0.06	*0.03*	0.03	*0.02*	0.05		**101.05**	**8.007**
	Core		0.12	32.76	0.08	65.72	1.54			*0.01*			*0.06*	0.09	*0.06*	*0.06*	*0.01*	*0.02*	*0.01*		0.23		*0.02*		**100.79**	**8.017**
	Core		0.06	32.72		65.96	0.64					*0.01*		*0.04*		*0.05*	0.08	*0.03*		0.06	*0.01*				**99.64**	**8.001**
ZrBd-08	Core	$Ca(OH)_2$	0.03	32.71	*0.02*	66.12	1.08		*0.01*				*0.02*				*0.04*			*0.03*			*0.01*		**100.07**	**8.000**
	Core		0.03	32.78	*0.03*	65.95	1.47		0.07						0.10	*0.01*		*0.05*		*0.05*	*0.01*	0.03			**100.58**	**8.003**
	Unaltered rim		0.09	32.37	0.07	64.96	1.21	0.02	*0.02*	*0.01*						*0.04*		0.12				0.04	0.03		**98.99**	**8.004**
ZrBd-08	Core	$Ca(OH)_2$	0.07	32.73	0.06	65.15	1.28	0.02	0.04		0.05			0.11			*0.06*	0.20	*0.03*	*0.01*			0.10		**99.92**	**8.009**
	Core		0.04	32.62		64.96	1.60	0.03	0.15		*0.01*		0.07	0.10	0.13				*0.03*	0.06	0.01	0.04		0.03	**99.89**	**8.007**

Table 2. (continued)

Experiment	Comment	Fluid	P_2O_5	SiO_2	TiO_2	ZrO_2	HfO_2	ThO_2	UO_2	Al_2O_3	Y_2O_3	Ce_2O_3	Pr_2O_3	Nd_2O_3	Sm_2O_3	Gd_2O_3	Dy_2O_3	Ho_2O_3	Yb_2O_3	Lu_2O_3	CaO	MnO	FeO	PbO	Σ mass %	Σ cat ions
ZrBd-13	Core	$Ca(OH)_2$	0.10	32.85		65.68	1.22					0.13			0.16	0.11	*0.03*	*0.01*	*0.04*		0.05	*0.01*	*0.01*		**100.39**	**8.006**
	Core		0.05	32.77		65.85	1.07		0.04	*0.01*					0.08	*0.03*			0.06		0.03				**100.00**	**8.003**
ZrBd-13	Core	$Ca(OH)_2$	0.08	32.72	0.08	65.36	0.82	*0.01*							0.12			*0.02*	0.10	0.08	0.01	0.06			**99.46**	**8.005**
	Core		0.04	32.93	*0.03*	65.53	1.23	*0.01*						0.09	*0.06*	*0.06*	*0.04*	*0.03*	*0.03*	*0.04*					**100.14**	**8.003**
	Core		0.06	32.85	*0.02*	65.82	1.16	*0.01*				0.08			0.12	*0.06*	*0.04*	0.18	0.06	0.06	*0.01*				**100.53**	**8.004**
	Core		0.03	32.76	*0.03*	65.96	1.25					0.07		0.13	0.02	*0.03*	*0.02*	*0.05*			*0.01*	0.03		*0.01*	**100.39**	**8.005**
	Core		0.08	32.76	*0.03*	65.69	1.28			*0.01*		0.05	*0.01*	*0.06*		0.12	*0.06*	*0.04*			0.01	*0.01*			**100.21**	**8.004**
ZrBd-16	Core	$CaCl_2$	0.07	32.90	0.08	65.92	1.24	*0.01*	*0.01*	*0.01*	0.07			*0.03*		*0.06*		*0.02*	0.07	*0.04*		*0.01*	*0.03*		**100.56**	**8.004**
	Unaltered rim		0.07	32.62	0.06	65.08	1.57		0.03			*0.02*	*0.02*	*0.02*	*0.03*		*0.04*	*0.03*	0.06	0.05	0.06	*0.03*		0.02	**99.80**	**8.007**
ZrBd-16	Core	$CaCl_2$	0.09	32.94	0.06	66.03	1.64	0.02				0.06	*0.04*	0.12	0.08		0.09		0.05	0.08	0.01				**101.31**	**8.004**
	Unaltered rim		0.03	32.66		66.37	0.79					*0.02*		*0.06*		*0.06*	*0.01*	0.15	*0.03*		*0.01*		0.08		**100.28**	**8.008**
ZrBd-09	Baddeleyite	$Ca(OH)_2$	0.04	0.50	0.09	97.49	1.78	*0.01*	0.03	*0.01*		*0.02*	0.12		*0.02*	0.08	0.11		0.16	0.07	0.66	*0.03*			**101.23**	**8.067**
	Core		0.08	32.33	0.04	65.72	0.66						0.09	*0.02*			*0.01*	*0.06*	0.05		*0.01*				**99.07**	**8.001**
ZrBd-09	Baddeleyite	$Ca(OH)_2$	0.12	0.50	0.13	99.44	1.52	*0.01*	*0.01*	*0.01*					*0.04*	*0.01*	0.11		*0.02*		0.47		*0.01*		**102.39**	**8.040**
	Core		0.03	32.54	*0.00*	65.46	1.67	*0.01*	0.03				*0.05*			*0.07*		0.12	0.07		0.03		*0.02*		**100.10**	**8.006**
	Altered rim		0.02	32.59	*0.01*	64.65	2.14		*0.02*			0.05			0.08		0.08	0.15	*0.01*	*0.04*	0.04				**99.89**	**8.007**
ZrBd-09	Core	$Ca(OH)_2$	0.07	32.41		65.80	0.83	*0.01*							0.19		*0.05*		0.07		0.01		*0.03*		**99.47**	**8.003**
ZrBd-09	Core	$Ca(OH)_2$	0.07	32.41	0.05	65.10	0.90		0.07						*0.01*			0.08	0.14			*0.02*			**98.85**	**8.001**
	Altered rim		0.03	32.46	*0.02*	65.12	0.95	0.03	*0.01*		0.13	0.08	0.12				*0.05*		0.10	*0.03*	0.01		0.06		**99.20**	**8.009**
ZrBd-10	Baddeleyite	$Ca(OH)_2$	0.04	0.14	0.06	97.73	1.30		0.03							*0.03*	*0.02*	*0.06*	0.05		0.06				**99.52**	**8.006**
	Baddeleyite		0.04	0.12	0.09	97.89	2.07	0.03				*0.03*		*0.01*				*0.04*	*0.04*	*0.04*	0.06				**100.46**	**8.007**
	Baddeleyite		0.04	0.21	0.05	93.42	2.09		0.05								*0.05*			*0.03*	0.04	*0.01*	*0.03*		**96.02**	**8.007**
	Core		0.10	32.06		64.76	0.84	0.04	0.04		0.14		*0.05*	0.11			0.11	*0.01*	0.09		0.06		0.08		**98.51**	**8.012**
ZrBd-10	Baddeleyite	$Ca(OH)_2$	0.12	0.24	0.05	98.38	1.42		*0.01*			0.06			*0.05*	*0.06*	0.08	0.17	0.09		0.08		*0.02*		**100.83**	**8.011**
	Core		0.06	32.50	0.06	65.30	1.04	*0.01*	0.03					*0.05*	0.12		*0.01*		0.08			*0.03*			**99.29**	**8.002**
ZrBd-10	Baddeleyite	$Ca(OH)_2$	0.03	0.59	0.04	95.12	1.56			0.03		*0.02*			0.07			*0.05*		*0.01*	0.16				**97.69**	**8.018**
	Baddeleyite		0.18	0.30	*0.01*	97.83	1.33		0.09	*0.01*					*0.02*	*0.03*		0.09	*0.03*		0.50				**100.41**	**8.040**
	Core		0.03	32.50		65.41	1.19					*0.04*		*0.06*			*0.04*	0.15	*0.03*		0.03				**99.47**	**8.005**
ZrBd-10	Baddeleyite	$Ca(OH)_2$	0.33	0.22	*0.03*	97.34	1.34		0.06					0.09	*0.03*	*0.03*	0.12	*0.03*	0.08		0.12	0.04	0.05		**99.91**	**8.010**
	Core		0.06	32.43	*0.03*	65.36	1.48		0.06	*0.01*		*0.04*			*0.05*	*0.02*		*0.01*	*0.01*		0.01		*0.03*		**99.61**	**8.002**
ZrBd-11	Core	$CaCl_2$	0.04	32.60	0.05	65.50	1.41					*0.04*		*0.03*		0.20		0.10		*0.01*	0.02	*0.02*	*0.01*		**100.04**	**8.005**
ZrBd-11	Core	$CaCl_2$	0.03	32.42	*0.03*	64.96	0.99	*0.01*						*0.05*			*0.06*		0.06		*0.01*	0.04	*0.01*		**98.67**	**8.003**
ZrBd-12	Core	$CaCl_2$	0.07	32.55		65.49	0.80	*0.01*				0.11	0.07					0.12	0.09		0.01	*0.02*	*0.01*		**99.35**	**8.004**
	Altered rim		0.08	32.54		65.85	1.35					0.05		*0.05*	*0.06*	*0.03*		0.08		*0.04*	0.01				**100.14**	**8.002**
ZrBd-12	Core	$CaCl_2$	0.07	32.36		65.48	0.96	*0.01*						*0.06*		0.11		*0.02*			*0.01*				**99.08**	**8.001**

Table 2. (continued)

Experiment	Comment	Fluid	P_2O_5	SiO_2	TiO_2	ZrO_2	HfO_2	ThO_2	UO_2	Al_2O_3	Y_2O_3	Ce_2O_3	Pr_2O_3	Nd_2O_3	Sm_2O_3	Gd_2O_3	Dy_2O_3	Ho_2O_3	Yb_2O_3	Lu_2O_3	CaO	MnO	FeO	PbO	Σ mass %	Σ cat ions
ZrBd-14	Core	$Ca(OH)_2$	0.03	32.40		65.10	1.05	*0.01*	*0.01*	*0.01*			0.07			0.10	0.14	*0.01*			0.18	*0.01*	0.04		**99.15**	**8.018**
	Band		0.04	21.10	0.07	44.35	0.57			0.06				0.06		0.10	*0.01*	*0.06*	*0.02*	0.09	32.19	*0.01*	0.04		**98.76**	**10.293**
	Rim		0.03	10.99	0.12	63.20	0.87			0.16			*0.04*						0.09	*0.01*	23.91	*0.02*	0.05		**99.49**	**9.868**
ZrBd-14	Core	$Ca(OH)_2$	0.05	32.57	0.06	64.96	0.85		0.03	0.05				*0.04*	*0.06*	0.08		0.09	*0.01*	0.05	0.06		*0.02*		**98.98**	**8.009**
	Altered rim		0.04	9.50	*0.03*	66.27	0.92	*0.01*		0.15			0.07	*0.06*			*0.01*	0.08		*0.02*	21.92		0.05		**99.14**	**9.748**
	Altered rim		0.06	2.67	0.08	77.07	1.69	0.03		0.16			0.10	0.18		*0.02*	*0.01*		*0.01*	*0.01*	14.76		*0.02*		**96.87**	**9.302**
ZrBd-14	Core	$Ca(OH)_2$	0.02	32.56	*0.02*	65.32	1.44	*0.01*					0.08		0.10	0.13		*0.06*	0.06	*0.02*	0.13		*0.01*		**99.95**	**8.014**
	Core		0.06	32.66		65.57	1.23					*0.03*		*0.05*	*0.06*	*0.03*					0.11		0.06		**99.86**	**8.012**
	Band		0.04	21.10	0.10	44.33	0.88	0.02	*0.02*	0.06		*0.02*	0.16	0.14						*0.02*	32.72	*0.01*	*0.01*		**99.63**	**10.314**
	Altered rim		0.03	10.41	*0.02*	64.86	1.46			0.15				*0.04*		0.11	0.15	*0.07*	*0.01*	*0.01*	22.89	0.05	0.08	0.02	**100.36**	**9.801**
	Altered rim		0.05	2.89	0.09	77.21	1.69		0.03	0.16			0.16		0.14	*0.03*		0.08	*0.01*	0.14	15.03		0.12		**97.83**	**9.323**
ZrBd-14	Core	$Ca(OH)_2$	0.06	32.93	0.06	65.64	1.50						*0.06*		0.10	*0.06*		0.11	0.09	0.08	0.06				**100.74**	**8.007**
	Band		0.03	20.87	*0.03*	45.03	1.09			0.07		*0.04*	0.08					0.09		*0.01*	32.88		*0.01*		**100.22**	**10.318**
	Altered rim		0.05	9.15	0.06	67.10	0.89		*0.01*	0.10		*0.04*	0.07	*0.02*		*0.04*			*0.02*	*0.04*	21.14	0.04			**98.78**	**9.696**
ZrBd-15	Core	$CaCl_2$	0.07	32.38	0.06	64.33	1.32	0.02	0.04		0.21		*0.05*	*0.01*		*0.05*		*0.07*	0.09				0.04		**98.76**	**8.008**
	Altered rim		0.04	32.59	0.13	65.15	1.22		0.03	*0.01*						0.12	0.16		*0.01*			*0.01*			**99.46**	**8.003**
ZrBd-15	Core	$CaCl_2$	0.10	32.51		64.25	0.63	0.06	*0.01*		0.35	0.07		0.08	*0.05*	0.12			0.14	*0.04*	*0.01*	*0.02*		0.02	**98.45**	**8.010**
	Core		0.18	32.30	*0.03*	63.90	0.67	0.07	0.12		0.74	*0.02*	0.10			0.15	0.12	0.08	0.17			*0.01*	*0.02*		**98.69**	**8.016**
	Altered rim		0.07	32.81	*0.03*	65.29	1.17	0.02						*0.02*	0.11		*0.04*	0.11	*0.04*		*0.01*				**99.72**	**8.002**
	Altered rim		0.05	32.47	0.05	65.25	0.89	*0.01*								0.09				*0.02*	0.02	*0.02*			**98.87**	**8.001**
ZrBd-17	Baddeleyite	$Ca(OH)_2$	0.08	0.50	0.07	97.11	2.46	0.02	0.19	0.02			*0.01*		*0.05*	*0.04*			0.07		0.23	0.04			**100.87**	**8.023**
	Core		0.06	32.61	0.17	64.91	1.58	*0.01*				*0.04*				*0.02*		*0.02*	*0.01*	0.05	0.10	*0.01*			**99.57**	**8.008**
	Core		0.09	32.64	*0.01*	65.05	1.24	0.02	0.03		0.09			0.15			*0.07*		0.08		0.05	*0.01*	*0.02*		**99.54**	**8.006**
	Altered rim		0.03	32.79	0.05	65.80	1.00		0.05	*0.01*		0.07				*0.02*	*0.03*	*0.04*	*0.03*		0.06	*0.02*			**99.99**	**8.006**
ZrBd-17	Core	$Ca(OH)_2$	0.07	32.48		65.37	0.84	*0.01*	*0.01*				*0.01*			0.12	*0.06*	0.11	0.06		0.16		0.03		**99.32**	**8.014**
	Core		0.07	32.57	*0.02*	65.90	0.78		*0.01*				*0.02*	*0.02*		0.10	0.08	*0.04*			0.05	0.03	*0.01*		**99.70**	**8.006**
ZrBd-17	Core	$Ca(OH)_2$	0.11	32.61	*0.01*	65.43	0.90					0.08	*0.02*	*0.03*	*0.02*	0.09			*0.03*		0.01				**99.34**	**8.000**
	Altered rim		0.04	32.43		64.91	1.77		0.12				*0.01*				0.13	*0.01*	0.09	0.06	0.02		*0.01*	0.03	**99.64**	**8.005**
ZrBd-17	Core	$Ca(OH)_2$	0.09	32.35		64.78	1.22	0.02	*0.02*					*0.05*	0.09	*0.01*		*0.04*	0.08		0.08	*0.01*			**98.83**	**8.006**
	Core		0.06	32.60	0.04	65.52	0.89	0.03	0.03						0.12			0.16	*0.03*		0.05		*0.01*		**99.54**	**8.005**
	Altered rim		0.04	32.36	*0.03*	64.99	1.08	*0.01*	0.04	*0.01*		*0.03*		*0.05*	0.11	*0.04*	*0.04*		0.04	0.05	0.31	*0.03*		*0.01*	**99.24**	**8.024**
ZrBd-18	Bd	$Ca(OH)_2$	0.05	7.53	0.04	89.09	1.99	0.02	0.16		0.03	0.10	0.14	0.08	0.14	*0.04*		0.16	0.13	0.06	0.14				**99.92**	**8.022**
	Core			32.09	0.05	63.52	0.91	0.06	0.36	*0.01*	0.02	0.23		0.15	0.12	0.11	*0.04*		*0.01*	0.12	0.15		*0.02*		**97.97**	**8.021**
	Core		0.02	32.16	*0.02*	63.51	1.36	*0.01*	0.07		0.18	0.19	0.07	0.10	0.08	0.18		0.09	0.07	*0.01*	0.17				**98.28**	**8.022**
ZrBd-18	Core	$Ca(OH)_2$	0.07	32.17	0.06	65.13	0.93		*0.01*									*0.07*			0.12	*0.02*	0.01		**98.60**	**8.008**
	Altered rim		0.02	32.40	*0.03*	64.90	1.32		*0.02*					*0.02*			0.16				0.18	0.04	*0.03*		**99.11**	**8.018**
ZrBd-18	Core	$Ca(OH)_2$	0.04	32.29	*0.03*	64.13	1.26	*0.01*	0.07	*0.01*	0.18	0.18	0.14	0.14	*0.04*	0.13	0.23		0.12		0.18		*0.02*		**99.21**	**8.026**
ZrBd-18	Core	$Ca(OH)_2$	0.04	32.46		64.65	1.11		*0.02*					0.14	0.07		0.08	0.09	0.06	*0.04*	0.14		*0.03*		**98.92**	**8.014**
	Altered rim		0.03	31.90		63.78	1.01	0.06	0.06		0.08				*0.06*	0.11		*0.05*		0.06	0.16				**97.36**	**8.014**

Table 3. SEM-EDS analyses for ZrBd-10. Empty cell = below detection limit.

Comment	Si	Zr	Hf	Al	Ca	O	Σ mass %
Baddeleyite		85.77	1.24			30.31	117.32
Baddeleyite		87.33	0.99			30.81	119.13
Baddeleyite		84.73				29.72	114.45
Baddeleyite		86.63	1.23			30.60	118.46
Baddeleyite		91.19	1.24			32.21	124.64
Baddeleyite		77.53				27.19	104.72
Baddeleyite		86.53	1.08		0.36	30.68	118.65
Baddeleyite		89.80	1.23			31.73	122.76
Baddeleyite		85.96	1.16			30.35	117.47
Baddeleyite		90.24	1.13			31.86	123.23
Baddeleyite		86.37	1.24			30.53	118.14
Baddeleyite		88.95	1.20			31.42	121.57
Baddeleyite		85.31				29.93	115.24
Baddeleyite		86.45	1.21			30.54	118.20
Baddeleyite		86.84	1.15			30.67	118.66
Baddeleyite		80.87	1.23			28.59	110.69
Baddeleyite		84.02				29.47	113.49
Baddeleyite		85.50	1.08			30.18	116.76
Baddeleyite		83.12				29.16	112.28
Baddeleyite		87.16	1.30			30.80	119.26
Baddeleyite		81.63				28.63	110.26
Core	13.44	55.65				34.83	103.92
Core	13.47	56.00				34.98	104.45
Core	13.30	55.18				34.50	102.98
Core	13.33	55.13				34.52	102.98
Core	13.63	56.74				35.43	105.80
Core	13.83	57.25				35.84	106.92
Altered rim	7.13	42.98			16.42	29.76	96.29
Altered rim	12.14	26.22			26.90	33.76	99.02
Altered rim	8.60	39.53			19.95	31.62	99.70
Altered rim	11.66	31.90			26.30	34.96	104.82
Altered rim	10.99	31.52			24.17	33.22	99.90
Altered rim	11.89	24.80			26.87	32.98	96.54
Altered rim	9.98	30.68			22.96	31.29	94.91
Altered rim	1.27	77.17		0.42	3.30	30.19	112.35
Altered rim	11.13	30.94			24.89	33.46	100.42
Altered rim	10.34	34.99			23.08	33.27	101.68
Altered rim	10.59	27.87		0.31	24.49	31.91	95.17
$Ca(OH)_2$?					36.37	14.52	50.89
$Ca(OH)_2$?					35.66	14.24	49.90
Wollastonite	23.26				33.85	40.02	97.13
Wollastonite	23.21				33.90	39.97	97.08
Wollastonite	23.01				33.72	39.67	96.40
Wollastonite	22.31				31.73	38.08	92.12
Wollastonite	23.06				33.53	39.67	96.26
Wollastonite	22.78				33.07	39.29	95.14
Wollastonite	22.39				32.72	38.58	93.69

4.3 Energy dispersive x-ray analyses

SEM-EDS data for ZrBd-10 is presented in Table 3 and plotted in Figure 9. Analysed grain types or grain parts are: unaltered zircon cores, altered zircon rims, baddeleyite domains and reaction products other than zircon. A part from that altered rims are showing elevated Ca content, a pure Ca silicate component is also identified, showing mass percentages corresponding to wollastonite. It is important to note that analyses containing Zr are flawed (probably systematic instrument error), for unaltered zircon giving Zr values elevated by ~10 mass% compared to a theoretical zircon. Many analyses are also showing total mass percentages significantly differing from 100%. Hence, the EDS data should not and cannot be compared with the EMP data.

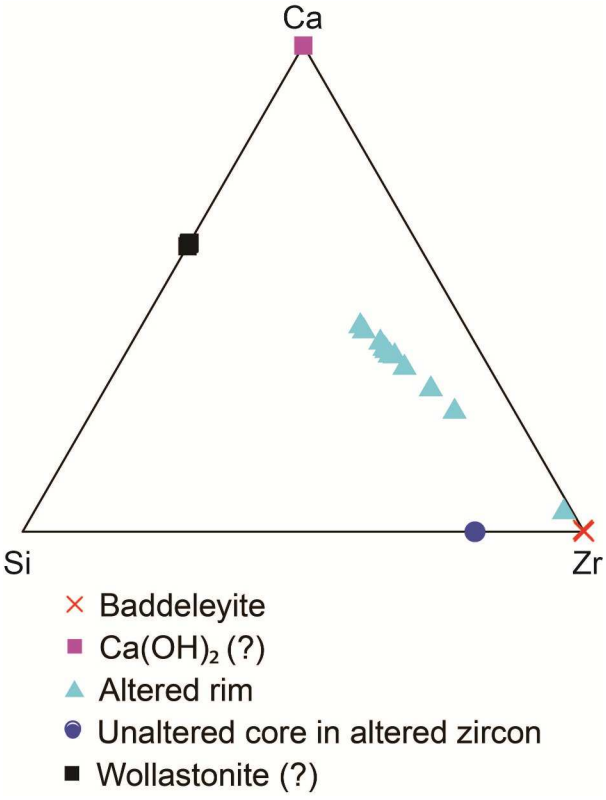

Fig. 9. Ternary Si-Ca-Zr plot based on SEM-EDS data (Table 3) from ZrBd-10. Possible wollastonite grains are found to contain only Si and Ca as major elements. Analyses of altered rims are plotting on a trajectory between the wollastonite analyses and the baddeleyite analyses. It is also noteworthy that a pure Ca phase is analysed as a reaction product, the low total wt% values of this phase could indicate high H content.

5 Discussion

5.1 Zircon-baddeleyite stability

Zircon is a robust mineral and assumed to withstand metamorphic and hydrothermal processes at most conditions, without participating in reactions or equilibrating its composition with the environment. The stability field of zircon in relation to different silica varieties is presented in Figure 10.

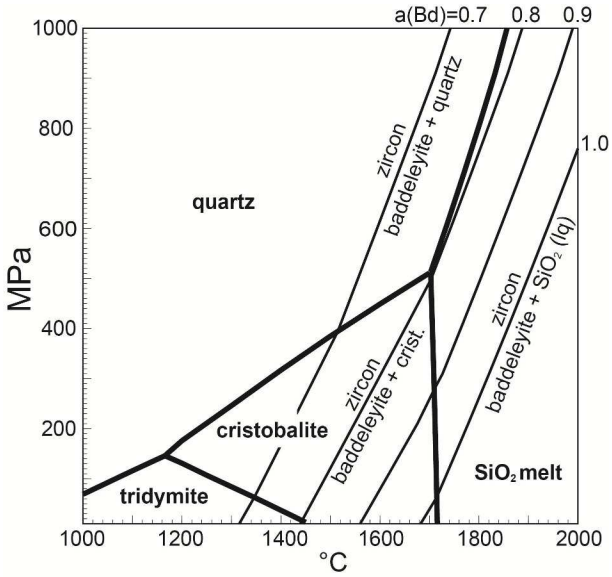

Fig 10. Phase diagram showing the stability fields of quartz and other silica phases. In addition, lines for the breakdown reaction of zircon to baddeleyite + a silica phase are drawn out for a range of baddeleyite activities ranging from 0.7 to 1. Interestingly, the conditions used in this study (380-1,000 MPa and 600-900 °C) are not even near the conditions where the observed reaction takes place in a silica saturated system. Based on thermodynamic data from Holland & Powell (1998) and constructed by Alexander Proyer (personal communication) using Thermo-Calc 3.30.

Despite the fact that zircon should not react to form baddeleyite at the P and T conditions used in this study, baddeleyite has formed. Silica activity is one parameter that would affect zircon-baddeleyite stability, where a silica activity below one would make dissolved zircon partially re-precipitate as baddeleyite. All experiments but one that were conducted at silica under-saturated conditions in this study are also showing extensive alteration of zircon to baddeleyite, supporting the previous statement. However, a number of experiments conducted at silica saturated conditions are showing the same alteration and baddeleyite formation. Hence, I would like to propose that the silica activity in the system somehow is lowered during these experiments.

It is notable that (with exception for ZrBd-20) not all grains are altered in the experiments that gave baddeleyite formation. This could be a random effect, but also a matter of reaction time or that different zircon grains have varying reactiveness, a combination of all, or other parameters. No simple explanation can be provided by the observations and data included in this study.

5.2 Model for baddeleyite formation

How can the silica activity be lowered to a(Si) < 1 in a system that initially is silica saturated? One way would be if the fluid in the system is preferentially dissolving Zr before Si, making the fluid silica under saturated, meaning that shortage in silica would make dissolved zircon to some extent re-precipitate as baddeleyite. Experimental work has showed that several salt-water solutions, e.g. NaCl and $CaCl_2$, yield decreasing quartz solubility with increasing mole fraction salt (X_{salt}) compared to pure water. For NaCl-H_2O solutions a salt -in effect is present at the lower P and T conditions used in this study, meaning that quartz solubility is enhanced at low X_{salt} (< 0.1). At X_{salt} > 0.1 quartz solubility is decreasing with increasing X_{salt}. At the higher P and T conditions used in this study no salt-in effect is observed (Newton and Manning 2000; Shmulovich et al. 2006). However, this salt-in effect is not observed for $CaCl_2$-H_2O solutions, which can be explained through solutions containing doubly charged cations (e.g. $Ca2^+$) seemingly have greater negative impact on quartz solubility than singly charged cations (e.g. Na^+), and is true for both P and T conditions used in this study (Shmulovich et al. 2006). In this study an $X_{salt} \approx 0.1$ was used, and according to Shmulovich et al. (2006) this would yield a quartz solubility just below half the one of pure water at 800 °C and 900 MPa (approximately the high P and T conditions used in this study), and just above half the one of pure water at 500 °C and 500 MPa (approximately the low P and T conditions used in this study).

Furthermore, Ryzhenko et al. (2008) have shown experimentally that several acidic and basic, salt and non-salt, aqueous solutions (e.g. NaOH) yield increased zirconium solubility with increased concentration acid or base. At $X_{NaOH} \approx 0.004$, 500 °C and 100 MPa, the zirconium solubility is about three times as high as in pure water. It should be noted that Ryzhenko et al. (2008) do not include P and T conditions comparable to this study, nor $CaCl_2$ or $Ca(OH)_2$. However, these results are not undisputed, and the zirconium solubility values are proposed to be elevated (Migdisov et al. 2011). Migdisov et al. (2011) are also proposing that zircon (not zirconium) solubility in a zircon-K-feldspar-muscovite-quartz-NaCl-KCl-HF sys -tem would decrease with increased temperature at a 100 MPa isobar, and they are also pointing out the importance of HF concentration as Zr is concluded to be transported in Zr-F-OH complexes meaning that increased HF concentration would enhance zircon solubility. However, I would still like to suggest that there is a possibility that the presence of calcium salts in a fluid is enhancing zirconium solubility.

Experiments conducted using $Ca(OH)_2$ generally result in stronger reaction than those conducted using $CaCl_2$, suggesting that $Ca(OH)_2$ would be a more potent reactant. Firstly, one should note that $Ca(OH)_2$ is a strong base and that a basic system might enhance the general rate of dissolution, implying increased reactiveness. However, no references in the literature exploring change in zircon dissolution as a function of basicity can be found to support this statement. Furthermore, according to Evans (2007) a fully dissociated salt would yield much higher negative effect on quartz solubility than a fully associated salt. It is unlikely that $CaCl_2$ would be significantly dissociated as Ca has a large charge to radius ratio (implying high ion association) and $CaCl_2$ should be regarded as fully associated at the conditions used in this study (Evans 2007). In contrast, one should be able to assume that $Ca(OH)_2$ (being a strong base) is near fully dissociated and by analogy to Evans (2007) thereby lowering the quartz solubility by at least twice as much as $CaCl_2$ does. If this is true, it would imply that a $Ca(OH)_2$ bearing fluid would more readily preferentially dissolve zirconium than a $CaCl_2$ bearing fluid.

Another way to lower the silica activity in the system would be if Si is reacting and forming complexes or compounds with Ca. Si would then be effectively immobilised, making the fluid highly silica undersaturated, significantly lowering the silica activity below one. Dissolved zirconium would then, in accordance with previous statements, partially or completely re-precipitate as baddeleyite rather than zircon. The fact that experiments run with a Ca:Si ratio << 1 (Table 1) did not produce baddeleyite supports this idea, as the Ca content in these experiments was too low to immobilise enough Si to make the fluid silica under saturated. Further support comes from the fact that a Ca silicate component is present as a reaction product (Figs. 7 & 9) and as part of altered zircon rims. Semi-quantitative SEM-EDS analyses (Table 3) of the pure Ca silicate show mass percentages for Si and Ca corresponding to those of the mineral wollastonite ($CaSiO_3$). EMP data for a number of altered zircon rims are also plotting on a trajectory between baddeleyite and a theoretical wollastonite point, indicating that the seemingly porous baddeleyite reaction rims (seen in e.g. ZrBd-14) are not porous but rather an intergrowth between baddeleyite and wollastonite. This can also be seen in the EMP element maps (Fig. 8). It is impossible to tell whether the wollastonite is forming simultaneously with the baddeleyite, or is simply filling pores created by the coupled dissolution-reprecipitation process.

As a result of the previous discussion, I would like to propose the following model for partial alteration of zircon to baddeleyite, also conceptually presented in Figure 11. Initially the system (zircon, water, silica and $Ca(OH)_2$ or $CaCl_2$) is silica saturated. Increased temperature (600-900 °C) and pressure (400-1000 MPa) give two effects; (1) reduced quartz solubility and possibly enhanced zirconium solubility, (2) complex bonding between Ca and Si implying immobilisation of Si. The system would now be effectively silica under saturated, as an effect of (1), (2) or both combined. With increased time the reaction front moves further into a zircon grain, gradually dissolving it and preferentially dissolving Zr as Si solubility is reduced by Ca ions. The dissolved material is gradually re-

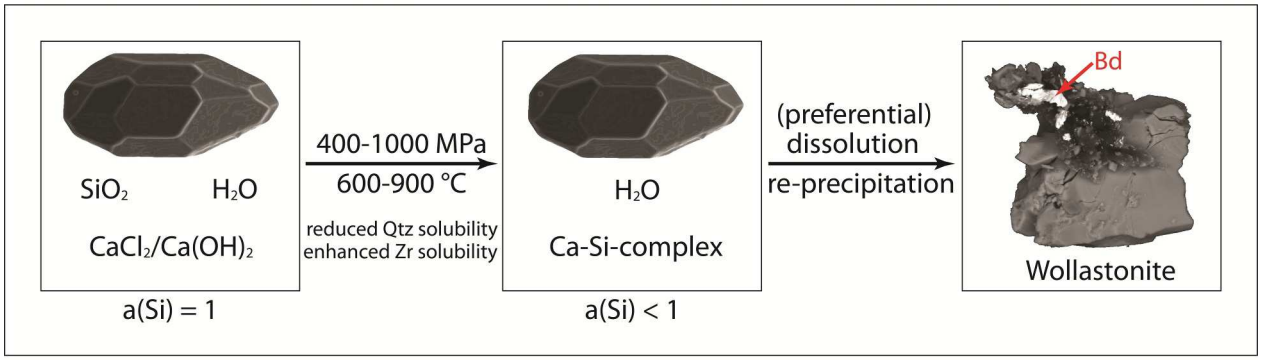

Fig. 11. A conceptual drawing of the proposed model for how alteration of zircon to baddeleyite takes place. Initially the system is silica saturated. Increased pressure and temperature reduces quartz solubility, possibly enhanced zirconium solubility and probable complex bonding between calcium and silicon, all together resulting in reduced silica activity. The process of coupled dissolution-reprecipitation will alter the zircon, now in a silica under-saturated system. Depending on how low the silica activity is, varying amounts of baddeleyite will replace the original zircon.

precipitating; as zircon if Si is available, as baddeleyite if Si is unavailable and as wollastonite if Ca is available. Depending on how much the silica activity is reduced, the result will be zircon varyingly partially altered to baddeleyite.

5.3 Geological implications

In nature, as described by Lewerentz (2010), altered zircon grains seemingly are occurring at random with respect to mineralogy. In some cases altered zircon are situated only a few µm from unaltered ones. The experiments carried out in this study are showing the same result. This suggests that the reactivity of a zircon grain is a more important factor than petrological factors in the host rock (mineralogy, textures, cracks, etc.), controlling whether a zircon grain will be altered or not.

Coupled dissolution-reprecipitation as the mechanism for metasomatic alteration of zircon is re-equilibrating the zircon chemistry with the fluid chemistry. It is reasonable to believe that a hydrothermal fluid is enriched in terms of elements such as Al, Fe, Ca and Na. These elements are non-stoichiometric in zircon and could therefore be enriched in the resulting zircon reaction rim. The reacted zircon areas are also reported being porous in comparison to unreacted areas (Geisler et al. 2007). This is also seen in the natural baddeleyite containing zircon grains from southern West Greenland (Lewerentz 2010). Reacted zircon grains from this study are showing a prominent and porous reaction rim and recrystallisation front encapsulating an unreacted core. EMP analyses show elevated values of Ca within reaction rims, and possibly indicating the same for Al. This study, constructed to mimic a hydrothermal fluid system, is showing results conforming to both other experimental studies and examples from nature. Thus, I conclude that baddeleyite intergrowths in the zircon from southern West Greenland are a result of fluid induced hydrothermal alteration (i.e. metasomatism), with coupled dissolution-reprecipitation being the underlying mechanism.

Metasomatic alteration of rocks probably took place along localised zones, i.e. where fluids could move forth. This can however not be observed in field. It is possible that macro-scale alteration textures or structures have been overprinted by later deformation and metamorphism, as the complex geological history of southern West Greenland contains numerous metamorphic events. On the micro scale, both plagioclase and K-feldspar are commonly showing signs of alteration in these rocks. One possibility is that plagioclase, being a Ca bearing mineral, during alteration released enough Ca to enable alteration of zircon to baddeleyite. However, SEM-EDS analyses of plagioclase show homogeneous An contents within all four rocks (see 1.4 Natural zircon and Appendix 1). If plagioclase was altered to some extent within the rock and that this enabled zircon alteration, it might be assumed that An contents should be more heterogeneous. Based on this I would like to suggest that an external fluid is responsible for alteration of zircon and other minerals.

Fluid chemistry is an important factor on whether baddeleyite will form or not. Ca bearing fluids are used and resulting in baddeleyite formation in this study. As Ca-Si complex bonding is proposed to be part of the model behind baddeleyite formation, it is reasonable to assume that any fluid containing an element complexing with Si could alter zircon to baddeleyite. However, such an element must also be one of the major rock forming elements to be available in quantities large enough to effectively neutralise the silica activity in a silica saturated system. Daniel E. Harlov (personal communication) has conducted experiments with zircon using the same P and T conditions as in this study, but except $Ca(OH)_2$ also used different K and Na compounds as fluids. However, only $Ca(OH)_2$ based fluids resulted in baddeleyite formation. Thus, I propose that fluids responsible for baddeleyite formation in zircon are Ca bearing.

Both zircon and baddeleyite are important minerals for U-Pb geochronology, as they incorporate U but not Pb during formation. If baddeleyite is forming due to metasomatism, this baddeleyite should also incorpo-

rate U in its structure but not Pb. Furthermore, the reacted zircon is assumed to undergo depletion of trace elements (such as Pb). CL images (Figs. 5 and 6) of zircon reaction rims are indicating depletion of trace elements. Trace element depletion can however not be detected in the EMP data, due to insufficient detection limits. EMP element maps (Fig. 8) are showing an apparent enrichment of Hf in altered zircon rims, although this is probably an effect of volume change and no real significant concentration change. In nature, metasomatically altered zircon is reported to show trace element depletion in altered areas (Rubatto et al. 2008; Soman et al. 2010). Similarly, trace element loss in reaction rims is also observed as a result of metasomatism and partial alteration of monazite (Harlov et al. 2011). Conclusively, there should be two separate possibilities to use U-Pb geochronology to date a metasomatic event, either by dating the baddeleyite or the zircon reaction rim, where total Pb-loss and U-Pb resetting is expected. The extent of e.g. Pb-loss must however be confirmed by using precise and accurate U-Pb microanalyses of e.g. experimentally altered zircon, where t=0 is well established.

6 Further studies

To confirm that metasomatically formed baddeleyite and altered zircon areas can be dated, precise and accurate U-Pb micro-analyses would be useful. Analyses of REE and other trace elements would also provide further insight in the mechanisms of the underlying processes. Lastly, TEM would give valuable nano scale information on the behaviour of the transition between altered and unaltered zircon.

7 Conclusions

- Baddeleyite intergrowths in zircon form due to metasomatic alteration (i.e. coupled dissolution -reprecipitation).
- In order to reprecipitate baddeleyite in an initially silica saturated system, the silica activity must be lowered.
- The silica activity could be lower by Ca-Si complexing and or preferential Zr dissolution.
- Ca-bearing fluids were probably responsible for the alteration of zircon to baddeleyite in the four studied silica saturated rocks from southern West Greenland.
- U-Pb dating of altered zircon areas and metasomatically formed baddeleyite should yield an age representing the time of alteration.

8 Acknowledgements

First of all I would like to thank my supervisor Dr. Anders Scherstén for valuable comments and suggestions throughout the project. None the less, my co-supervisor Dr. Daniel E. Harlov (GFZ) should also have thanks for comments, suggestions and above all for providing methodological experience in the field of experimental petrology. I would also like to thank Prof. Wilhelm Heinrich (Head of Section 3.3, GFZ) for allowing me to conduct the experimental work of this study, using machines and materials at the GFZ. Others I would like to thank are Dr. Dieter Rehde for EMP analyses, Dr. Leif Johansson for providing Önnestad and Varberg starting materials, Dr. Nicolas Norberg for help with general things at the GFZ (such as making grain mounts). In general I would also like to thank other staff, guests and students at both GFZ and Lund University for rewarding discussions and support.

9 References

Austrheim, H., Putnis, C.V., Engvik, A.K. & Putnis, A., 2008: Zircon coronas around Fe–Ti oxides: a physical reference frame for metamorphic and metasomatic reactions. *Contributions to Mineralogy and Petrology 156*, 517-527.

Beech, E. & Chadwick, B., 1980: The Malene supracrustal gneisses of northwest Buksefjorden: Their origin and significance in the Archaean crustal evolution of southern West Greenland. *Precambrian Research 11*, 329-355.

Champness, P.E., 1995: Analytical electron microscopy. *In* Potts, P.J., Bowles, J.F.W., Reed, S.J.B. & Cave, M.R. (eds.): Microprobe Techniques in the Earth Sciences. *Mineralogical Society Series 6*, 91-139. London, Chapman & Hall.

Christoffel, C.A., Connelly, J.N. & Åhäll, K.-I., 1999: Timing and characterization of recurrent pre-Sveconorwegian metamorphism and deformation in the Varberg–Halmstad region of SW Sweden. *Precambrian Research 98*, 173-195.

Coe, K., 1980: Nûk gneisses of the Buksefjorden region, southern West Greenland, and their enclaves. *Precambrian Research 11*, 357-371.

Compton, P., 1978: Rare earth evidence for the origin of the Nûk gneisses, Buksefjorden region, southern West Greenland. *Contributions to Mineralogy and Petrology 66*, 283-293.

Evans, K., 2007: Quartz solubility in salt-bearing solutions at pressures to 1 GPa and temperatures to 900°C. *Geofluids 7*, 451-467.

Friend, C.R.L., Nutman, A.P., Baadsgaard, H., Kinny, P.D. & McGregor, V.R., 1996: Timing of late Archaean terrane assembly, crustal thickening and granite emplacement in the Nuuk region, southern West Greenland. *Earth and Planetary Science Letters 142*, 353-365.

Geisler, T., 2002: Isothermal annealing of partially metamict zircon: evidence for a three-stage recovery process. *Physics and Chemistry of Minerals 29*, 420-429.

Geisler, T., Pidgeon, R.T., Kurtz, R., van Bronswijk, W. & Schliecher, H., 2003a: Experimental hydrothermal alteration of partially metamict zircon. *The American mineralogist 88*, 1496-1513.

Geisler, T., Schaltegger, U. & Tomaschek, F., 2007: Re-equilibration of zircon in aqueous fluids and melts. *Elements 3*, 43-50.

Geisler, T., Ulonska, M., Schliecher, H., Pidgeon, R.T. & van Bronswijk, W., 2001: Leaching and differential recrystallization of metamict zircon under experimental hydrothermal conditions. *Contributions to Mineralogy and Petrology 141*, 53-65.

Geisler, T., Zhang, M. & Salje, E.K.H., 2003b: Recrystallization of almost fully amorphous zircon under hydrothermal conditions: An infrared spectroscopic study. *Journal of Nuclear Materials 320*, 280-291.

Grenholm, M., 2011: Petrology of Birimian granitoids in southern Ghana - petrography and petrogenesis. *Dissertations in Geology at Lund University,* Bachelor's thesis, No. 285, 38 pp. 15 ECTS credits.

Harlov, D.E., Wirth, R. & Hetherington, C.J., 2011: Fluid-mediated partial alteration in monazite: the role of coupled dissolution–reprecipitation in element redistribution and mass transfer. *Contributions to Mineralogy and Petrology 162*, 329-348.

Holland, T.J.B. & Powell, R., 1998: An internally consistent thermodynamic data set for phases of petrological interest. *Journal of Metamorphic Geology 16*, 309-343.

Johannes, W., 1973: Eine vereinfachte Piston-Zylinder-Apparatur hoher Genauigkeit. *Neues Jahrbuch für Mineralogie Monatshefte 1973*, 337-351.

Johannes, W., Bell, P.M., Mao, H.K., Boettcher, A.L., Chipman, D.W., Hays, J.F., Newton, R.C. & Seifert, F., 1971: An interlaboratory comparison of piston-cylinder pressure calibration using the albite-breakdown reaction. *Contributions to mineralogy and petrology 32*, 24-38.

Johansson, Å., 1990: Age of the Önnestad syenite and some gneissic granites along the southern part of the Protogine Zone, southern Sweden. *In* Gower, C.F., Rivers, T., & Ryan, B. (eds.): Mid-Proterozoic Laurentia-Baltica. *Geological Association of Canada Special Paper 38*, 131-148.

Keulen, N., Scherstén, A., Schumacher, J.C., Næraa, T. & Windley, B.F., 2009: Geological observations in the southern West Greenland basement from Ameralik to Frederikshåb Isblink in 2008. *Geological Survey of Denmark and Greenland Bulletin 17*, 49-52.

Kolb, J., Dziggel, A., Koppelberg, M., Stoltz, N.B., Kisters, A.F.M. & Bergen, A., 2010: Controls of hydrothermal quartz vein mineralisation and wall rock alteration between Sermilik and Grædefjord, southern West Greenland. *Danmarks og Grønlands Geologiske Undersøgelse Rapport 2010/47*. Copenhagen, Geological Survey of Denmark and Greenland, 73 pp.

Lenting, C., Geisler, T., Gerdes, A., Kooijman, E., Scherer, E.E. & Zeh, A., 2010: The behavior of the Hf isotope system in radiation-damaged zircon during experimental hydrothermal alteration. *The American Mineralogist, 95*, 1343-1348.

Lewerentz, A., 2010: On the occurrence of baddeleyite in zircon in silica-saturated rocks. *Dissertations in Geology at Lund University*, Bachelor's thesis, No. 261, 54 pp. 15 ECTS credits.

Long, J.V.P., 1995: Microanalysis from 1950 to the 1990s. *In* Potts, P.J., Bowles, J.F.W., Reed, S.J.B., & Cave, M.R. (eds.): Microprobe Techniques in the Earth Sciences. *Mineralogical Society Series 6*, 1-48. London, Chapman & Hall.

Migdisov, A.A., Williams-Jones, A.E., van Hinsberg, V. & Salvi, S., 2011: An experimental study of the solubility of baddeleyite (ZrO_2) in fluoride-bearing solutions at elevated temperature. *Geochimica et Cosmochimica Acta 75*, 7426-7434.

Næraa, T. & Scherstén, A., 2008: New zircon ages from the Tasiusarsuaq terrane, southern West Greenland. *Geological Survey of Denmark and Greenland Bulletin 15*, 73-76.

Newton, R.C. & Manning, C.E., 2000: Quartz solubility in H_2O-NaCl and H_2O-CO_2 solutions at deep crust-upper mantle pressures and temperatures: 2-15 kbar and 500-900°C. *Geochimica et Cosmochimica Acta 64*, 2993-3005.

Nutman, A.P., Friend, C.R.L., Baadsgaard, H. & McGregor, V.R., 1989: Evolution and assembly of Archean gneiss terranes in the Godthåbsfjord region, southern West Greenland: structural, metamorphic and isotopic evidence. *Tectonics 8*, 573-589.

Nutman, A.P., Friend, C.R.L., Barker, S.L.L. & McGregor, V.R., 2004: Inventory and assessment of Palaeoarchaean gneiss terrains and detrital zircons in southern West Greenland. *Precambrian Research 135*, 281-314.

Páez, G.N., Ruiz, R., Guido, D.M., Jovic, S.M. & Schalamuk, I.B., 2011: Structurally controlled fluid flow: High-grade silver ore-shoots at Martha epithermal mine, Deseado Massif, Argentina. *Journal of Structural Geology 33*, 985-999.

Pidgeon, R.T. & Kalsbeek, F., 1978: Dating of igneous and metamorphic events in the Fiskenaesset region of southern west Greenland. *Canadian Journal of Earth Sciences 15*, 2021-2025.

Putnis, A., 2002: Mineral replacement reactions: from macroscopic observations to microscopic mechanisms. *Mineralogical Magazine 66*, 689-708.

Putnis, A., 2009: Mineral Replacement Reactions. *Reviews in Mineralogy & Geochemistry 70*, 87-124.

Putnis, A. & Austrheim, H., 2010: Fluid-induced processes: metasomatism and metamorphism. *Geofluids 10*, 254-269.

Reed, S.J.B., 1995: Electron microprobe microanalysis. *In* Potts, P.J., Bowles, J.F.W., Reed, S.J.B. & Cave, M.R. (eds.): Microprobe Techniques in the Earth Sciences. *Mineralogical Society Series 6*, 49-89. London, Chapman & Hall.

Rubatto, D., Müntener, O., Barnhoorn, A. & Gregory, C., 2008: Dissolution-reprecipitation of zircon at low-temperature, high-pressure conditions (Lanzo Massif, Italy). *The American Mineralogist 98*, 1519-1529.

Ryzhenko, B.N., Kovalenko, N.I., Prisyagina, N.I., Starshinova, N.P. & Krupskaya, V.V., 2008: Experimental determination of zirconium speciation in hydrothermal solutions. *Geochemistry International 46*, 328-339.

Schiøtte, L., Compston, W. & Bridgwater, D., 1988: Late Archaean ages for the deposition of clastic sediments belonging to the Malene supracrustals, southern West Greenland: evidence from an ion probe U-Pb zircon study. *Earth and Planetary Science Letters 87*, 45-58.

Schiøtte, L., Compston, W. & Bridgwater, D., 1989: U-Pb single-zircon age for the Tinissaq gneiss of southern West Greenland: A controversy resolved. *Chemical geology 79*, 21-30.

Schumacher, J.C., van Hinsberg, V.J. & Keulen, N., 2011: Metamorphism in supracrustal and ultramafic rocks in southern West Greenland and South-West Greenland 64 – 61.5°N. *Danmarks og Grønlands Geologiske Undersøgelse Rapport 2011/6*. Copenhagen, Geological Survey of Denmark and Greenland, 30 pp.

Shmulovich, K.I., Yardley, B.W.D. & Graham, C.M., 2006: Solubility of quartz in crustal fluids: experiments and general equations for salt solutions and H_2O-CO_2 mixtures at 400-800 °C and 0.1-0.9 GPa. *Geofluids 6*, 1-14.

Smith, M.P., Henderson, P. & Campbell, L.S., 2000: Fractionation of the REE during hydrothermal processes: Constraints from the Bayan Obo Fe-REE-Nb deposit, Inner Mongolia, China. *Geochimica et Cosmochimica Acta 64*, 3141-3160.

Soman, A., Geisler, T., Tomaschek, F., Grange, M. & Berndt, J., 2010: Alteration of crystalline zircon solid solutions: a case study on zircon from an alkaline pegmatite from Zomba-Malosa, Malawi. *Contributions to Mineralogy and Petrology 160*, 909-930.

Steenfelt, A., Garde, A.A. & Moyen, J.-F., 2005: Mantle wedge involvement in the petrogenesis of Archaean grey gneisses in West Greenland. *Lithos 79*, 207-228.

Thomas, J.R., 1973: Petrography of gneisses south of Bjørnesund in the Fiskenæsset region: *Rapport Grønlands Geologiske Undersøgelse, 51*, 31-36.

Windley, B.F. & Garde, A.A., 2009: Arc-generated blocks with crustal sections in the North Atlantic craton of West Greenland: crustal growth in the Archean with modern analogues. *Earth-Science Reviews 93*, 1-30.

Åhäll, K.-I., Samuelsson, L. & Persson, P.-O., 1997: Geochronology and structural setting of the 1.38 Ga Torpa granite; implications for charnockite formation in SW Sweden. *GFF 119*, 37-43.

Appendix 1. SEM-EDS analyses of plagioclase in thin sections.

Sample	Si	Al	Ca	K	Na	O	Σ mass%	%An
468720	28.55	13.11	4.23		6.43	48.11	100.42	27.45
	28.89	13.32	4.46	0.21	6.42	48.82	102.11	28.16
	28.25	13.19	4.60		6.21	47.91	100.16	30.10
	28.11	13.12	4.48	0.27	6.30	47.73	100.01	28.57
	28.23	12.95	4.36		6.38	47.64	99.57	27.88
	28.21	13.13	4.26	0.22	6.11	47.70	99.63	28.43
	28.24	13.16	4.45	0.20	6.20	47.86	100.12	29.13
	28.22	13.17	4.49		6.28	47.84	100.00	29.13
	28.28	13.53	4.71	0.19	6.14	48.31	101.15	30.10
	28.32	13.15	4.46	0.25	6.29	47.98	100.46	28.57
	28.32	13.15	4.46	0.25	6.29	47.98	100.46	28.57
	28.32	13.15	4.46	0.25	6.29	47.98	100.46	28.57
	28.32	13.15	4.46	0.25	6.29	47.98	100.46	28.57
	28.32	13.15	4.46	0.25	6.29	47.98	100.46	28.57
	28.32	13.15	4.46	0.25	6.29	47.98	100.46	28.57
	27.99	13.15	4.61	0.18	6.41	47.69	100.03	28.97
	28.08	13.18	4.41		6.21	47.64	99.53	29.13
	28.30	13.18	4.35	0.23	6.31	47.94	100.31	27.88
	28.24	12.98	4.28	0.28	6.16	47.63	99.57	28.16
	28.04	13.14	4.41	0.17	6.30	47.62	99.68	28.57
468720							**Average %An:**	**28.65**
							σ:	**0.66**
510155	29.41	12.29	3.04	0.21	7.04	48.15	100.16	19.61
	29.56	12.49	2.96		7.23	48.48	100.72	18.63
	29.50	12.22	3.08	0.31	7.04	48.22	100.37	19.42
	29.34	12.49	3.07	0.22	7.07	48.27	100.46	19.23
	29.75	12.33	3.17	0.25	7.09	48.64	101.23	20.19
	29.50	12.36	3.00	0.20	7.10	48.31	100.48	19.42
	29.54	12.19	3.05	0.25	7.15	48.25	100.42	19.23
	28.75	12.50	3.64	0.17	6.73	47.70	99.49	23.08
	29.17	12.22	2.96	0.21	7.12	47.80	99.46	19.23
	29.28	12.18	3.03	0.30	7.16	47.95	99.89	19.05
	29.36	12.43	3.22	0.19	6.98	48.26	100.43	20.59
	29.05	12.20	3.08	0.16	7.07	47.67	99.24	20.00
	28.93	12.26	3.17	0.17	6.96	47.59	99.08	20.39
	29.02	12.22	2.93	0.20	7.05	47.59	99.00	19.23
	29.19	12.27	3.11	0.25	7.00	47.89	99.71	20.19
	28.98	12.06	3.04		7.06	47.42	98.56	19.42
	28.93	12.04	3.01	0.24	6.81	47.28	98.31	19.61
	29.28	12.17	3.03	0.20	7.05	47.88	99.60	19.42
	29.44	12.34	3.15		7.25	48.30	100.48	20.00
	29.45	12.31	3.03	0.18	7.30	48.28	100.55	19.05
510155							**Average %An:**	**19.75**
							σ:	**0.93**

Sample	Si	Al	Ca	K	Na	O	Σ mass%	%An
512028	27.42	13.79	5.18		5.90	47.63	99.92	33.65
	27.17	13.67	5.04		5.64	47.09	98.61	33.66
	27.09	13.83	5.51		5.75	47.36	99.54	35.24
	27.23	13.73	5.44		5.64	47.36	99.39	35.92
	27.17	13.54	5.35		5.64	47.10	98.81	34.95
	27.07	13.61	5.32		5.63	47.03	98.66	34.95
	27.19	13.62	5.25		5.69	47.17	98.93	34.95
	27.08	13.70	5.41		5.54	47.13	98.88	36.27
	27.07	13.69	5.43		5.62	47.14	98.95	35.92
	27.01	13.85	5.38		5.63	47.20	99.08	35.29
	27.09	13.81	5.62		5.63	47.35	99.50	36.54
	27.09	13.81	5.62		5.63	47.35	99.50	36.54
	27.11	13.60	5.30		5.30	47.05	98.69	34.95
	27.37	13.40	5.00		5.84	47.12	98.73	33.01
	27.09	13.66	5.40		5.47	47.08	98.70	36.27
	27.39	13.67	5.33		5.72	47.48	99.59	34.95
	27.01	13.61	5.31		5.52	46.91	98.36	35.29
	27.41	13.86	5.59	0.16	5.47	47.72	100.20	36.27
	27.26	13.71	5.28		5.64	47.32	99.21	35.29
	26.94	13.64	5.47		5.61	46.96	98.62	35.92
512028							**Average %An:**	**35.29**
							σ:	**0.98**
512075	27.20	15.11	6.99		5.13	49.01	103.45	44.23
	27.22	15.04	6.89		5.25	48.96	103.36	42.86
	26.47	14.49	6.70		5.09	47.49	100.25	42.86
	27.04	15.22	6.94		5.00	48.86	103.06	42.16
	26.60	14.57	6.68		4.98	47.67	100.51	43.27
	25.91	14.22	6.32		4.88	46.39	97.73	41.35
	26.95	14.59	6.72		5.06	48.12	101.43	43.27
	27.52	14.74	6.63		5.35	48.97	103.21	44.23
	26.76	15.14	6.97		5.03	48.48	102.38	45.10
	26.60	15.06	6.99		4.88	48.19	101.73	45.54
510155							**Average %An:**	**43.49**
							σ:	**1.30**

Appendix 2. Complete SEM image record of starting materials

Varberg charnockite zircon (all scale bars are x μm)

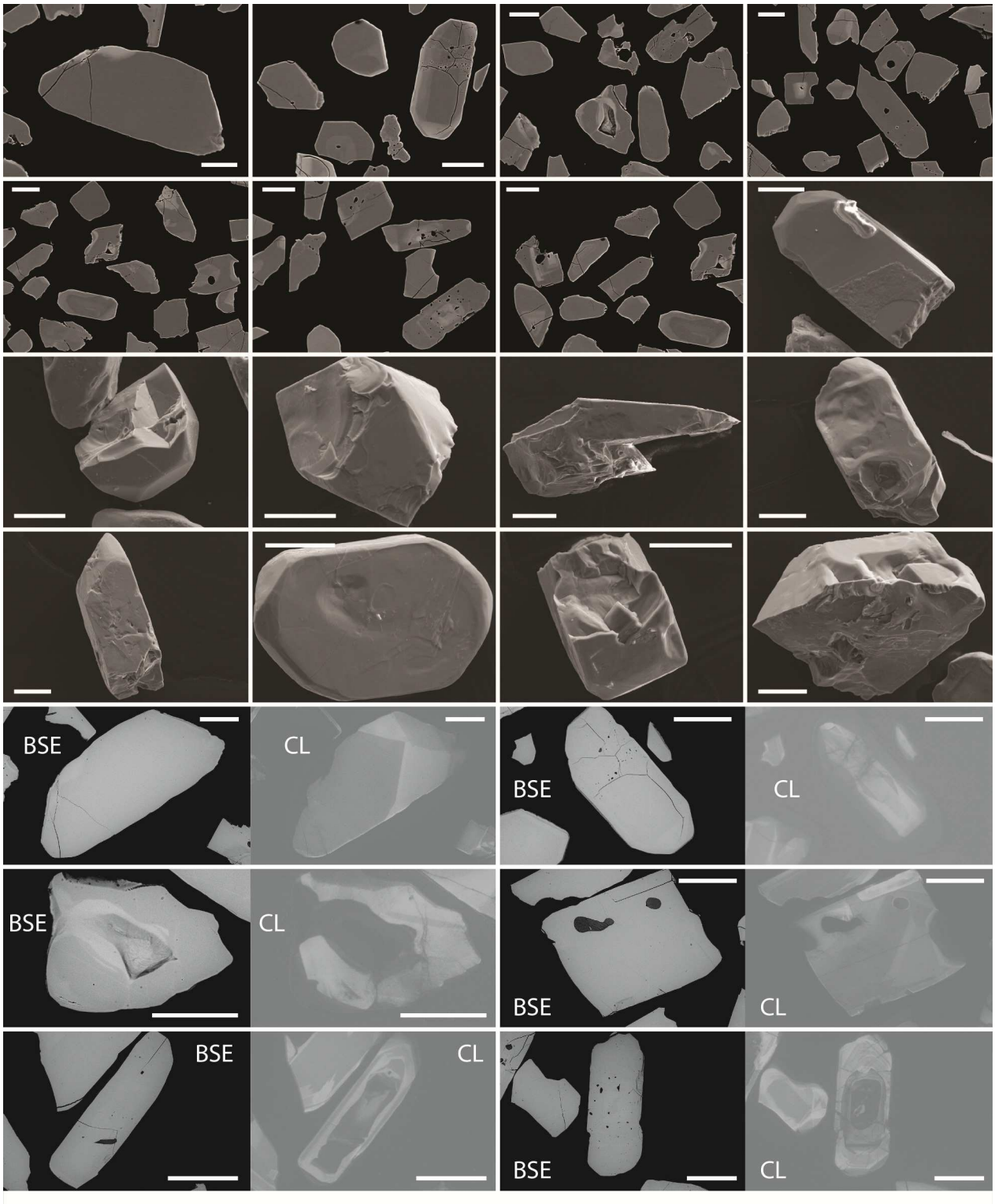

Önnestad syenite zircon (all scale bars are x µm)

ASGH007A tonalite zircon (all scale bars are x μm)

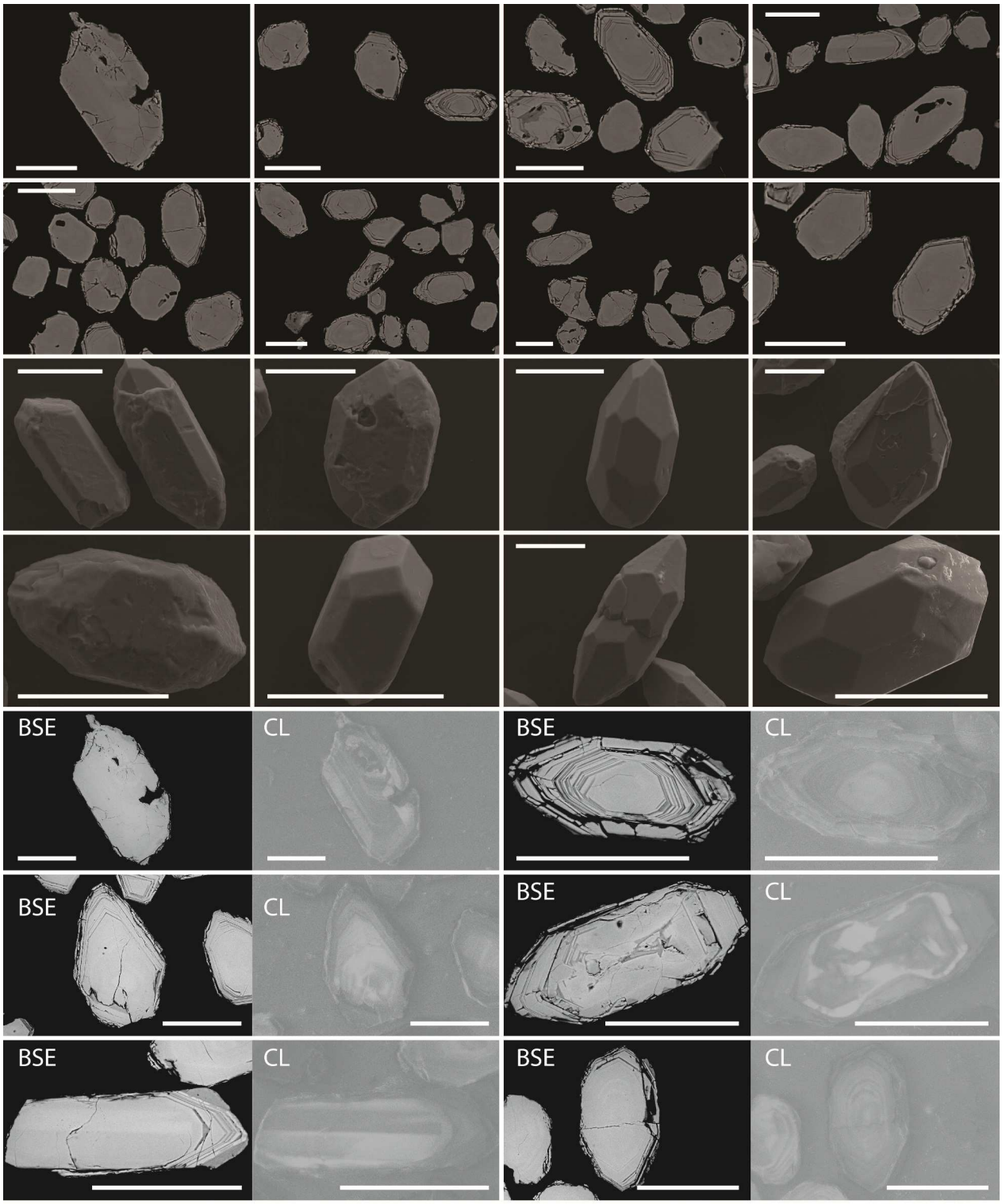

Appendix 3. Complete SEM image record of experimental runs

ZrBd-01 (all scale bars are 80 μm)

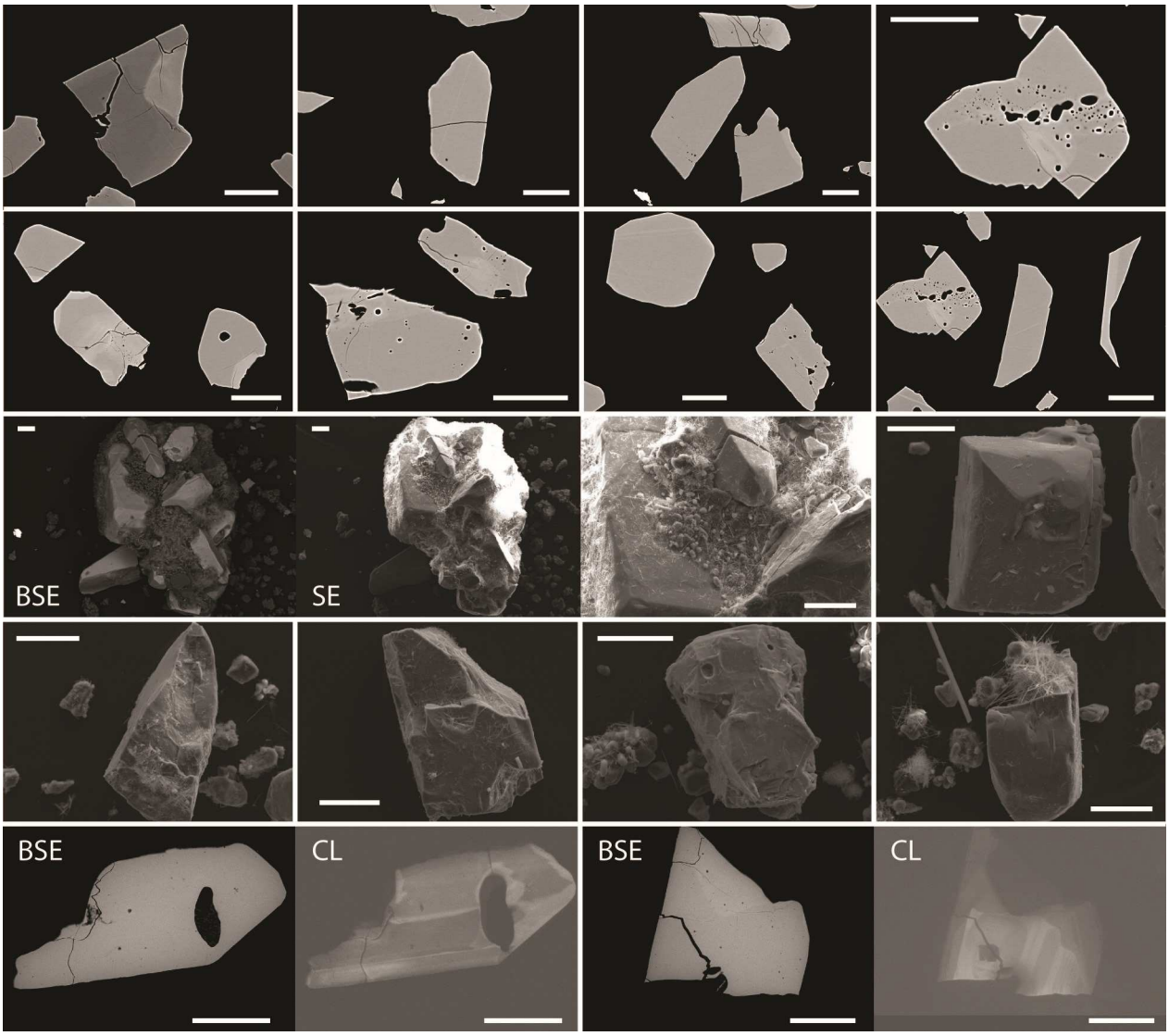

ZrBd-02 (all scale bars are 80 μm)

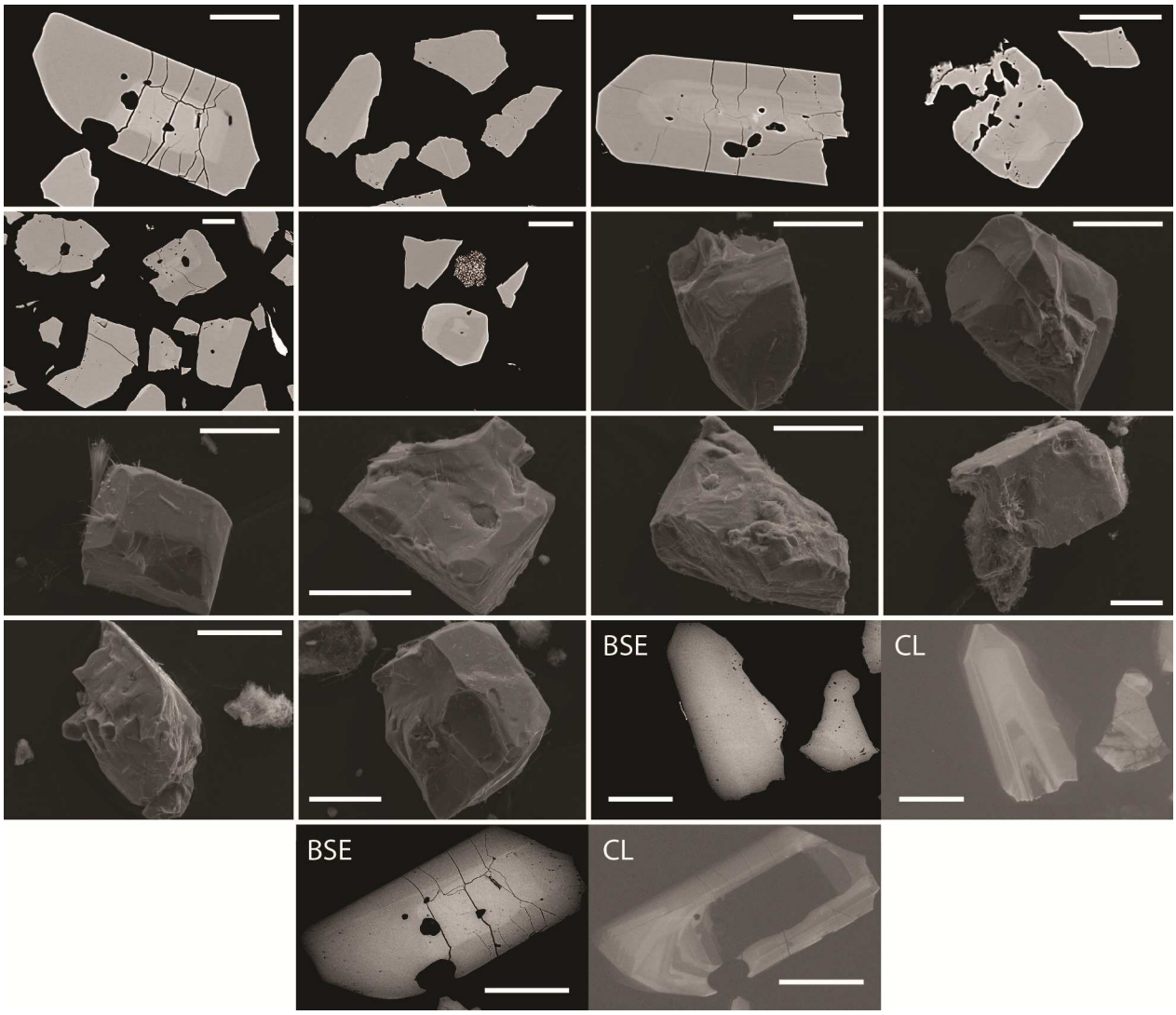

ZrBd-03 (all scale bars are 80 μm)

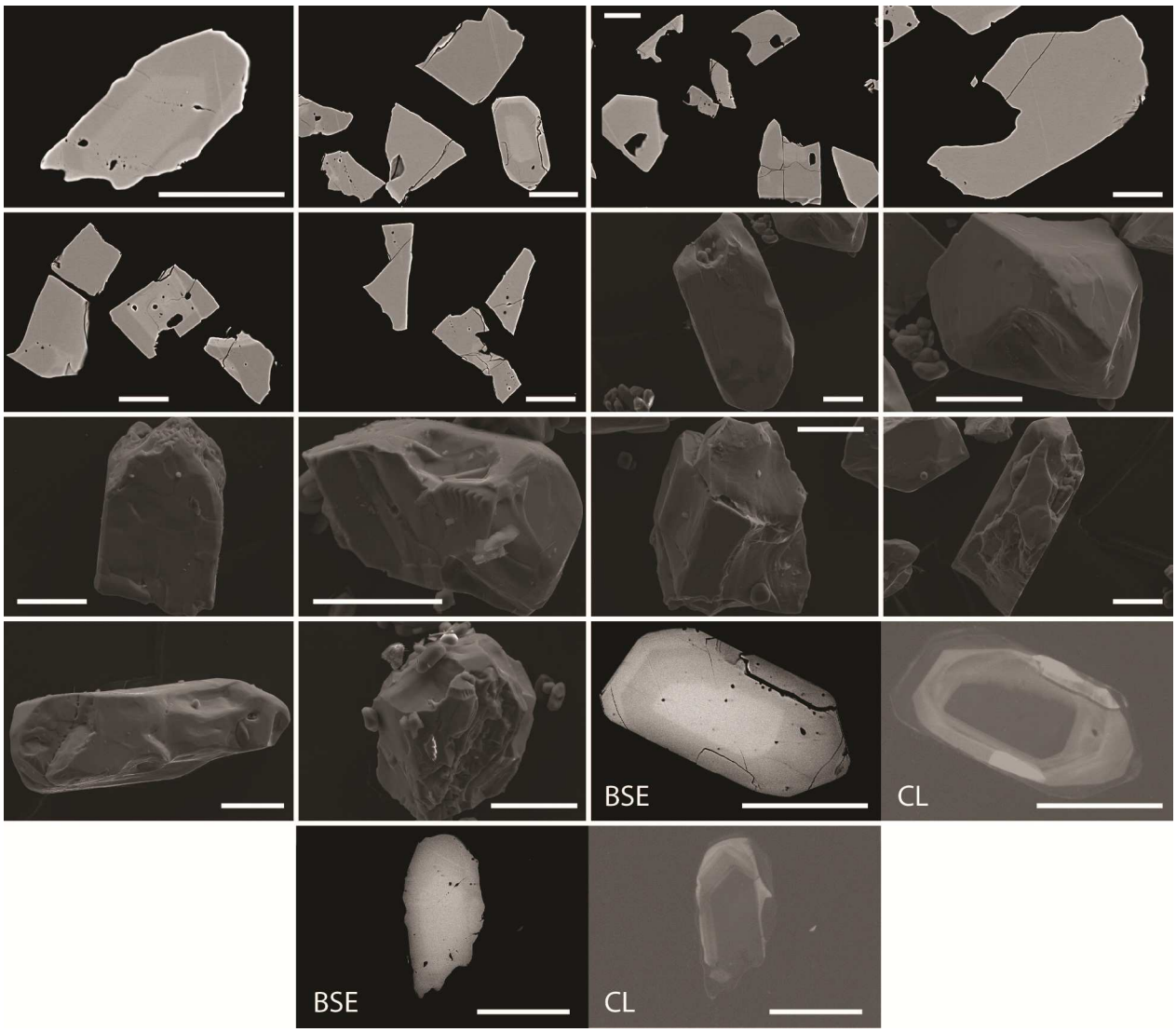

ZrBd-04 (all scale bars are 80 μm)

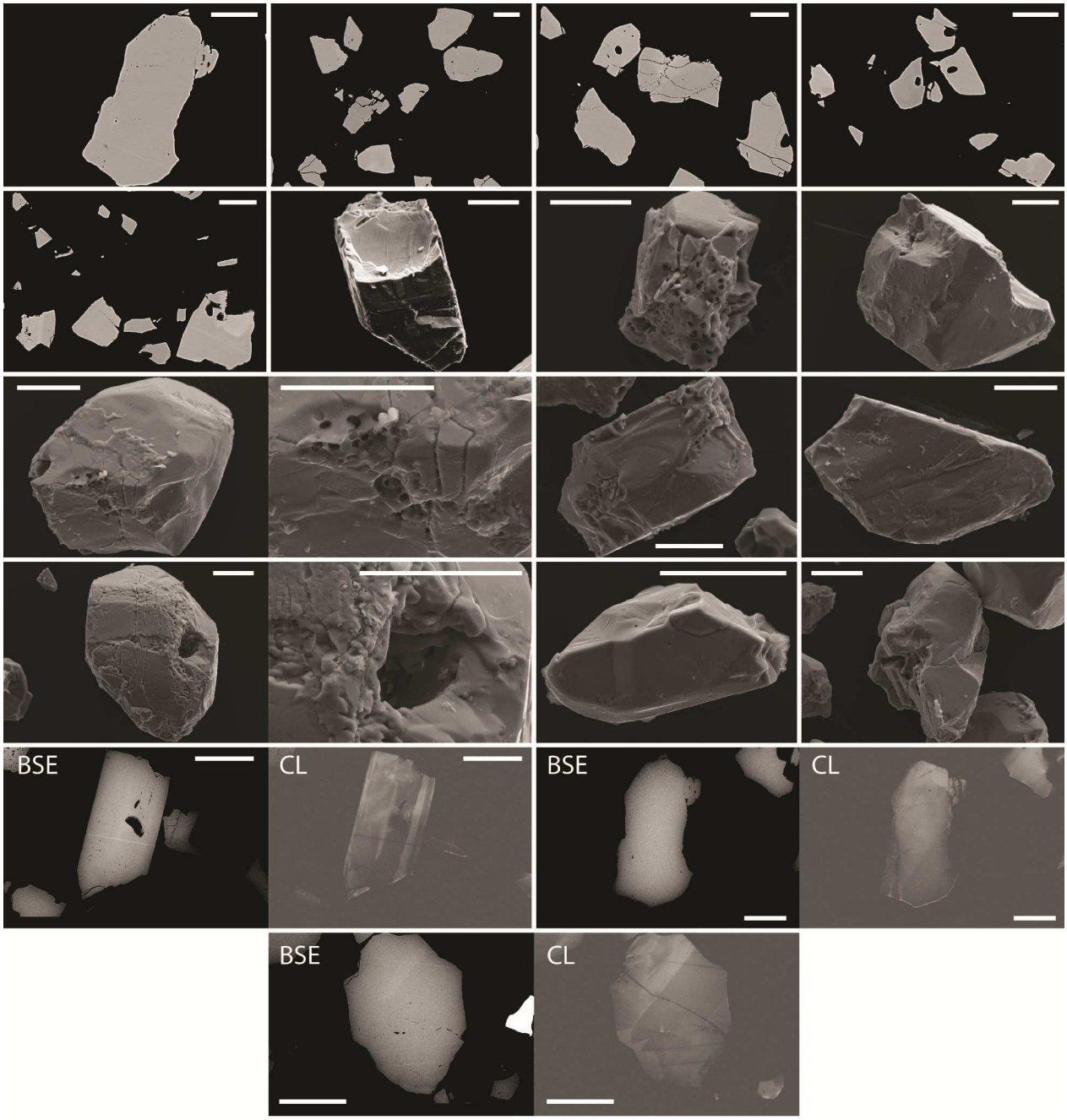

ZrBd-05 (all scale bars are 80 μm)

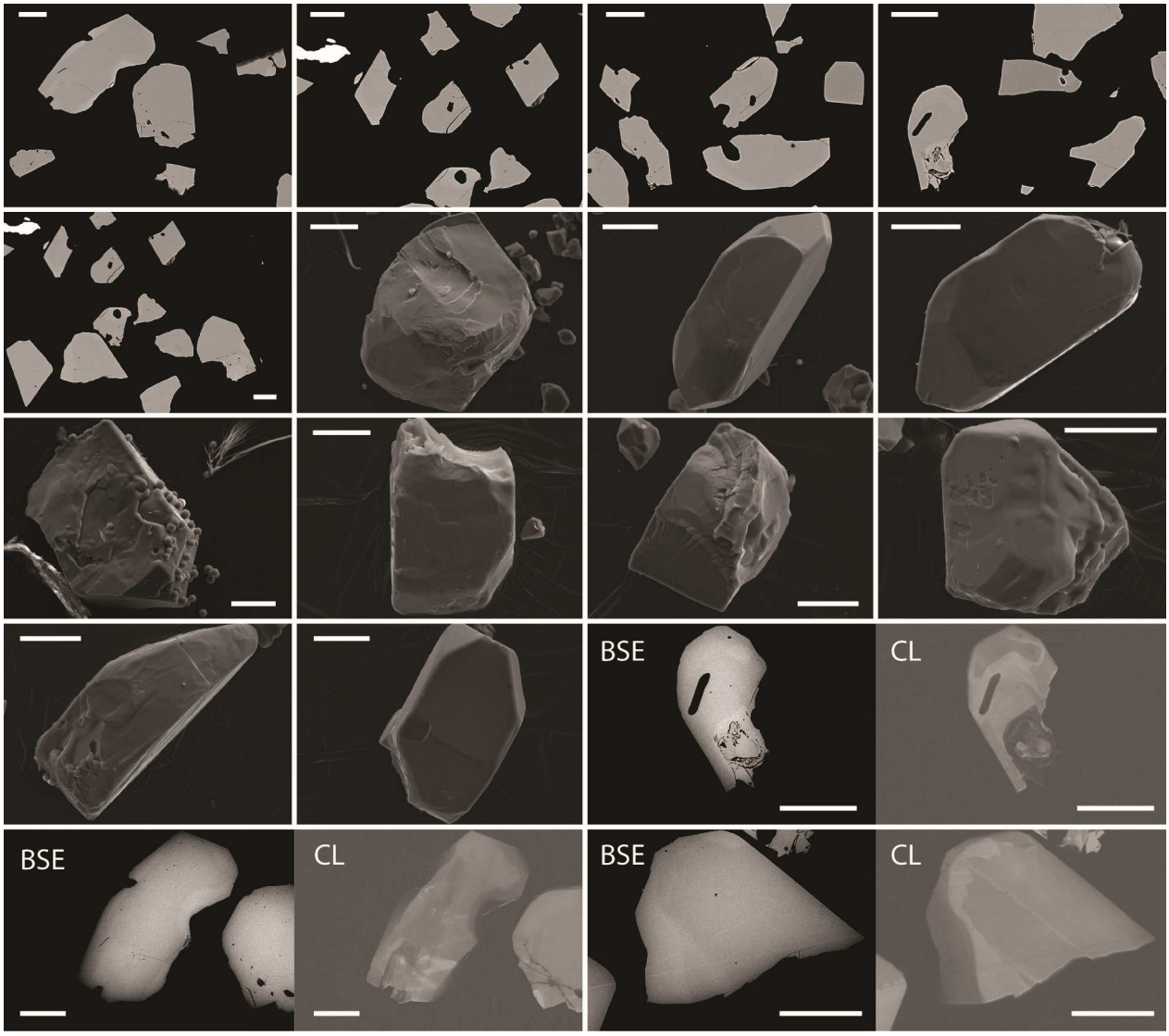

ZrBd-06 (all scale bars are 80 μm)

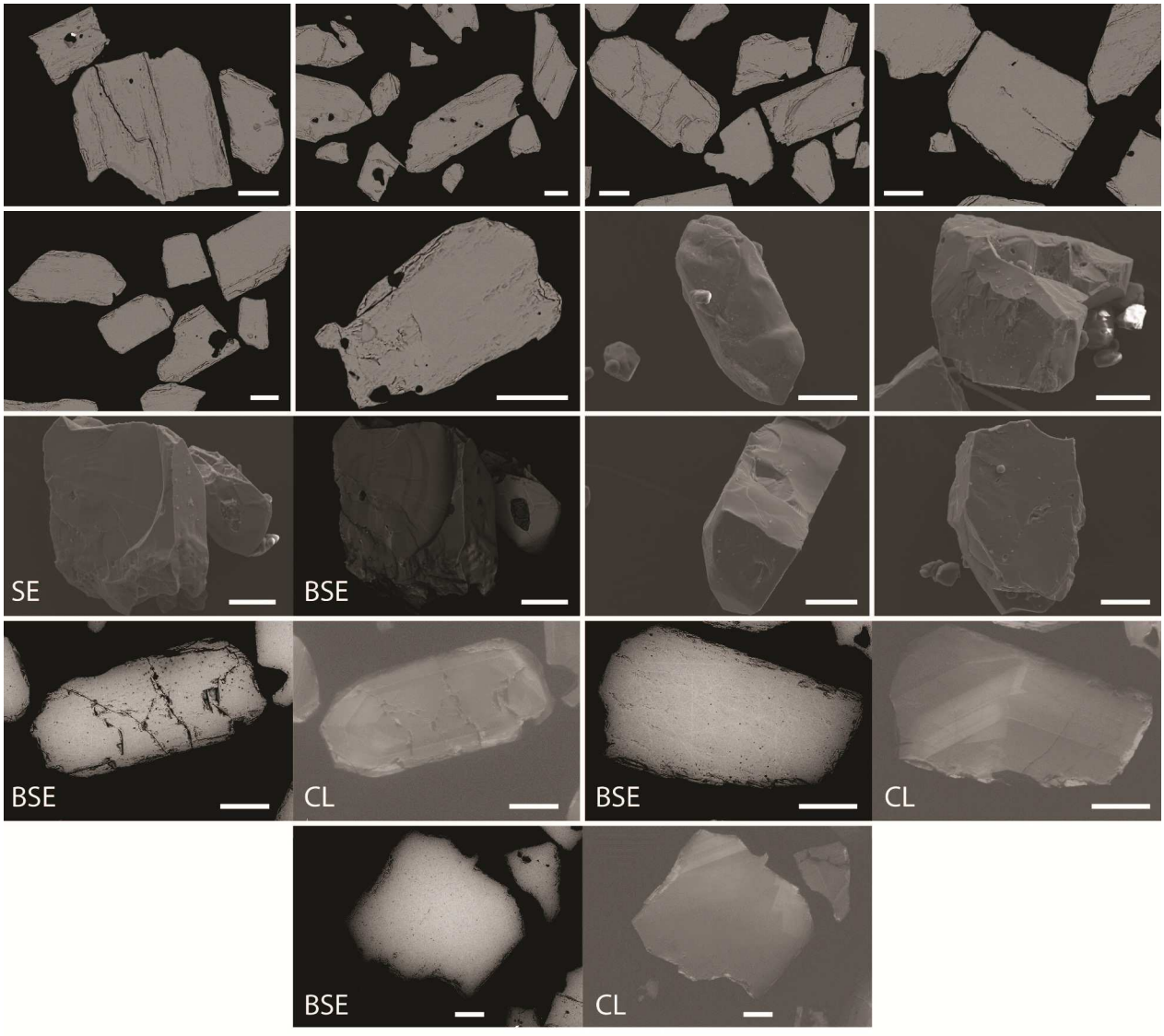

ZrBd-07 (all scale bars are 80 μm)

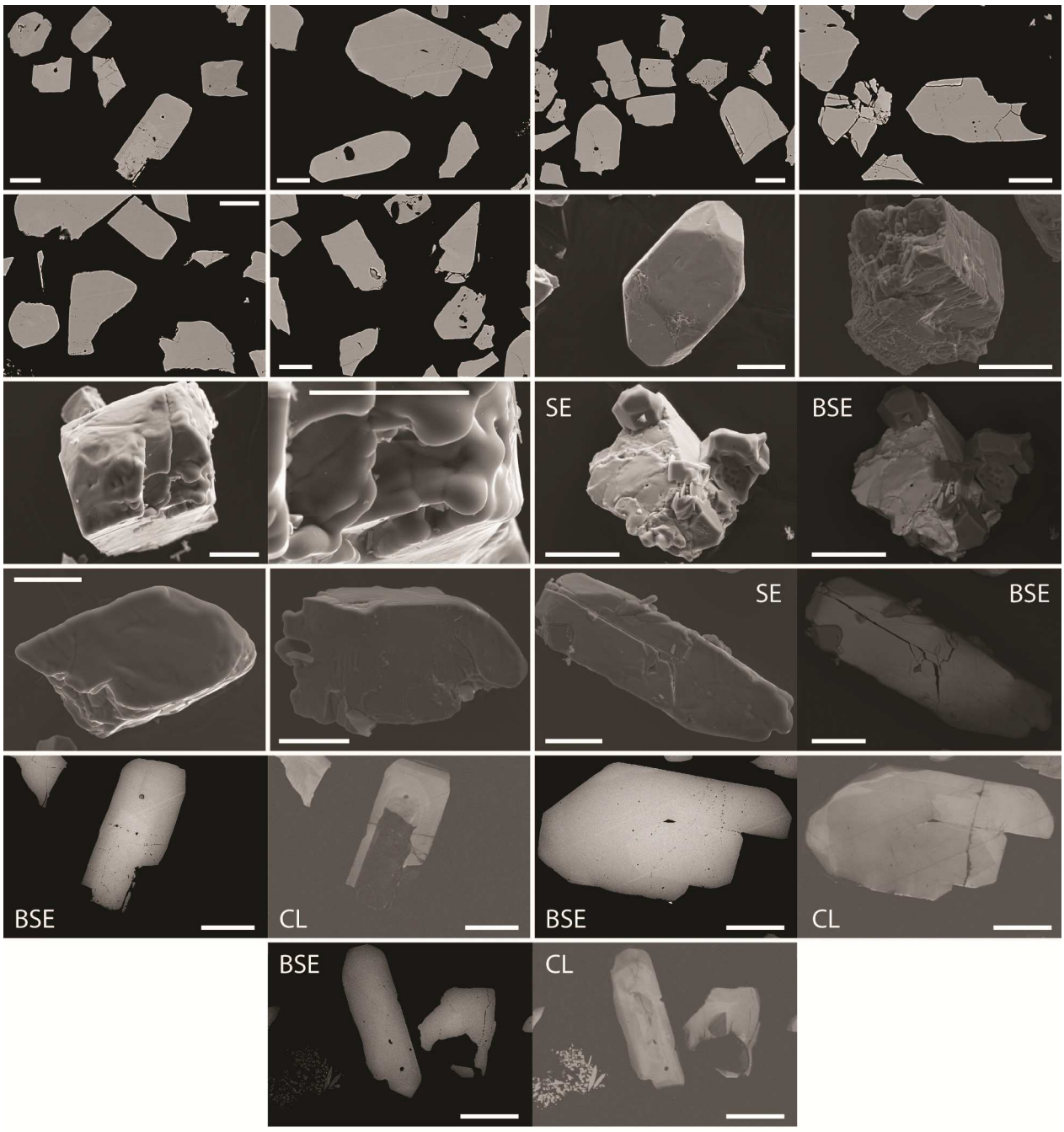

ZrBd-08 (all scale bars are 80 μm)

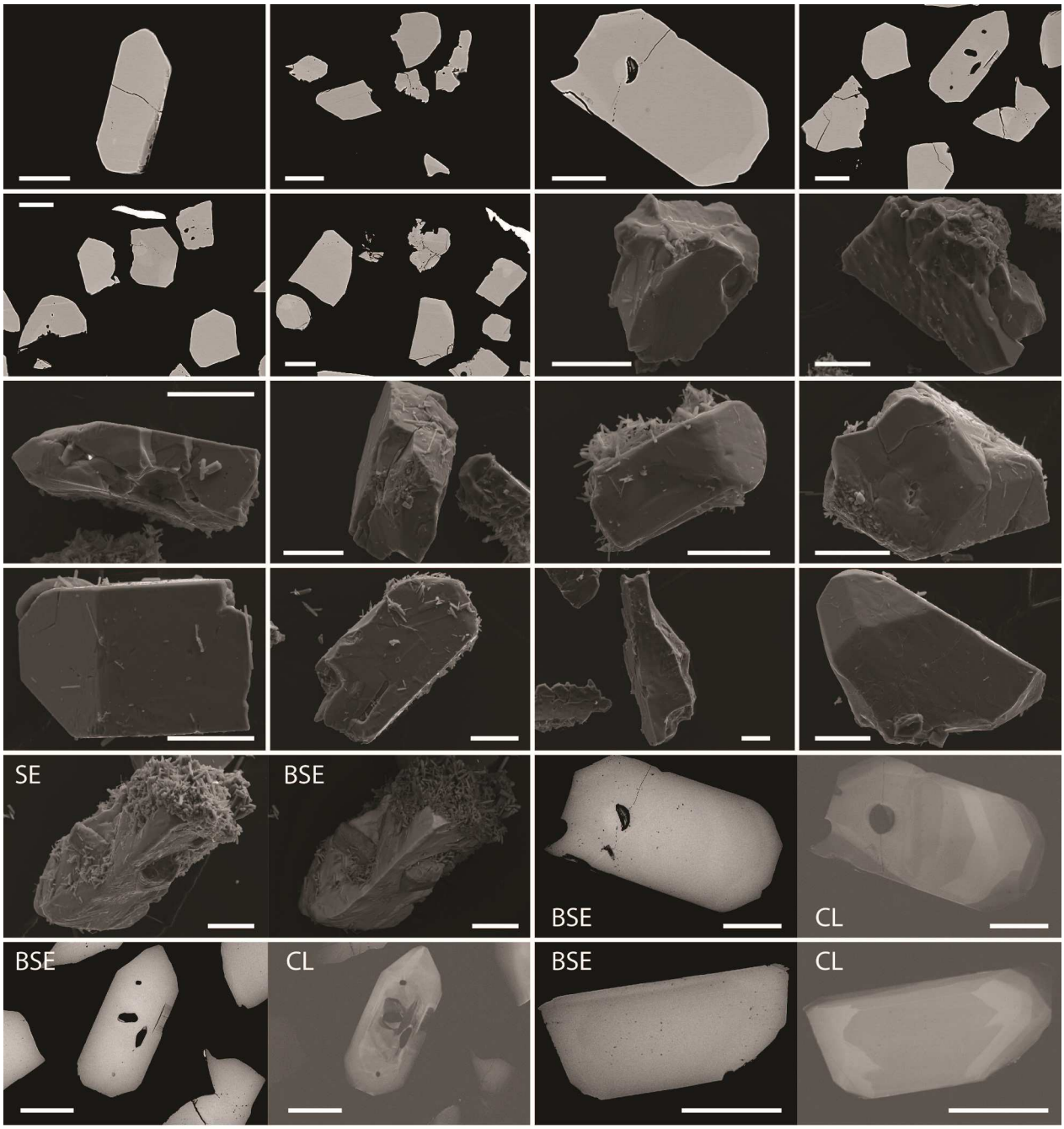

ZrBd-09 (all scale bars are 80 μm)

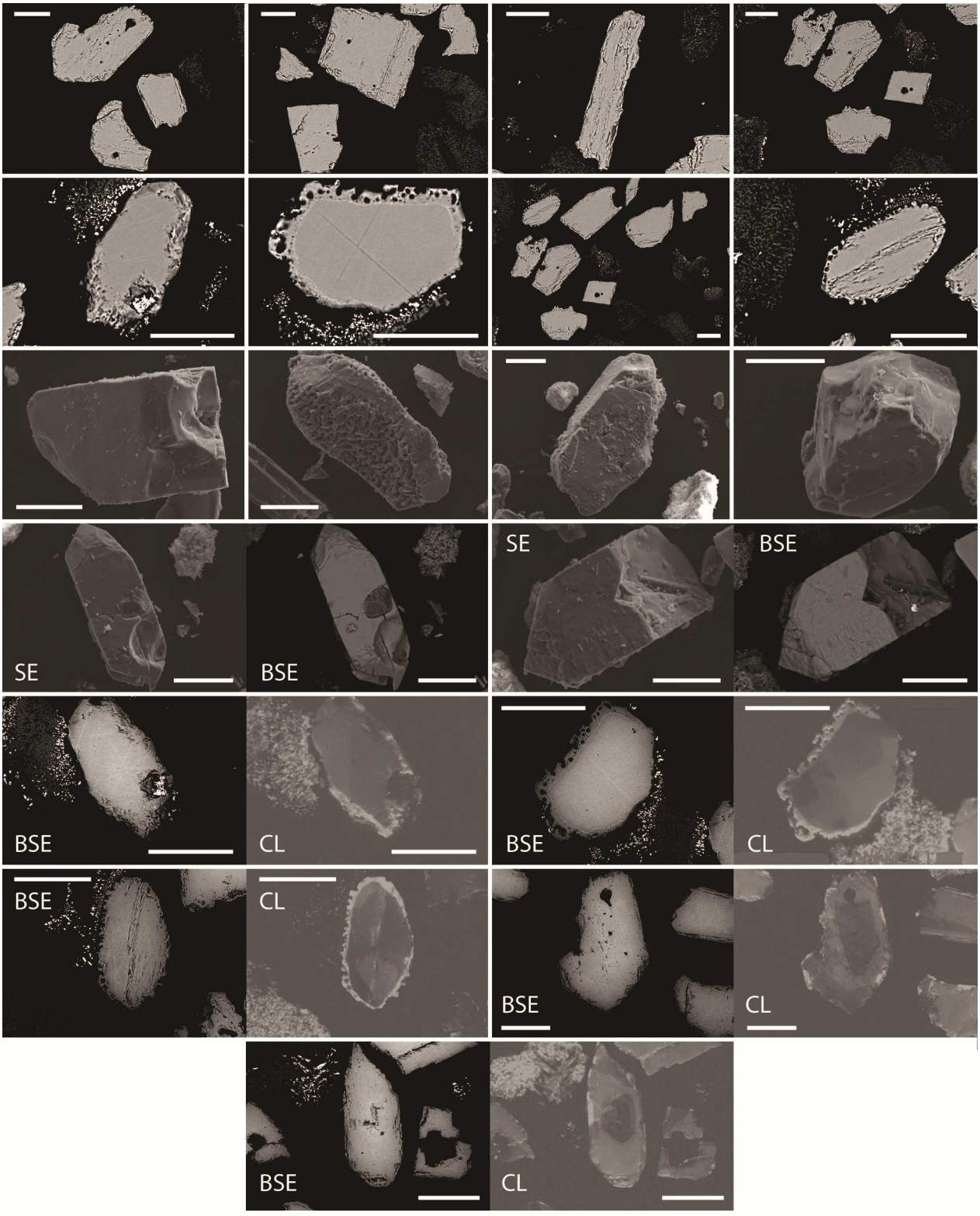

ZrBd-10 (all scale bars are 80 μm)

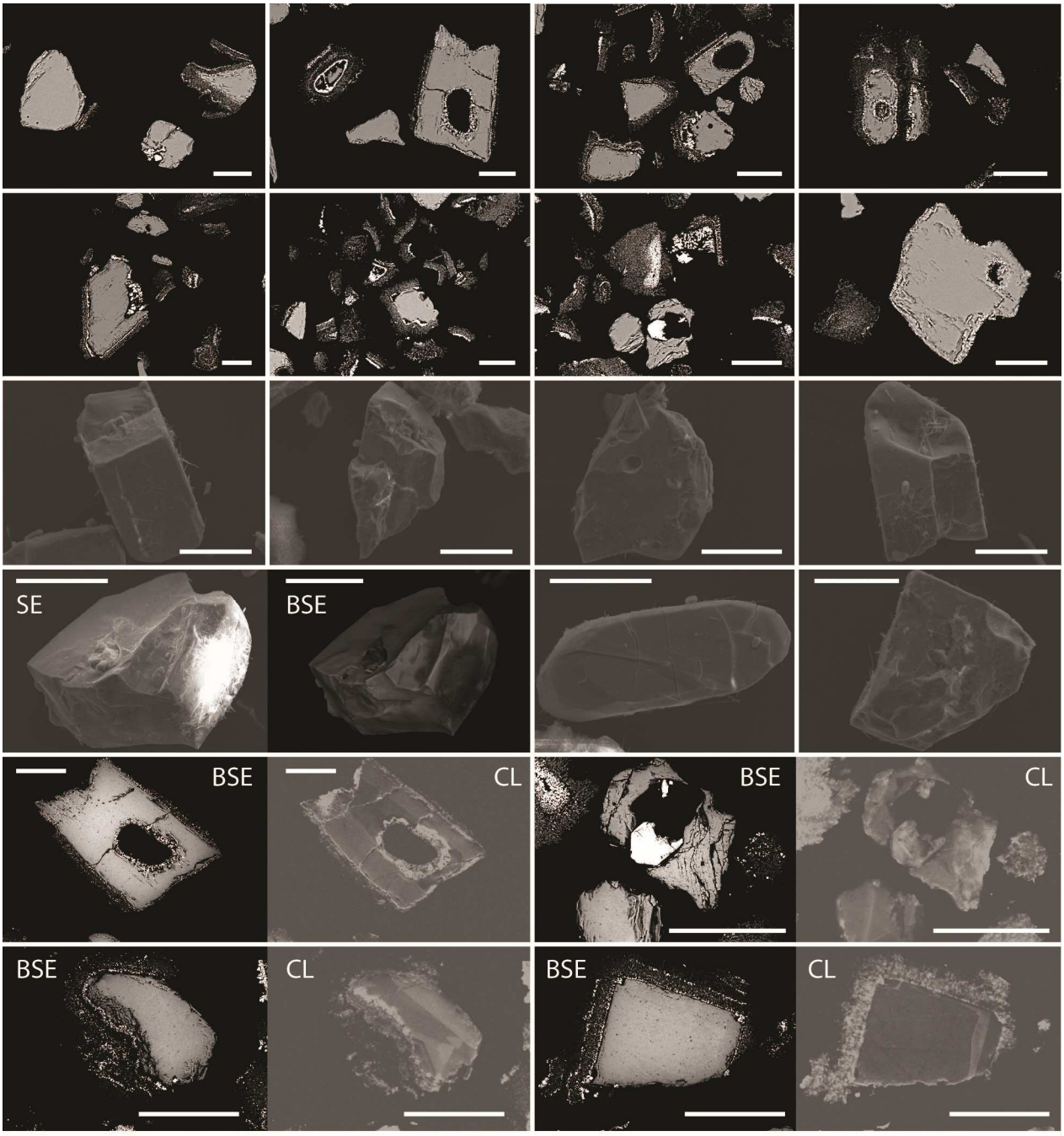

ZrBd-11 (all scale bars are 80 μm)

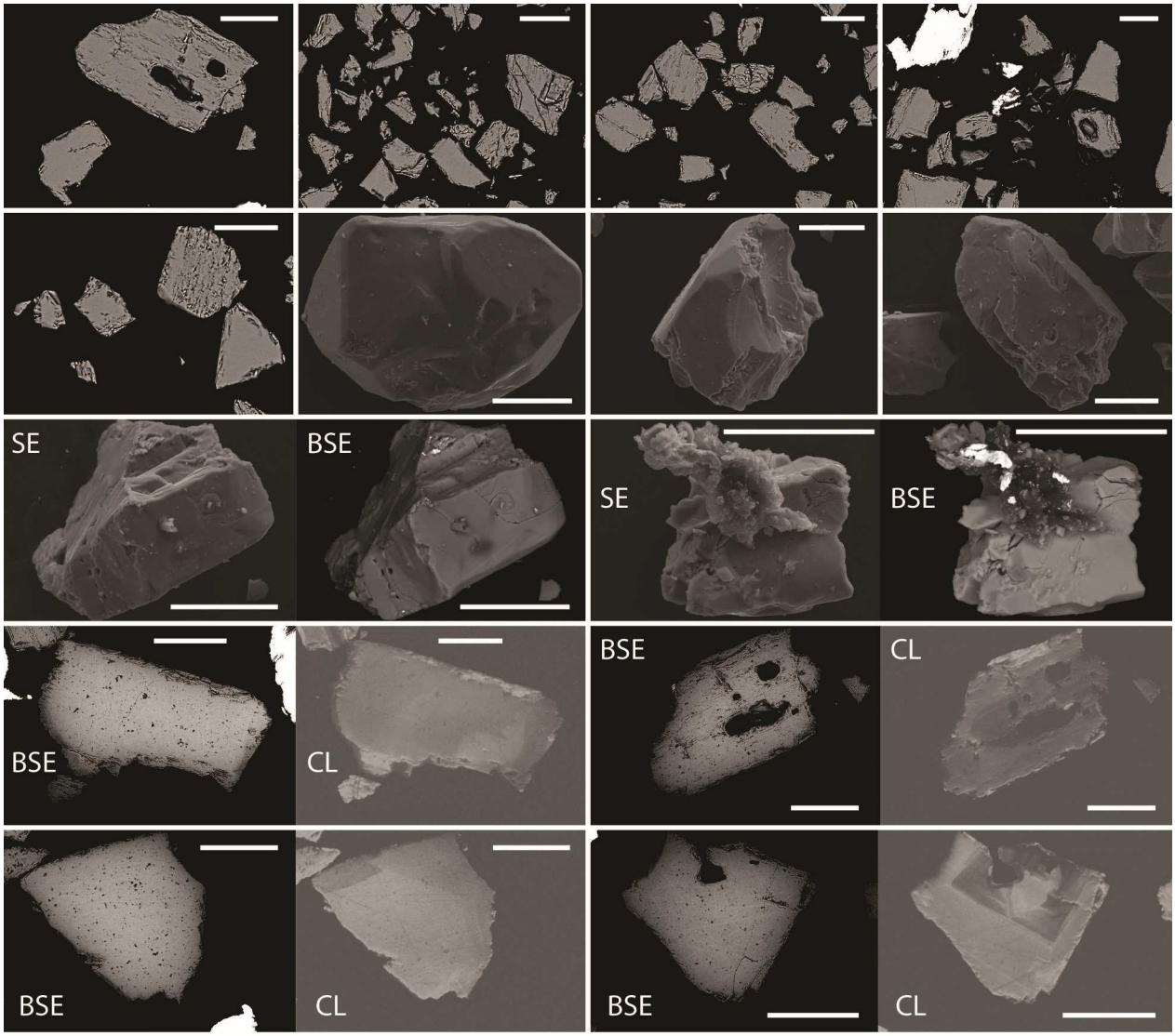

ZrBd-12 (all scale bars are 80 µm, unless other stated)

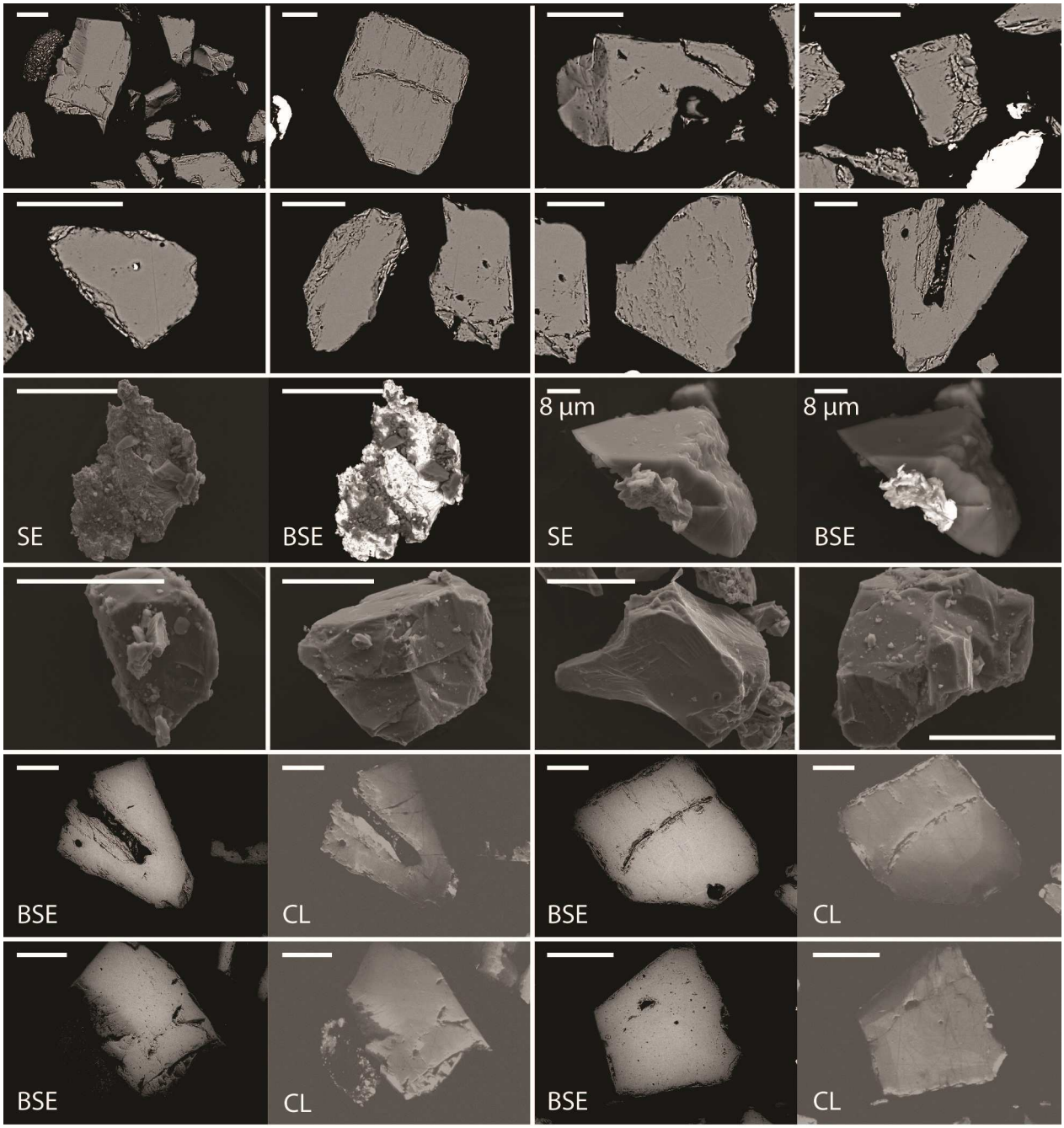

ZrBd-13 (all scale bars are 80 μm)

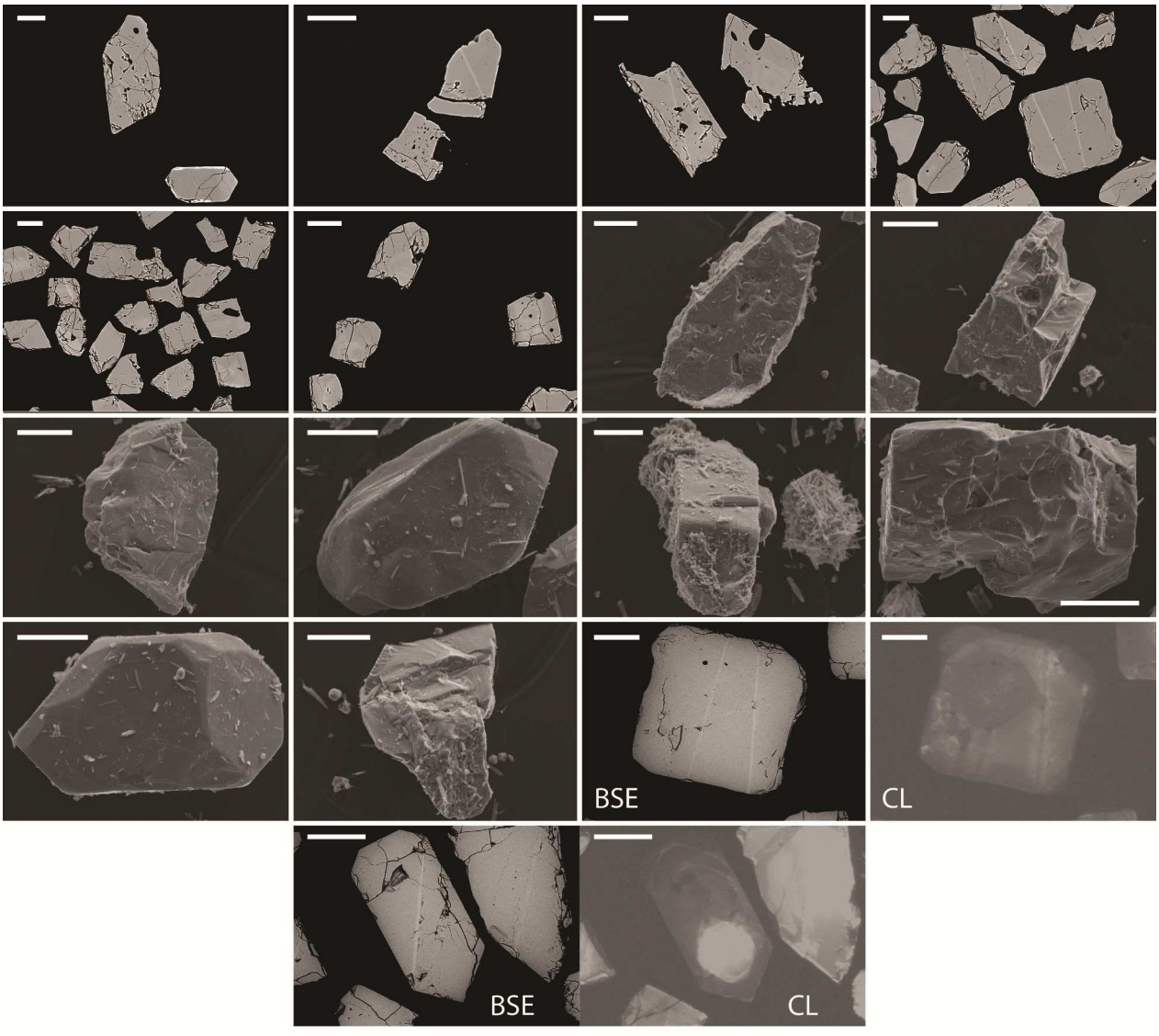

ZrBd-14 (all scale bars are 80 μm)

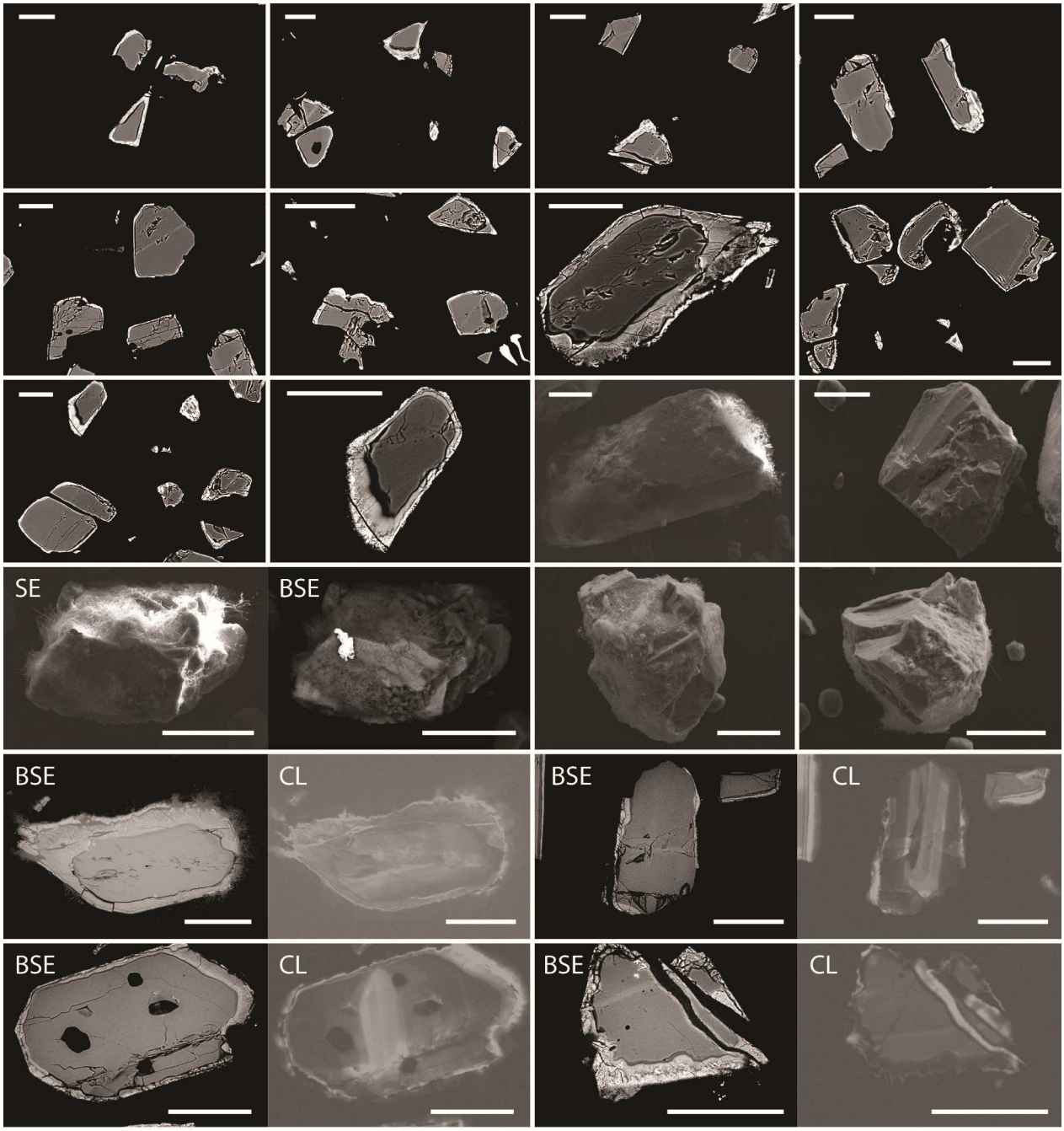

ZrBd-15 (all scale bars are 80 μm)

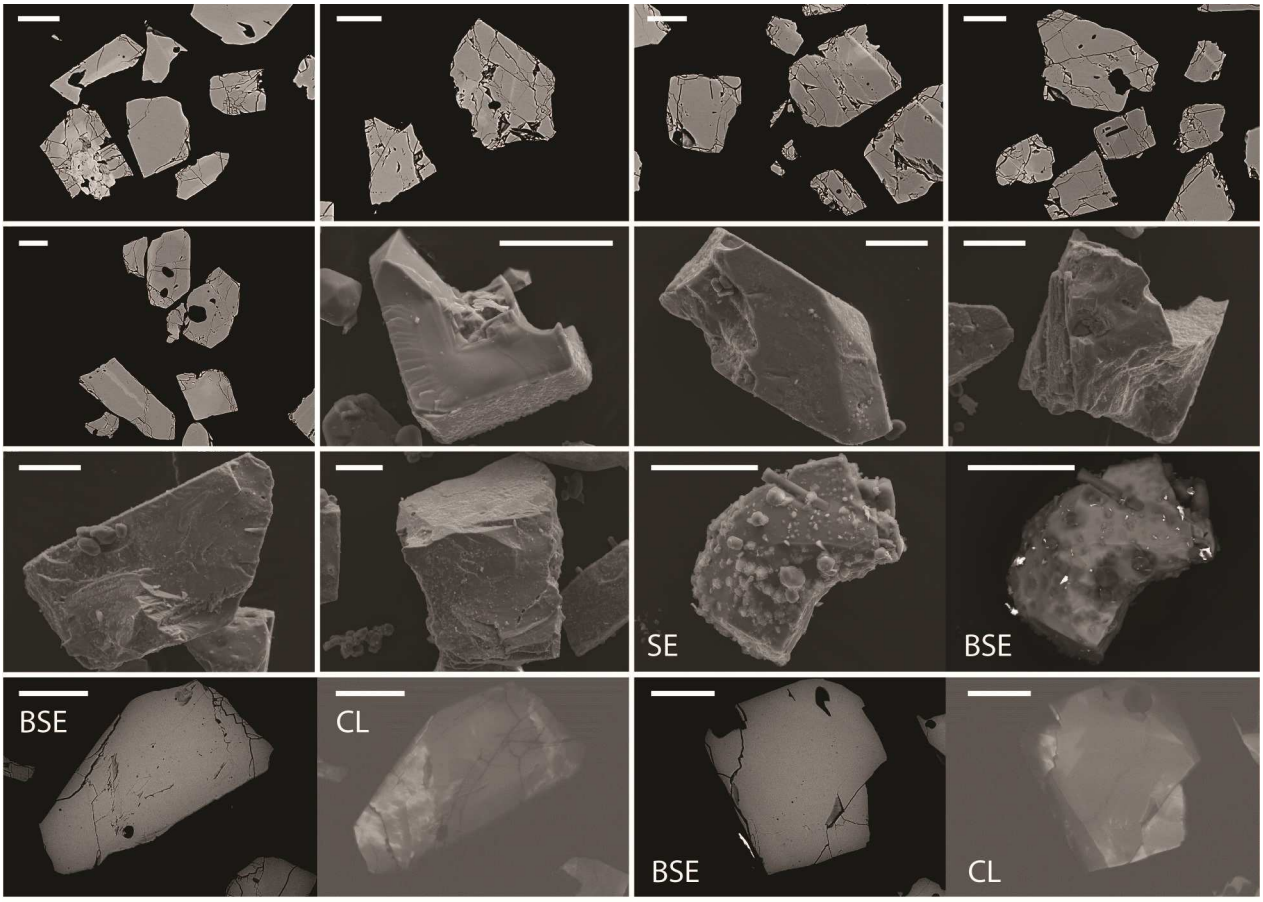

ZrBd-16 (all scale bars are 80 μm)

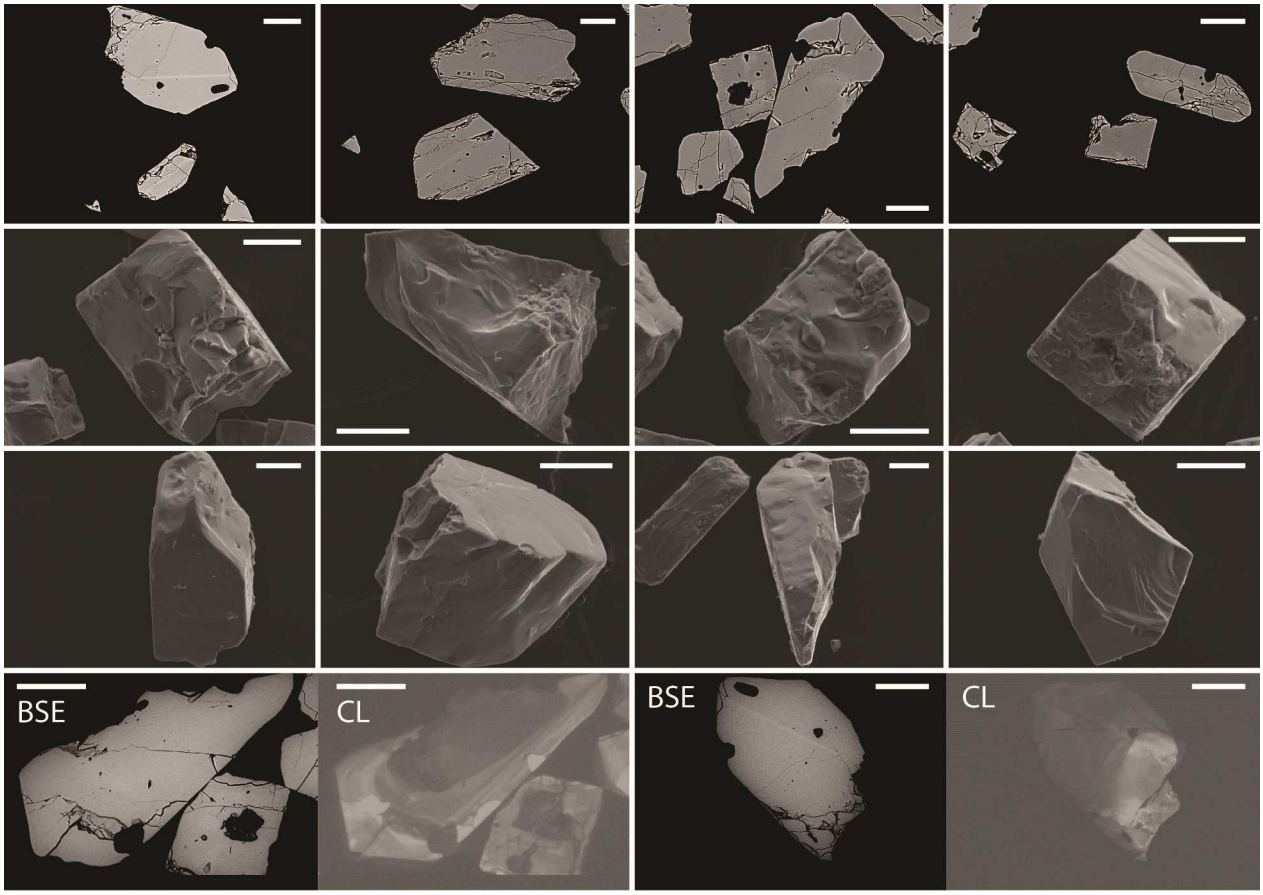

ZrBd-17 (all scale bars are 80 μm)

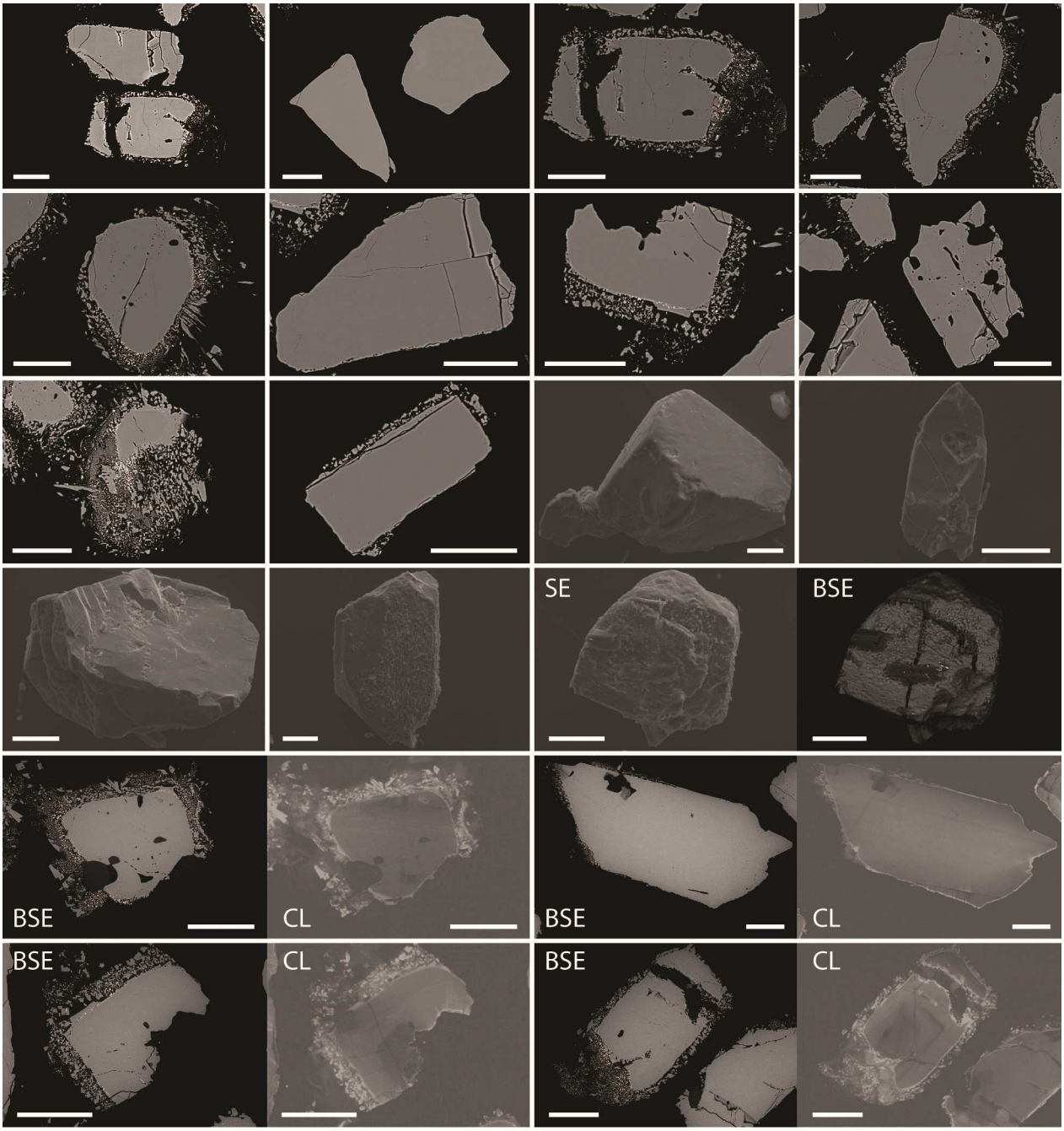

ZrBd-18 (all scale bars are 80 μm)

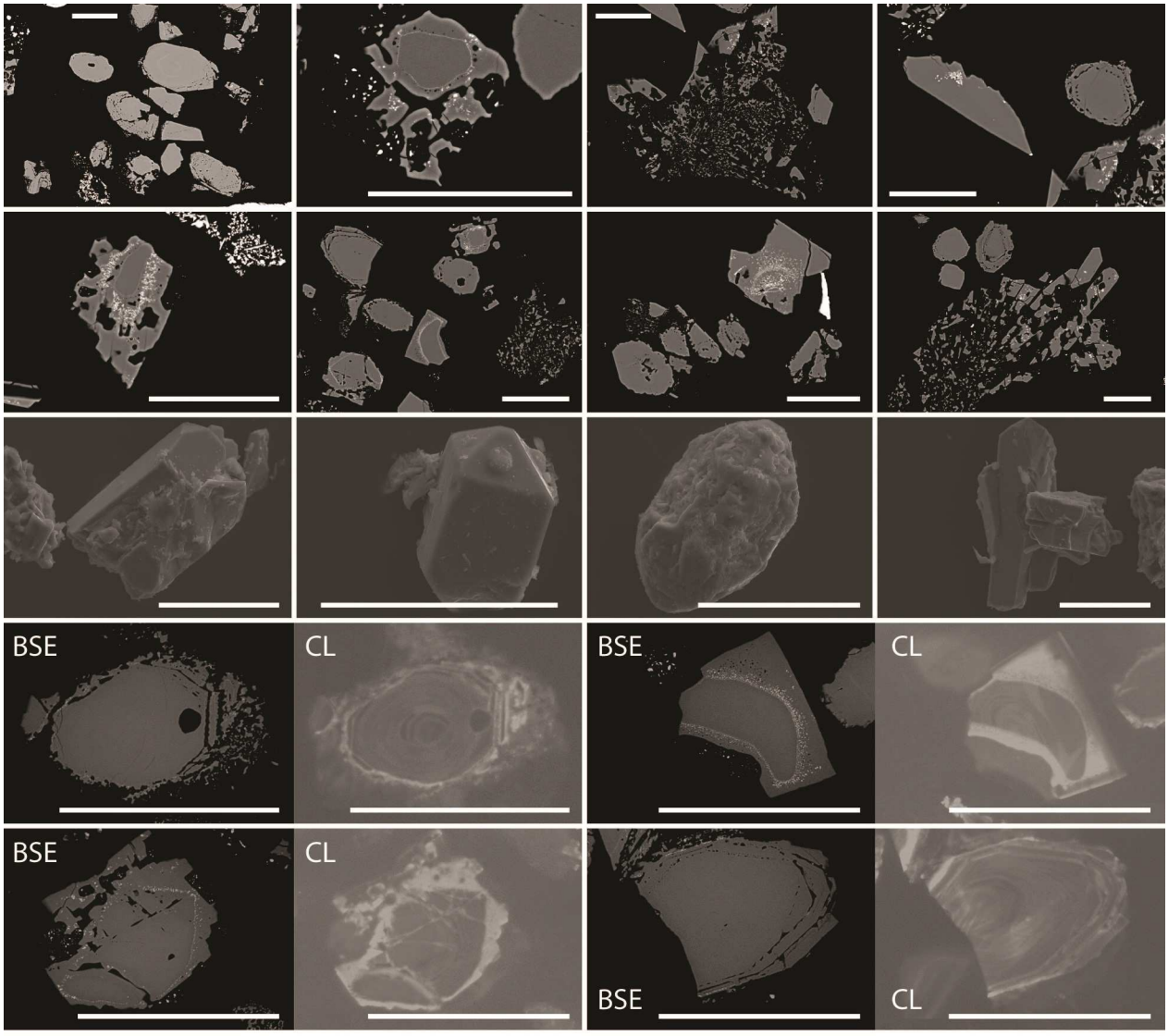

ZrBd-19 (all scale bars are 80 μm)

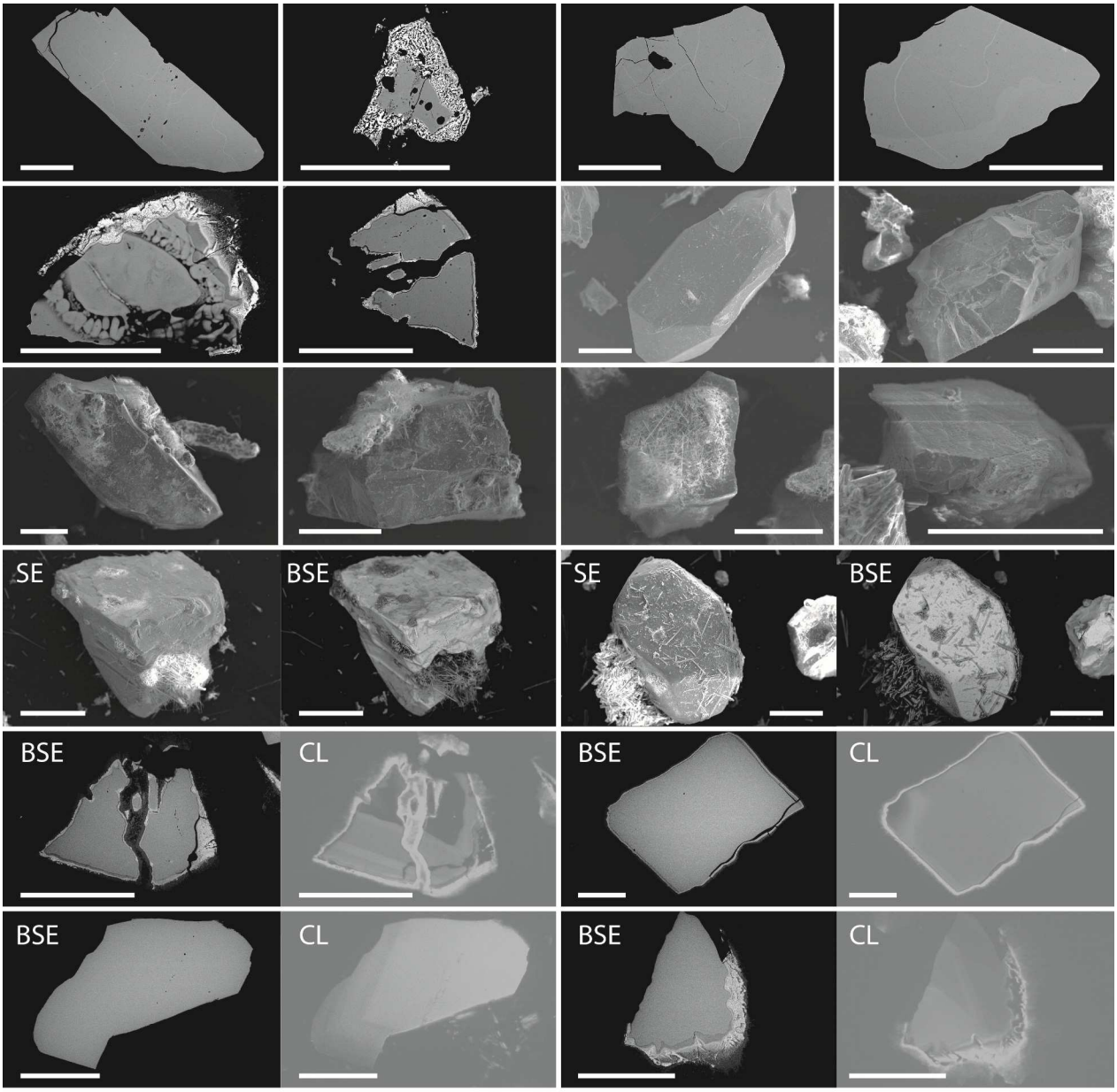

ZrBd-20 (all scale bars are 80 μm)

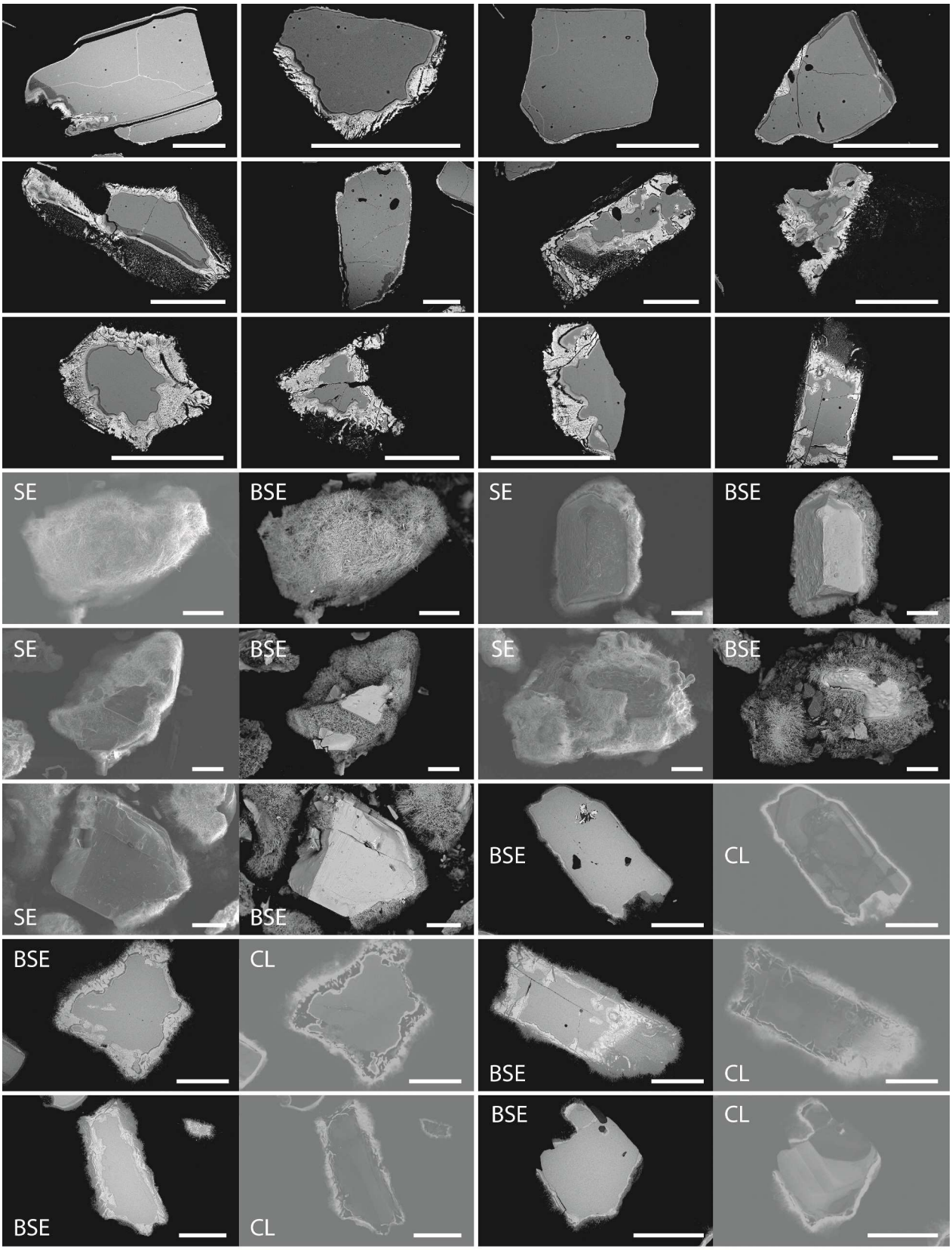

Tidigare skrifter i serien ”Examensarbeten i Geologi vid Lunds Universitet”:

244. Olsson, Håkan, 2009: Climate archives and the Late Ordovician Boda Event. (15 hskp)
245. Wollein Waldetoft, Kristofer, 2009: Svekofennisk granit från olika metamorfa miljöer. (15 hskp)
246. Månsby, Urban, 2009: Late Cretaceous coprolites from the Kristianstad Basin, southern Sweden. (15 hskp)
247. MacGimpsey, I., 2008: Petroleum Geology of the Barents Sea. (15 hskp)
248. Jäckel, O., 2009: Comparison between two sediment X-ray Fluorescence records of the Late Holocene from Disko Bugt, West Greenland; Paleoclimatic and methodological implications. (45 hskp)
249. Andersen, Christine, 2009: The mineral composition of the Burkland Cu-sulphide deposit at Zinkgruvan, Sweden – a supplementary study. (15 hskp)
250. Riebe, My, 2009: Spinel group minerals in carbonaceous and ordinary chondrites. (15 hskp)
251. Nilsson, Filip, 2009: Föroreningsspridning och geologi vid Filborna i Helsingborg. (30 hskp)
252. Peetz, Romina, 2009: A geochemical characterization of the lower part of the Miocene shield-building lavas on Gran Canaria. (45 hskp)
253. Åkesson, Maria, 2010: Mass movements as contamination carriers in surface water systems – Swedish experiences and risks.
254. Löfroth, Elin, 2010: A Greenland ice core perspective on the dating of the Late Bronze Age Santorini eruption. (45 hskp)
255. Ellingsgaard, Óluva, 2009: Formation Evaluation of Interlava Volcaniclastic Rocks from the Faroe Islands and the Faroe-Shetland Basin. (45 hskp)
256. Arvidsson, Kristina, 2010: Geophysical and hydrogeological survey in a part of the Nhandugue River valley, Gorongosa National Park, Mozambique. (45 hskp)
257. Gren, Johan, 2010: Osteo-histology of Mesozoic marine tetrapods – implications for longevity, growth strategies and growth rates. (15 hskp)
258. Syversen, Fredrikke, 2010: Late Jurassic deposits in the Troll field. (15 hskp)
259. Andersson, Pontus, 2010: Hydrogeological investigation for the PEGASUS project, southern Skåne, Sweden. (30 hskp)
260. Noor, Amir, 2010: Upper Ordovician through lowermost Silurian stratigraphy and facies of the Borenshult-1 core, Östergötland, Sweden. (45 hskp)
261. Lewerentz, Alexander, 2010: On the occurrence of baddeleyite in zircon in silica-saturated rocks. (15 hskp)
262. Eriksson, Magnus, 2010: The Ordovician Orthoceratite Limestone and the Blommiga Bladet hardground complex at Horns Udde, Öland. (15 hskp)
263. Lindskog, Anders, 2010: From red to grey and back again: A detailed study of the lower Kundan (Middle Ordovician) ‘Täljsten’ interval and its enclosing strata in Västergötland, Sweden. (15 hskp)
264. Rääf, Rebecka, 2010: Changes in beyrichiid ostracode faunas during the Late Silurian Lau Event on Gotland, Sweden. (30 hskp)
265. Petersson, Andreas, 2010: Zircon U-Pb, Hf and O isotope constraints on the growth versus recycling of continental crust in the Grenville orogen, Ohio, USA. (45 hskp)
266. Stenberg, Li, 2010: Geophysical and hydrogeological survey in a part of the Nhandugue River valley, Gorongosa National Park, Mozambique – Area 1 and 2. (45 hskp)
267. Andersen, Christine, 2010: Controls of seafloor depth on hydrothermal vent temperatures - prediction, observation & 2D finite element modeling. (45 hskp)
268. März, Nadine, 2010: When did the Kalahari craton form? Constraints from baddeleyite U-Pb geochronology and geo-chemistry of mafic intrusions in the Kaapvaal and Zimbabwe cratons. (45 hp)
269. Dyck, Brendan, 2010: Metamorphic rocks in a section across a Svecnorwegian eclogite-bearing deformation zone in Halland: characteristics and regional context. (15 hp)
270. McGimpsey, Ian, 2010: Petrology and lithogeochemistry of the host rocks to the Nautanen Cu-Au deposit, Gällivare area, northern Sweden. (45 hp)
271. Ulmius, Jan, 2010: Microspherules from the lowermost Ordovician in Scania, Sweden – affinity and taphonomy. (15 hp)

272. Andersson, Josefin, Hybertsen, Frida, 2010: Geologi i Helsingborgs kommun – en geoturistkarta med beskrivning. (15 hp)
273. Barth, Kilian, 2011: Late Weichselian glacial and geomorphological reconstruction of South-Western Scania, Sweden. (45 hp)
274. Mashramah, Yaser, 2011: Maturity of kerogen, petroleum generation and the application of fossils and organic matter for paleotemperature measurements. (45 hp)
275. Vang, Ina, 2011: Amphibolites, structures and metamorphism on Flekkerøy, south Norway. (45 hp)
276. Lindvall, Hanna, 2011: A multi-proxy study of a peat sequence on Nightingale Island, South Atlantic. (45 hp)
277. Bjerg, Benjamin, 2011: Metodik för att förhindra metanemissioner från avfallsdeponier, tillämpad vid Albäcksdeponin, Trelleborg. (30 hp)
278. Pettersson, Hanna, 2011: El Hicha – en studie av saltstäppssediment. (15 hskp)
279. Dyck, Brendan, 2011: A key fold structure within a Sveconorwegian eclogite-bearing deformation zone in Halland, southwestern Sweden: geometry and tectonic implications. (45 hp)
280. Hansson, Anton, 2011: Torvstratigrafisk studie av en trädstamshorisont i Viss mosse, centrala Skåne kring 4 000 - 3 000 cal BP med avseende på klimat- och vattenståndsförändringar. (15 hp)
281. Åkesson, Christine, 2011: Vegetationsutvecklingen i nordvästra Europa under Eem och Weichsel, samt en fallstudie av en submorän, organisk avlagring i Bellinga stenbrott, Skåne. (15 hp)
282. Silveira, Eduardo M., 2011: First precise U-Pb ages of mafic dykes from the São Francisco Craton. (45 hp)
283. Holm, Johanna, 2011: Geofysisk utvärdering av grundvattenskydd mellan väg 11 och Vombs vattenverk. (15 hp)
284. Löfgren, Anneli, 2011: Undersökning av geofysiska metoders användbarhet vid kontroll av den omättade zonen i en infiltrationsdamm vid Vombverket. (15 hp)
285. Grenholm, Mikael, 2011: Petrology of Birimian granitoids in southern Ghana - petrography and petrogenesis. (15 hp)
286. Thorbergsson, Gunnlaugur, 2011: A sedimentological study on the formation of a hummocky moraine at Törnåkra in Småland, southern Sweden. (45 hp)
287. Lindskog, Anders, 2011: A Russian record of a Middle Ordovician meteorite shower: Extraterrestrial chromite in Volkhovian-Kundan (lower Darriwilian) strata at Lynna River, St. Petersburg region. (45 hp)
288. Gren, Johan, 2011: Dental histology of Cretaceous mosasaurs (Reptilia, Squamata): incremental growth lines in dentine and implications for tooth replacement. (45 hp)
289. Cederberg, Julia, 2011: U-Pb baddelyit dateringar av basiska gångar längs Romeleåsen i Skåne och deras påverkan av plastisk deformation i Protoginzonen (15 hp)
290. Ning, Wenxing, 2011: Testing the hypothesis of a link between Earth's magnetic field and climate change: a case study from southern Sweden focusing on the 1st millennium BC. (45 hp)
291. Holm Östergaard, Sören, 2011: Hydrogeology and groundwater regime of the Stanford Aquifer, South Africa. (45 hp)
292. Tebi, Magnus Asiboh, 2011: Metamorphosed and partially molten hydrothermal alteration zones of the Akulleq glacier area, Paamiut gold province, South-West Greenland. (45 hp)
293. 293. Lewerentz, Alexander, 2011: Experimental zircon alteration and baddeleyite formation in silica saturated systems: implications for dating hydrothermal events. (45 hp)

LUNDS UNIVERSITET

Geologiska enheten
Institutionen för geo- och ekosystemvetenskaper
Sölvegatan 12, 223 62 Lund